Monitoring Moisture Content and Mass Flow of Wood Chips Using Electrical Capacitance Tomography

by

Pengmin Pan

A dissertation submitted to the Graduate Faculty of
Auburn University
in partial fulfillment of the
requirements for the Degree of
Doctor of Philosophy

Auburn, Alabama
December 13, 2014

Keywords: capacitance,image,permittivity,moisture content,mass flow,dynamic

Approved by

Timothy McDonald, Chair, Associate Professor of Biosystems Engineering
John Fulton, Associate Professor of Food, Agricultural,
and Biological Engineering, Ohio State University
Brian Via, Associate Professor, School of Forestry and Wildlife Sciences
John Hung, Professor of Electrical and Computer Engineering

Abstract

Woody biomass is currently sold on a wet basis, a system that works because moisture content of harvested trees normally fluctuates within a narrow range and wood from multiple sources can be considered a uniform product. Wet wood, however, is not an optimal energy feedstock and various methods have been proposed to reduce moisture content in woody biomass prior to its sale. Once moisture content can vary outside its typical range, however, the use of wet weight as a basis for selling timber products becomes untenable. Promoting a robust bioenergy market will, therefore, require the development of reliable sensors for measuring moisture content of wood in the field. A logical place at which to measure moisture content of woody biomass would be just prior to shipment for final conversion. For biomass harvested from pine plantations prevalent in the US South, that would most likely be between the chipping and loading operations. To avoid handling the biomass an extra time, however, a moisture sensor should work accurately on a moving stream of chips as they exit a chipper and are blown into a van for hauling. This type of high-speed, non-contact moisture sensor suitable for application in a rough environment is not currently available. Our goal in this study was to develop a sensor for measuring moisture content of a rapidly moving stream of pine chips that was robust, non-contact in operation, reliable, and accurate.

An 8-electrode electrical capacitance sensor was built for that purpose. The multiple electrode system was used to characterize the distribution of permittivity within the circular area (diameter = 16.5cm) enclosed by the sensor and surrounded by the electrodes (2.5x10 cm copper plates). The sensor was could be operated in two modes: a) static mode in which the cumulative permittivity between each combination of plates was the variable correlated with moisture (a bulk measurement), and b) a dynamic mode in which multiple sequential readings of electrode combinations was used to sample a stream of chips moving through the sensor enclosure, the result being a sequence of 2-D maps of permittivity. This method is referred to as electrical capacitance tomography (ECT).

The objectives of the research presented in this dissertation were:

1. Validate the accuracy of the sensor in static mode in predicting moisture content of fixed quantities of biomass, and investigate the sensor's limits of performance when subjected to variations in such confounding variables as quantity, location, and size of the material under test.

2. Develop the necessary hardware and software systems to perform dynamic (ECT) mode characterization of moving streams of biomass, and establish the accuracy of moisture content predictions.

Static mode calibration of the sensor was carried out on wood chips having uniform moisture content. Tests were made on chips ranging in moisture content of from 4% to 140% (dry basis), and the results compared with the widely-accepted near infrared spectroscopy (NIR) method. For tests on individual wood chips (about 10 g each), the root mean squared errors of prediction (RMSEP) were 13.52% and 48.43% for NIR and ECT, respectively. In bulk measurements (multiple chips, 40-80 in number), RMSEPs were found to be 15.39% and 11.65% for the NIR and ECT methods, indicating the main difference between the two methods: NIR predictions were independent of sample mass, the ECT estimates were not. Two additional measurement procedures were developed using the capacitance sensor, one using multiple excitation frequencies and the other assuming a fixed sample mass based on volume, to remove its dependency on sample mass. The RMSEPs for the two methods were similar (13.0% and 10.9% for the fixed volume and two-frequency methods, respectively) and also comparable to the previous methods when sample mass was known. It was concluded the capacitive approach was very comparable to NIR in its ability to accurately predict moisture content of biomass using either approach (unknown or known mass), and the capacitive sensor was superior in predicting moisture content of bulk materials. On quantities of wood near the detection limit of the capacitance sensor (about 10g), however, the NIR approach was preferable.

Dynamic mode tests of the sensor were made in two steps, the first involving simultaneous independent measurement of mass flow using another sensor (plus moisture content from the sensor in capacitive mode), and the second using the sensor in ECT mode to estimate both total mass flow and moisture content simultaneously. In the first tests, an impact measurement approach was used to estimate mass flow. In the second, the ECT tomographic mode was used to image the variation in permittivity of the flowing stream of wood chips. The images also provided a means to estimate chip volume within the sensor, which, assuming uniform density, provided a mass value. The RMSEP of moisture content predictions using the impact and ECT mass flow estimation methods were 11.86% and 17.71%, respectively. It was concluded these tests proved the feasibility of using electrical capacitance tomography as a means of measuring moisture content of moving biomass streams. Further development of the techniques to increase the sampling rates above that achieved in these tests will be required to make the system practical.

Acknowledgments

First of all, I would like to thank foremost my advisor, Professor Timothy McDonald, for his advice and guidance. Without his help, it would be much more challenging for me to complete the Ph.D. study. I am a lucky person to have an advisor whom I admire his profession and respect his personality. I am also grateful to Professor John Fulton (The Ohio State University), Professor John Hung and Professor Brian Via for being on my committee. Thanks Professor Tony Grift (UIUC) for being my dissertation reader. Their suggestions and feedbacks are greatly improving my research. I also thank Professor Yifen Wang, Professor Songming Zhu (Zhejiang University, China) and my master advisor Professor Jianping Li (Zhejiang University, China), who introduced me to Auburn University.

I would like to express my gratitude to Professors and colleagues of Biosystems Engineering Department. Especially thank Professor Oladiran Fasina for allowing to use his ovens for the research. Thanks to Rees Bridges for his great help in both my laboratory works, data analysis and my life. Thanks to USDA and DOE for funding the project. Thanks to John Klepac for providing research equipment. Thanks to local mills who provided woodchips for the study. Thanks to all my friends who brought wonderful time to my life in Auburn. Thanks to Auburn University for bringing me so many good friends all over the world!

Finally and as always, I want to give a special acknowledgement to my parents and grandparents. No words can ever express their love, support and encouragement.

Table of Contents

List of Figures

List of Tables

Chapter 1

INTRODUCTION

Woody biomass is often transported and used in chipped form, in the pulp and paper industry and potentially as a feedstock for a future biomass energy industry. Predictions from the leading information provider for the global forest products industry, RISI's (Repository of Industrial Security Incidents) Wood Biomass Market Report, indicate increasing demand for wood chips in the future. Estimates for North America predict demand for up to 54 million green tons of wood chips annually, mostly from loblolly pine, through the year 2015.

With the increasing demand for wood chips, especially for energy, a potential problem is raised. Woody biomass is currently sold on a wet basis, a system that works because moisture content (MC) of green harvested trees normally fluctuates within a narrow range and wood from multiple sources can be considered a uniform product. This is acceptable when chips are used for pulp, but water is considered a contaminant for thermo-chemical processes producing energy. Energy-producing consumers would prefer to pay for raw material on an energy basis, rather than wet weight, to favor those suppliers bringing the driest wood chips. Feedstock value, therefore, is directly related to moisture content. Once moisture content can vary outside its typical range the use of wet weight as a basis for selling timber products becomes untenable, but there is no effective, rapid method available to assess moisture content of biomass chips, or other material, that can be applied in an industrial setting. In both production and process control applications, chips are moved at high velocity and a sensor that can detect variations in MC in those circumstances is not available.

In an in-woods setting, a logical place at which to measure MC would be just prior to shipment to a conversion facility. In pine pulp chip production, that would most likely be after stems were chipped and before the product was loaded into a truck. A sensor for that application would necessarily have the capability to obtain MC in a rapidly moving stream of chips as it was blown out of a chipper. Such an arrangement would afford the ability to sample MC for all biomass without having to handle it separately and was presumed to give the highest degree of utility in application.

The goal of this research was to develop a sensor for that application. It was anticipated a successful conclusion in the project might also lead to applications for the sensor in other process control settings, or for other biomass materials.

1.1 Overview of Published Work

Wood MC is defined as the weight percent of water in wood and can defined based either on a total weight (wood plus water, wet basis), or on the dry weight of wood (Siau 1984). In this thesis, MC is always presented on a dry basis, as equation (1.1).

$$MC = \frac{W_{\text{water}}}{W_{\text{wood}}} \times 100\% \tag{1.1}$$

For green wood, MC can vary from about 30% to more than 150%. The traditional way of measuring wood MC is to use the oven dry method. Wet sample weight (wood plus water) is measured before placing in an oven, and, when the weight of wood sample does not change with time, the sample is removed and the dry weight recorded. The weight lost during the drying process is considered to be only water. Although there exist some sources of error in the oven-dry moisture measurement, such as incorrect temperature, incomplete drying, water absorbtion from air, or volatile matter loss, the moisture value estimated from the oven dry method is very accurate and usually used as the true MC. However, the oven dry method is time consuming, typically taking 24 hours to fully dry a sample (Reeb and Milota, 1999). The method is not appropriate, however, when a real-time assessment of moisture is necessary, as in resolving payment systems based on dry matter, or in process control settings. As a means toward this end, multiple types of rapid moisture sensors have been developed. These sensors can be classified into two categories: contact and non-contact types.

1.1.1 Contact Type Sensor

Contact moisture meters are mainly based on wood's electric or dielectric properties. Electric property sensors those sensitive to variations in conductance and resistance. The principle of conductance (or resistance) measurement is to calculate the flow of electric current through the material according to Ohm's law. Prediction models are built based on the relationship between MC and conductance (or resistance) (James 1998).

Wood is a dielectric material. The dielectric property describes how much potential electrical energy could be kept in an electric field established within the material itself. The energy storage capacity depends on the material's permittivity, which can be greatly affected by the presence of water, and this is true in biomass materials, including wood.

Capacitance sensors are often used in measuring the variation in permittivity of biomass materials with moisture content. The simplest type of capacitor is built using two parallel conductive plates between which is sandwiched a dielectric material. The capacitance of the device is related to the electric field established across the plates (by applying a voltage), plus the permittivity of the material between them. Compared to other biomass components (e.g., wood), the permittivity of water is significantly larger (for details see section 2.1) and this property has led to development of moisture sensors for numerous materials such as corn, peanuts, wheat, grain and other bio-products (Kandala & Sundaram 2010, Kandala & Puppala 2012), with very good precision. A capacitance-type sensor has been built to measure the permittivity change of wood with MC (Saxena 1981). A perfect dielectric material can completely discharge any charge polarization if the applied electric field is removed. However, wood is not a perfect dielectric material and will dissipate energy during a time-varying charge-discharge cycle, a process known as hysteresis. Based on the amount of energy lost, another moisture sensor known as a power-loss type moisture meter has been developed. The amount of energy loss has been shown to have high correlation with MC (James 1998).

Although the electric moisture meters work well in measuring MC of wood, three disadvantages limit their applications:

1. High accuracy is obtained only when samples are under fiber saturation point (FSP), or under about 30% MC. There are two kinds of water that exist in wood: bound water and free water. Bound water exists as a component of cell walls; free water is that found in the lumen and may be liquid or vapor moving freely in cavities (Reeb 1995). Water under FSP is bound water only. However, since electrical moisture meters have significantly different responses with bound water and free water, their measuring range is limited (James 1998).

2. Moisture meters are usually designed with two fixed electrodes. A sample that is appropriate to apply must typically be in contact with both electrodes. MC of small sized materials, such as wood chips or powder, is not able to be measured.

3. Contact sensors usually require several seconds reading time, and thus are only applicable to static situations.

1.1.2 Non-Contact Measurement

Compared with contact sensors, non-contact methods have advantages, particularly for dynamic MC determination. The common principle of non-contact techniques is based on measuring changes in energy propagating through a material. The energy source includes electromagnetic radiation (X-ray, radio frequency (RF), microwave, near infrared (NIR)), acoustic (ultrasonic) waves, and simple electric fields (electrical capacitance tomography, ECT). Non-contact sensing systems typically consist of a signal emitter and a receiver with the test material located between them. The sensor is sensitive to some difference between the source and returned signals such as a change in amplitude, or phase, or both.

Acoustic wave techniques have been widely used in detecting and processing chemical components of biomass and foods. In measuring MC of biomass, two distinct acoustic systems were reported.

(1) Ultrasonic wave system. A typical wave measuring system equipped with 1MHz ultrasonic source wave to measure the change in wave velocity which was related to MC in wood. A strong linear relationship was observed if the MC was below FSP. However, the trend of change in wave velocity was totally different when MC exceeded 30%. An indirect method was introduced (Minamisawa *et al.* 1990) using longitudinal modulus as a connection between velocity of ultrasonic sound and MC above 30%. The relationship between longitudinal modulus and sound velocity was expressed as $M = \rho\nu^2$ (where M stood for longitudinal modulus, $kg/m \cdot s^2$, ρ was wood density, kg/m^3 and ν was the velocity of ultrasonic sound, m/s). Since the longitudinal modulus was also proportional to MC, a polygonal equation could be identified between sound velocity and MC. Two different models (for MC above and below 30%) were developed and connected with each other at FSP (MC = 30%).

(2) Impact sound measurement. The system was tested using cereal grains dropped at 10cm height to the impact surface to generate sound waves. An acoustic sensor was applied to collect sound wave with the output as voltage signals. The feed rate of grain was almost constant. Results indicated the sound pressure level variations were highly correlated with grains' MC. The standard error of validation set was 1.25% for a limited moisture range (8% to 20%).

X-ray projection is described as an accurate means to determine MC for porous materials. Implementing the method involves the following steps.

(1) System initialization. Determine the measuring space, set and record the distance between X-ray emitter and detector. Record the intensity of the original signal.

(2) Reference data. Dry sample, e.g. dry chips, should be measured as the reference data.

(3) Sample measurement. Acquire the transmitted X-ray intensity of test (wet) sample.

(4) Modeling. By comparing the transmitted X-ray intensity of test (wet) sample with the original intensity, MC could be estimated by equation 1.2.

$$\mathrm{MC} = -\frac{\rho_w}{\mu_w d}\left(\ln\left(I_{\mathrm{wet}}\right) - \ln\left(I_{\mathrm{dry}}\right)\right) \tag{1.2}$$

Here ρ_w is the density of water (g/cm^3), μ is the attenuation coefficient and d is the separation between emitter and detector, I_{wet} and I_{dry} are transmitted X-ray intensity through the dry and wet sample respectively, computed from equations:

$$I_{\mathrm{dry}} = I_0 e^{-\mu d} \tag{1.3}$$

$$I_{\mathrm{wet}} = I_0 e^{-\mu d - \mu_w d} \tag{1.4}$$

where I_0 is the intensity of original signal (Roel and Carmeliet 2006). Nordell and Vikterlo (2000) developed a dual energy X-ray system to measure MC in wood fuels accurately, with a standard error of 2.0%. The measuring range was greatly extended, compared to contact moisture meters (75.3% vs. 30%).

Radio frequency (RF) is an electromagnetic form of energy and at frequencies up to about 3 GHz (UHF) can be generated using an alternating current sent out through a relatively simple antenna. Phase and voltage attenuation for transmitting and receiving signal were analyzed for wood-based product MC measurement by Hanson and Kelly (1998). Energy loss at multiple frequencies were used as predictors for moisture content. The method could be extended to multiple types of wood-based boards such as hardboard, or particleboard. Liu *et al.* (2010) measured the specific gravity of wood chips using phase and voltage attenuation of RF energy. Polynomial equations were obtained relating MC and specific gravity, with a high correlation coefficient (0.87 and 0.89 respectively). Numerous other biofuel materials have also been successfully tested in MC prediction using the approach (Paz *et al.* 2006). Other wood properties, such as strength, have also been measured using an RF sensor (Steele and Cooper 2003). Water, however, strongly absorbs electro-magnetic energy at certain frequencies (Morrow 1980) and therefore the power of RF systems needs to be limited if applied in MC measurements to avoid sample damage.

A nuclear magnetic resonance (NMR) sensor has also been introduced to measure MC of wood chips at UHF frequencies (Barale *et al.* 2002). Samples were tested in a tube with a permanent magnetic field. Since permanent magnets are sensitive to temperature variations, the experiment was carried out in a temperature-controlled box. The MC measured from phase and voltage attenuation was compared with the oven drying method. The system required a few seconds for result calculation, but was generally accurate.

Microwave systems (above 3 GHz) can also be used for MC measurement in biomass materials. High accuracy prediction resulst were obtained for wood chips (Johansson 2001) with MC under FSP (standard error= 2.1%). However, due to interactions in the wood material that changed the phase of the incident radiation, the predicting error was greatly amplified when using 10 GHz microwaves to measure MC above FSP. As a solution to extend the measuring range, a lower frequency microwave system was designed with a 2.4 GHz signal (Vallejos 2009). The system was tested with *radiata spp.* pine boards. Results indicated the lower frequency system had the capability to extend the moisture measuring range and make it feasible to use for wood chips with a MC exceeding 30%. Other physical properties, including fiber direction and density, have also been successfully predicted using microwaves (Schajer and Orhan 2005, Hansson *et al.* 2005). However, microwave attenuation as used in these tests was sensitive to total mass of the sample, which also had to be known.

Due to O-H bond of water having significant absorption bands at 760, 970, 1450, 1940 and 2950 nm wavelength, near infrared radiation (NIR) is considered an efficient way to detect water content inside of materials (solid or other liquid) (Adepipe and Dawson 2008). An

NIR spectral dataset usually consists of hundreds of points and some mathematical approach is required to reduce the sample space of the measurements. Principal component analysis (PCA) is a common way to deal with these large datasets (Via *et al.* 2003). The method is used to extract linearly independent variables (principle components, PCs) from raw spectral data. A regression model can be built between MC and PCs, using regression methods such as multiple linear regression (MLR), principal component regression (PCR), or partial least square regression (PLS) (Zhang *et al.* 2010). The NIR technology has been verified as a rapid, accurate and stable method in predicting MC, as well as other chemical components. Its application field covers agriculture, food engineering, and chemical engineering. Recent research studies in NIR are mainly focused on improvements and dynamic applications:

(1) Improvements. Different combinations of view angles were studied in wood MC prediction. Tormanen and Makynen (2011) compared 12 different view angles on fresh veneer samples. An optimized combination was found and a highly correlated MC predicting model was built with R^2=0.891 and root-mean-square error of prediction (RMSEP) of 5.43%. Wavelength (Bull 1991) and temperature influence (Thygesen and Lundqvist 2000) was also studied to increase accuracy of wood MC measurement. Reflectance at 970nm was proved (Bull 1991) less sensitive to moisture variance because of greater penetration into the sample. 1300 nm was found as a relatively good reference wavelength for 1450nm (calculated as data at 1450nm divided by those at 1300nm), to improve the MC measurement of sawdust. For the influence from surface structure, size or color of wood, a single ray system was reported as unstable and imprecise. A dual ray system (Corluka *et al.* 2004) was developed to compensate for errors from the above sources, while the system cost was increased.

(2) On-line applications. Axrup *et al.* (2000) developed a dynamic wood chip and bark measuring system using miniature diode array NIR spectrometers, which were tested on moving samples with velocity of 1 m/s. The advantage of the array NIR detector was to avoid splits in spectra, which were observed if applying static NIR sensors to

measure dynamic samples. Spectra were calculated over a 3ms period. The root-mean-square error of calibration (RMSEC) and RMSEP for wood chip MC was 1.6% and 2.3% respectively. For bark samples, RMSEC and RMSEP were 3.5% and 5.1%. The system also had the capability to measure other chemical components of wood, such as carbohydrates, extractive, or lignin. The method has also been successfully applied for real time forage (Digman and Shinners 2008), corn or other biomass (John Deere, HarvestLab$^{\text{TM}}$ Sensor) harvester, hardwood pulp (Brink *et al.* 2010), pellet and biofuel (Lestander 2009), polymers (Leitner et al. 2003), and pharmaceutical powder (Demers et al 2012, Aditya *et al.* 2010).

Electrical capacitance tomography (ECT) systems generally consist of capacitance sensors, a data acquisition system, and a computer for image reconstruction and display. The principle of ECT is to use multiple estimates of permittivity across an enclosed space to measure its spatial distribution and reconstruct an image describing that variation (Yang and Conway 1998). The cross-sectional images can directly show the size and location of materials inside a closed vessel. Nurzharina (2011) developed a 12-electrode ECT sensor to measure the distribution and volume of water inside mixtures of sand and clay. However, no literature has been published yet for wood chips or other biomass applied in MC measurement.

1.1.3 Method Summary

As stated in 1.1.1 and 1.1.2, each method has its own power to predict MC for biomass, however, these technologies also have some limitations. Advantages and limitations were summarized in Table 1.1.

The purpose of reviewing these methods was to find an appropriate one for dynamic wood chip moisture determination. Key factors of an acceptable sensor would include: wide measuring range, low cost, robust in dusty and dirty environments, high sampling rate to assess rapidly moving streams of material, non-contact, and accurate. Although higher

Table 1.1: Comparison advantages, and disadvantages, of various moisture content measurement sensors.

Methods	**Advantages**	**Limitations**
Oven dry	Accurate,	Time consuming, destructive,
Contact meters	Robust, easy to use	Static measurement
X-ray, Microwave, Acoustic wave, RF	Rapid, non-contact	Expensive, fixed sample quantity, sensitive to particle size/density, single dimension measurement
NIR	Rapid, Non-contact	Surface and spot measurement, lens maintaince
ECT	Extremely fast, non-contact low cost	Weak signals

energy systems would probably provide better measuring results, equipment costs for theses type systems are usually high. The impact moisture measuring system was relatively lower cost, the range of moisture, however, was narrow and lower than the MC of green pine chips. The method may also be sensitive to the shape of the test material. Since the size of grain is small and its shape is uniform, the sensor accuracy is not affected by impact direction. However, wood chips have quite irregular shapes. Sound waves created by different impact points of chips would likely be different and the predicting accuracy could be significantly degraded. NIR is a surface measurement method, which is, unfortunately, imprecise in measuring materials with non-uniform moisture gradients between surface layers and the core, or between individual pieces in a bulk particulates. For dynamic samples, such as a wood chip stream, a single measured sample might not be representative of the whole population. Another limitation is the chipping process itself, which is very dusty and harsh by nature, and preserving lens and other optical structures in that type environment would be difficult. The ECT system outlined above does not have the limitations outlined above and has the potential to measure wood MC for samples in motion.

Although not much literature could be found to support ECT effectiveness in measuring biomass MC directly, results from single paired parallel plate capacitance sensor tests provided confidence in pursuit of measuring permittivity to predict MC. If the measuring speed could be made much higher than sample velocity, the sampling could be approximated as being of a static nature. Because a high sampling rate is an important feature of an ECT system, we choose this capacitance based technology to measure MC of biomass chips.

1.2 ECT Introduction

The ECT system is a relatively new technology developed from computed tomography (CT) in the 1980s. Compared to X-ray CT (the typical method used in medical scanning), ECT uses a much lower energy source signal probe the material under test. This approach greatly reduces the cost of system. The first 8-electrode ECT system was developed in 1988 to detect the distribution of sand in air (Huang *et al.* 1988). Nowadays, this technology has been well developed, both in hardware and software.

1.2.1 Hardware Improvements

Electrodes Multiple ECT sensors have been developed, electrode counts of which have ranged from 4 to 32, with multiple variations within that range. The increased electrode numbers divide the sensing area into more segments, which improves the resolution of reconstructed images. However, the combinations of capacitances measured are proportional to the square of electrode number. Increasing the electrode number significantly decreases the sampling rate achievable for a given data acquisition system, which reduces the number of frames per second that can be imaged. The effect of electrode number was analyzed by Peng *et al.* (2012) who suggested exceeding 12 would not contribute greatly to the quality of images. This conclusion was made based on a fixed measuring area and electrode size, which can varying dramatically among systems having different applications. According to the literature, besides 8 electrode sensors, typical electrode numbers for ECT systems in use

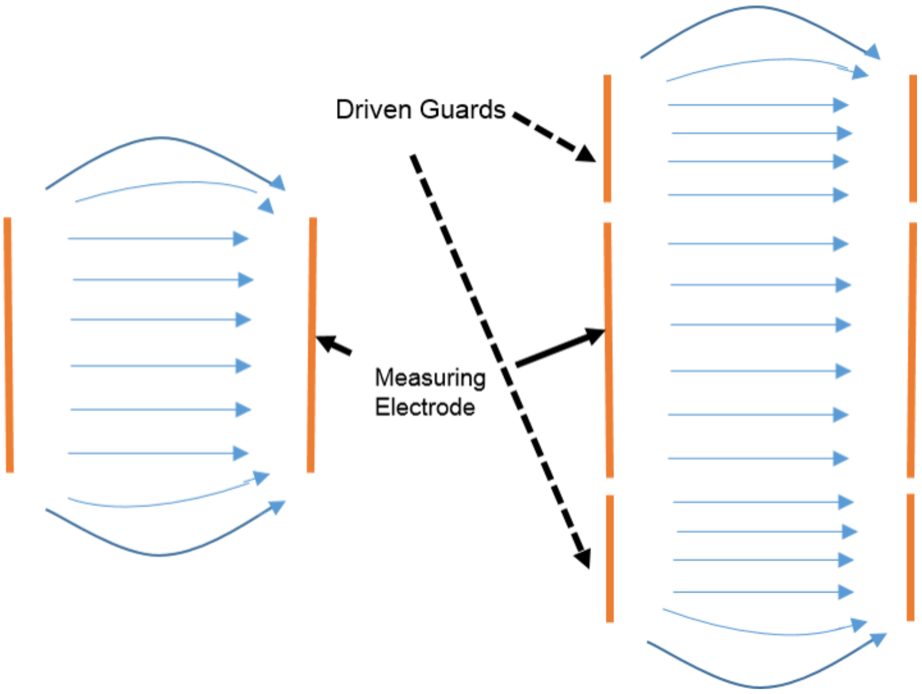

Figure 1.1: An illustration of the working principle of driven guards as applied in ECT measurements. The guards shift any fringe electric field physically away from sensor electrodes, increasing accuracy.

are 12 (Olmos *et al.* 2007) and 16 (Wang *et al.* 2009). The 16 electrode ECT could also be switched to 8 electrode mode. The effect of electrode size was also studied (Olmos *et al.* 2007).

Driven guard electrode and earthed screen The objective in adding the complexity of driven guard electrodes and an earthed screen was to reduce noise in the system. As shown in Figure 1.1, the driven guard electrodes, which are connected with the same signal as a source electrode, reduce the fringe electric field effect often observed to reduce accuracy in ECT systems. Details of the approach can be found in the papers by Yan *et al.* (1999 and 2008) and Yang (2006).

Data acquisition system To implement an ECT system a computer data acquisition system was required to effectively coordinate measurements and record results. Most data acquisition systems available can measure voltages quickly and inexpensively, therefore it was necessary to develop a means to convert the parameter of interest (capacitance) to a voltage signal that could be sampled. A capacitance to voltage transducer, therefore, is the basic but crucial element of an ECT system, as indicated in Huang *et al.* (1988). For such a transducer, its output voltage is proportional to an unknown capacitance. For an ECT system, the unkknown capacitance is that between any two paired electrode combinations. Dual transducer circuit have been developed to improve transducer quality (Johana et al. 2011, Yang 1995). The two signals obtained from such systems carried the same measuring result but in different sign (one positive from a circuit in a charging state and another negative from a discharging state). By subtracting negative output from the positive signal, the noise could be canceled the capacitance signal doubled (Jiang and Wang, 2009). Amplifiers have also been introduced to provide large gains to the output signal, but are more susceptible to noise (Yang 1999).

Sensor structures The traditional ECT was designed to attach surrounding a cylindrical vessel. For the purpose of extending their application scope, ECT systems for square vessels (Yang and Liu 1999), bending and T-junction cylindrical vessels were also developed (Wang *et al.* 2010). As the output of ECT was a two dimensional image, however, the results for these non-circular shapes were sometimes difficult to interpret. By correlating two sets of ECT sensors, three-dimensional ECT sensors have also been built and used to measure the volume of objects, instead of simply their cross section (Marashdeh and Teixeira 2004, Yan *et al.* 2011). The development of 3D ECT system was extremely useful for material properties measurement.

Multiple frequency The method uses two input signals at different frequencies. Two source signals were applied on two adjacent electrodes. By applying filters, output signals were separated with different frequency. Though the output data number was less than single frequency measurement, the dual method doubled the sampling rate (Mohamad *et al.* 2011).

1.2.2 Software Developments

Image reconstruction methods Image reconstructing algorithms are a fundamental part of ECT research. The common approach is to use the linear back projection (LBP) algorithm (Xie *et al.* 1992). Details are presented in Chapter 3. Since the LBP method tends to result in images with low precision, multiple algorithms have been developed to improve its estimates, such as: Landweber iteration method (Wang *et al.* 2012), BP neural network (Li *et al.* 2012; Chen *et al.* 2011), extended regularized total least squares method (Lei *et al.* 2008), genetic algorithm (Mou *et al.* 2005), fuzzy mathematical model (Abdelrahman *et al.* 2009), Gauss-Newton algorithm (Chen *et al.* 2009), Barzilai-Borwein algorithm (Liu *et al.* 2010), support vector machine method (Liu and Chen 2006), and sparse representation (Ye *et al.* 2014), among others.

1.2.3 Application Field Extended

Besides the application in detecting mixed solid distributions, the ECT sensor has been widely used in measuring flow of fluids in a closed nonconductive pipe. Most common examples are: measuring mixture of oil and water (Johana *et al.* 2011), gas/solid fluidized bed (Huang *et al.* 2003, Yang *et al.* 2009), gas/oil two phases (Li *et al.* 2008) and gas/oil/water flow measurement (Li *et al.* 2012). The application field has primarily been in multi-phase flow measurements, but ECT has also been used successfully to measure moisture distributions in mixtures of sand and clay (Karim and Ismail 2011).

1.3 Dissertation Objectives

This project's goal was to develop a MC measurement system providing accurate estimates on high-speed, pneumatically-conveyed streams of pine wood chips. Sensors are available that could potentially achieve this purpose, but most are either too expensive, or not likely to survive the conditions under which they might be deployed. A capacitance approach, however, appeared to be the method most likely capable of providing accurate measurements in biomass applications, and at low cost. Many capacitive sensing systems used to estimate moisture content in biomass, however, suffer from a significant confounding interaction with density of the material being probed (e.g., Virk *et al.* 2013). In a high-speed stream of chips, mass flow rate of material, and therefore density, is highly variable, which could dramatically lower the accuracy of estimates, at least over short periods of time. Because it can potentially sense both total quantity of material (through image) and total moisture (using capacitance), it was felt ECT was the most likely candidate for this application.

The overall hypothesis in this research was that ECT could simultaneously sense both dry matter and moisture flow rates in streams of wood chips with accuracy sufficient for its application in feedstock valuation or conversion process control.

To test this hypothesis, it was first necessary to build, understand, and verify the performance of the sensor itself. This was done using the following steps.

1. Design the prototype ECT sensor enclosure and electrodes based on a survey of literature.
2. Design, build, and verify the sensor capacitance-to-voltage electronics.
3. Build a data acquisition system capable of taking capacitance measurements at single-digit kHz speeds. Develop, based on a survey of literature, image reconstruction techniques to implement the construction of ECT images of permittivity distribution based on sensor measurements.
4. Investigate the sensitivity of the system to factors *other* than moisture content. Specifically, determine the influence of material physical properties such as size (volume),

plus variations in application of the sensor itself, such as location within the sensor enclosure, on the overall sensor response.

1.3.1 Research Objectives

The goal of the research project was to develop a robust, non-contact moisture sensing system for biomass. The unique aspect of the approach presented here was its use of imaging based on capacitance tomography. In order to establish the potential of the system as a practical means of sensing moisture in static and dynamic modes, however, its performance must be assessed relative to other accepted methods. The research objectives of this study were, therefore, as listed below.

1. Validate the accuracy of the sensor in static mode to predict moisture content of fixed quantities of biomass. Compare the capacitance sensor's accuracy to near-infrared reflectance spectroscopy, a well-established approach for determining moisture content in biomass materials.

2. Develop the necessary hardware and software systems to perform dynamic (ECT) mode characterization of moving streams of biomass, and establish the accuracy of moisture content predictions. Verify the ability of the ECT system to make simultaneous independent measurements of mass flow and moisture content.

1.4 Dissertation Outline

Chapter 2 covers the detailed design of the ECT system. It provides information on:

1. Hardware. The principle of ECT is presented, along with the hardware implementation developed for this study. All system design methods, parameters, theory and functions used in the development of the sensor were covered.

2. Software. This part covered sensor control, data acquisition system, and image reconstruction methods developed for the study.

In Chapter 3, the characteristics of the ECT system built for this project were tested and results summarized. The ability of the sensor to provide stable, repeatable capacitance measurements was evaluated, as well as the effects of distribution and size of the material under test.

Chapter 4 presents results of using the ECT sensor to measure MC of biomass when not in motion. Experiments were carried out for both single wood chips and bulk quantities to test the limits of detection of the sensor. NIR measurements of MC were used to validate ECT estimates and accuracy of both sensors was compared. Two alternative approaches of applying the ECT system were discussed as methods to eliminate the confounding effect of sample density.

Results covering tests on moving samples are covered in Chapter 5. A force transducer-based mass flow system was introduced and results from field and lab testing presented. This sensor was used to validate image-based measurements of mass flow derived from ECT. Two alternative MC prediction models for dynamic estimates based on ECT measurements were then discussed. Advantages and shortcomings of each were presented. Chapters 4 and 5 cover the research objectives outlined above.

Chapter 6 covers overall conclusions derived from the study and presents ideas for future work.

Chapter 2

ECT PRINCIPLE AND SYSTEM SETUP

2.1 Principle of ECT

Electrical capacitance sensing is, in general, a nondestructive, non-contact approach to describing variation in dielectric properties of a material occupying some space. It is an external measurement to describe the internal dielectric property variation within a closed space. An ECT system generally consists of three basic parts: capacitance sensors, data acquisition system and computer (data processing and image reconstruction), as Figure 2.1. Sensor electrodes are attached surrounding the testing vessel (non-conducting walls), each pair of sensors provides an independent capacitance value. The cross-section image can be reconstructed by adding all capacitor combinations together. For biomass materials, dielectric properties are typically used to predict some other important physical characteristic, in particular moisture content (Kandala & Sundaram 2010, Kandala & Puppala 2012).

The approach relies on observing the change in capacitance between two electrodes as the material between them (or otherwise within the range of their mutual electric field) varies. For the purposes of this study, it was desired to measure the MC of a moving stream of biomass within an enclosed conduit and this requirement was the basis for the sensor design. The approach was to develop a system placed in-line along a biomass conveyance system, preferably one in which a stream of material is conducted pneumatically along some closed conduit. Some portion of the conduit would be equipped with a system of electrodes that would be used to generate the electric fields necessary to measure dielectric constant of the two-phase air/biomass mixture flowing within. The realization of this sensor developed for this study used electrodes attached around the perimeter of a cylindrical, nonconductive vessel. At least two electrodes would be necessary to form the sensor, but additional

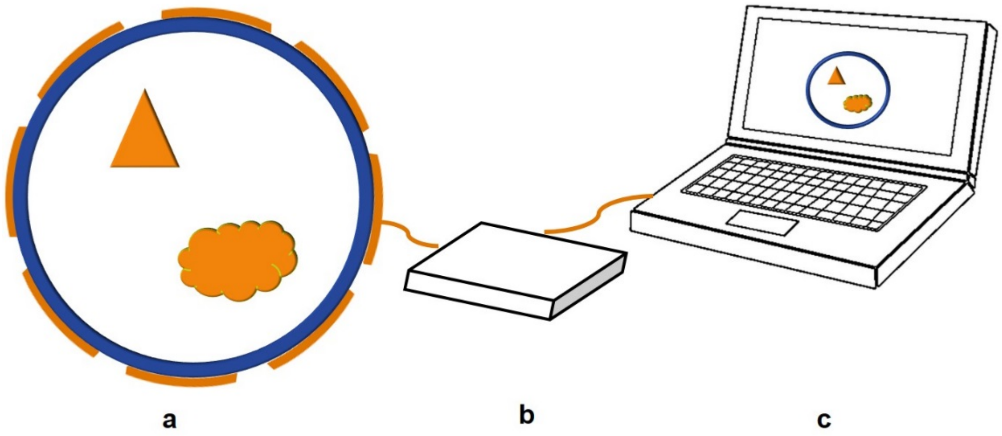

Figure 2.1: Schematic diagram of an ECT system. Elements shown are: (a) Capacitance sensors, (b) signal processing and data acquisition circuits, (c) computer to collect data and control the experiments.

electrodes were included in this design. For an N-electrode system $\binom{N}{2}$ combinations of electrode pairs would be available to characterize the distribution of dielectric constant of the material within the measurement enclosure.

The use of more than two electrodes in the measurement system provided redundancy in measurements as each unique pair of electrodes could be used to generate the electric field necessary for measuring dielectric constant. Their use also afforded, however, the additional opportunity of applying tomographic techniques to reconstruct the 2-D spatial variation of dielectric constant distributed throughout the sensor enclosure. This application of capacitive sensors, called electrical capacitance tomography, or ECT, has been applied in characterizing, for example, multi-phase flows or distribution of constituents within two component systems.

2.2 Hardware Design

For this study, an 8-electrode ECT sensor was designed to determine the MC of loblolly pine pulpwood chips.

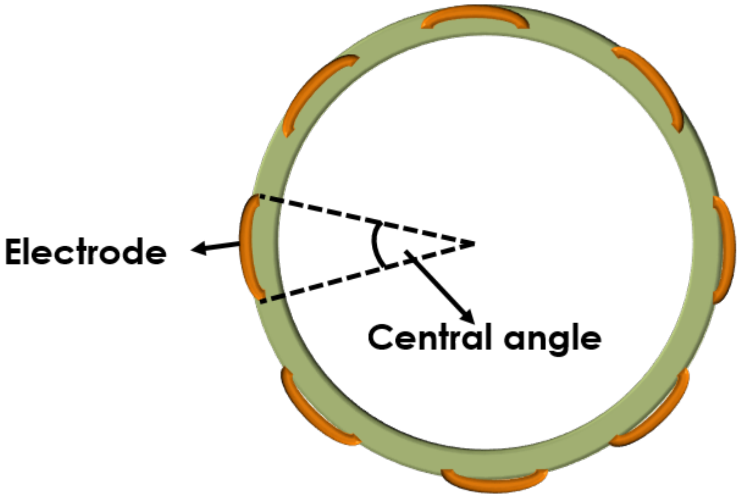

Figure 2.2: An illustration of the basic geometry of the design parameter referred in the text as 'central angle'.

2.2.1 Basic Design

A PVC pipe was selected as the measuring vessel. Electrodes were formed from copper plates adhered at uniform intervals around the external perimeter of the pipe. Details are shown in Table 2.1. The plates were used in pairs to generate an electric field within the pipe, the strength of which was related to the permittivity of the material between the electrodes. The pairs of electrodes could be viewed as a single capacitive element in a circuit generating an electric field. The capacitance of the electrode pairs would also be related to the permittivity of the material filling the void between them. Application of the ECT sensor therefore involved the sequential measurement of capacitance between each unique pair of electrodes.

2.2.2 Capacitance-to-Voltage Circuit

As noted in section 1.2, the capacitance to voltage transducer is a key element in the performance of an ECT system. The specifics of the sensing circuit used in this study to measure capacitance were adapted from Yang and York (1999), as in Figure 2.3. For this circuit and an input voltage V_s a sine wave, assuming an ideal op-amp ($i_- = 0$):

Table 2.1: Materials used and their parameters for the designed ECT sensor.

Components of capacitance sensors		**Parameters**
Electrode	Material	Copper
	Number	8
	Width	2.5 cm
	Length	10.0 cm
	Central Angle*	17.63°
Vessel	Material	PVC
	Outside Diameter	16.5 cm
	Inside Diameter	15.2 cm

* The ‘central angle’ of an electrode was the angle subtended by the two lines drawn from the center of the enclosure to either edge of a single electrode, as Figure 2.2. The width of each electrode is 2.54 cm, the total length of 8 is 20.32 cm. The outside perimeter of PVC pipe is 51.87 cm, therefore electrodes covered 39.18% of the perimeter of the pipe. The central angle of each electrode was calculated as: 360° × 39.18% / 8=17.63°.

$$\frac{V_s - V_A}{\frac{1}{j\omega C_x}} = \frac{V_A - V_o}{\frac{1}{j\omega C_f + \frac{1}{R_f}}} \tag{2.1}$$

$$V_o = -\frac{j\omega C_x R_f}{j\omega C_f R_f + 1} V_s \quad . \tag{2.2}$$

Given an appropriate feedback capacitance C_f and resistor R_f, when$|j\omega C_f R_f| \gg 1$ the output voltage V_o is proportional to the ratio of the known capacitance, C_f, to an unknown, C_x (equation 2.3). The unknown, in this case, would be the capacitance resulting from the material within the sample enclosure between any pair of copper plate electrodes.

$$V_o \approx -\frac{C_x}{C_f} V_s \tag{2.3}$$

Construction details of the capacitance-to-voltage transducer built for this project were shown in Table 2.2.

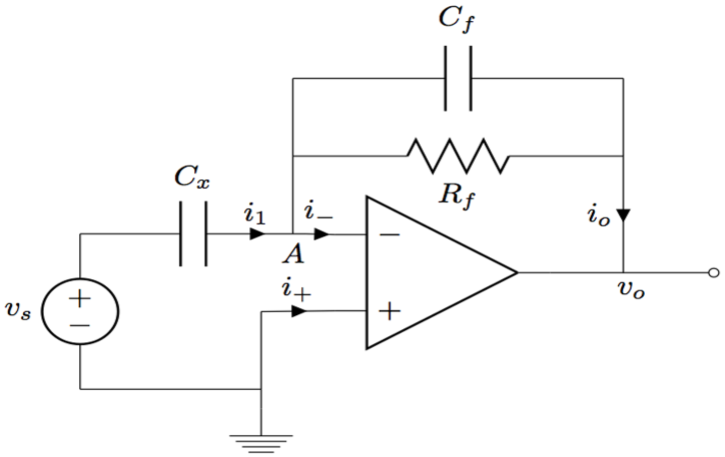

Figure 2.3: Capacitance-to-voltage conversion circuit

Table 2.2: Capacitance to voltage transducer circuit detail.

Element	Parameters	Feature
Op-Amp	AD 844	Wide bandwidth, low offset voltage, low quiescent current
Feedback Capacitors C_f	10 pf	$\lvert j\omega C_f R_f \rvert = 34.2$ for 800 kHz source signal
Feedback Resistor R_f	680 kΩ	

The measured capacitance C_x is very small, on the order of 0.01 pf to 1 pf, the change of capacitance from variation in MC is even smaller (Yang and York 1999). The feedback capacitance is necessarily small, according to equation 2.3, to sufficiently amplify the output signal, V_o. Thus to make $|j\omega C_f R_f|$ significantly larger than 1, the feedback resistor should be selected as large as possible. The choice of R_f can be several hundred kilo to several mega ohms. Selecting a large value for R_f ensures V_o is closer to $-\frac{C_x}{C_f}V_s$. However, the capacitance to voltage circuit is also a low pass filter, the cut-off frequency of which is $\frac{1}{2\pi C_f R_f}$. If $|j\omega C_f R_f| \gg 1$, the cut-off frequency is given by

$$\frac{1}{2\pi C_f R_f} \ll f_c \quad , \tag{2.4}$$

where f_c is the input frequency of the source signal, *rads*.

The frequency of the output signal V_o will be the same as V_s which, for this research, was an 800 kHz 10 V amplitude sine wave. If applying a very large feedback resistance (mega Ωs), R_f, to maximize gain, the cut-off frequency will be on the order of several thousand hertz, or much lower than the input sine wave. This could dramatically increase the signal to noise ratio (SNR) of the output signal. Taking both $|j\omega C_f R_f|$ and cut-off frequency into consideration, the feedback resistor was chosen for this study as 680 kΩ.

A capacitance to voltage circuit validation test was applied to 10 known capacitors (from 10 pf to 110 pf). The input sine wave was 800 kHz frequency and 2V amplitude. Circuit output voltage was measured using an oscilloscope. From equation 2.3, the measured capacitance was directly correlated with the amplitude of the output signal, V_o. For an input amplitude of 2V, $C_f = 10$ pf, the amplitude of the output signal would be $C_x = 0.2A_o$ (amplitude of V_o). Results were plotted in Figure 2.4. A highly correlated regression model suggested that the capacitance measuring circuit was reliable.

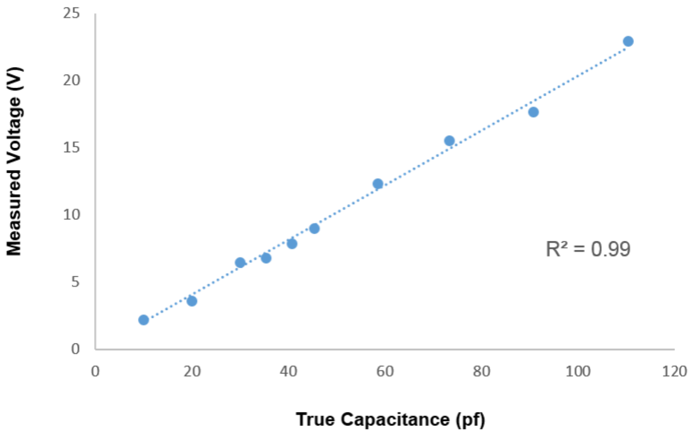

Figure 2.4: Test results for the capacitance-to-voltage conversion circuit. The data illustrate average sensor output amplitude, expressed in volts, as a function of an unknown input resistance, C_x in Figure 2.3.

2.2.3 Switching Network

To obtain 28 ($\binom{8}{2}$) different capacitances from 8 electrodes, any electrode should be able to connect either to the source signal or to the capacitance-to-voltage transducer to form a measurement pair. This function was achieved using a switching network. For each electrode connected to an independent capacitance-to-voltage transducer, the switching network itself became part of the capacitance to voltage circuit, and could, potentially, alter the measurements. The basic switching function could be achieved using a basic circuit as shown in Figure 2.5. When S1 is on and S2 off, the electrode was used as source. When the two switches were in the opposite states, that electrode was used as detector.

Theoretically, one double-pole switch could achieve this pattern of connection. However, the off state of any practical switch is not completely isolated. Part of the high frequency input signal could (and usually will) transmit across the air gap between switch contacts and be coupled into the detection circuit. For almost all real switches, this stray capacitance was much stronger than the capacitance between the electrodes themselves (very small gap compared to the separation of two electrodes, even though the leakage current was small). The basic switch system, as in Figure 2.5, was identified as a low SNR arrangement that

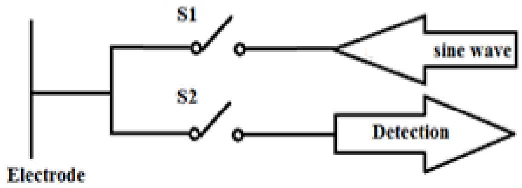

Figure 2.5: Basic switch arrangement. This implementation resulted in excessive stray capacitance.

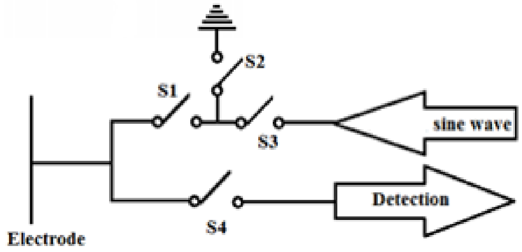

Figure 2.6: The switch arrangement developed to isolate the measurement circuits from switch-induced stray capacitance.

lost the sensitivity achievable without the switches in place (Yang and York 1999). An extra switch was therefore necessary to isolate the signal from the capacitance to voltage transducer when not in use. The advanced switching arrangement used in this project is shown in Figure 2.6. When the electrode was being used as detector, the switch S2 was grounded and undesirable signals would be led to ground. When the electrode was acting as source, nothing was measured from its detector circuit so no grounding switch was necessary in that case to block the stray capacitance.

A single three-state switch could perform this function, but, unfortunately, none were identified that did not introduce significant stray capacitance. We therefore chose to apply three Analog Devices ADG419 single-throw, double-pole switch devices for each electrode, one each to connect it to either the source (Figure 2.7 a) or filter circuits (Figure 2.7 b), plus another to shunt the electrode to ground when it was not actively involved in the

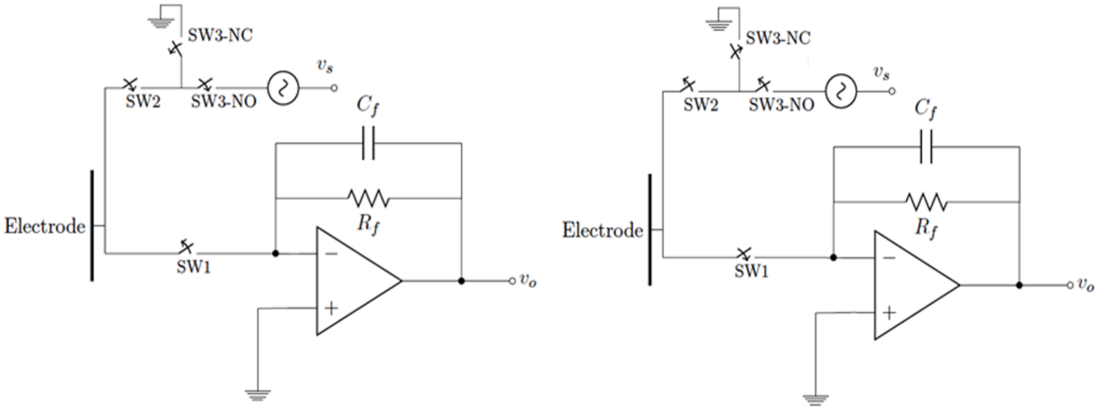

(a) (b)

Figure 2.7: Example showing the 2 states in which electrodes were operated and the switch configurations used to implement them. Electrode connected (a) to the source signal, or (b) to the output circuit.

measurements. The ADG419 devices were chosen because of their very low off-state leakage currents. Switch leakage currents effectively introduced a parallel capacitance to ground that, given the current was large enough, would overwhelm capacitance due to the dielectric material in the sensor.

Since no repeat measurement was taken, e.g. if using electrode 1 as source and measuring from electrode 2, then no measurement was acquired from electrode 1 when electrode 2 was excited, electrode 1 (the first electrode in the measuring sequence) would only need to take two states: source electrode and wait (no connection), and electrode 8 (the last electrode in the measuring sequence) was at either detecting or wait (no connection) status. The other 6 electrodes were working at either of two active states (source or detector) or a single inactive state, wait. The circuit requirements of the 8 electrodes were different, but considering the cost, all switching networks to voltage circuits were built using the same structure.

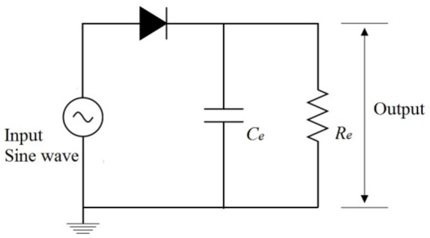

Figure 2.8: A half-wave envelope detector circuit.

2.2.4 Amplitude Extraction Circuit

The capacitance to be measured, C_x, was amplitude modulated in the output of the capacitance-to-voltage circuit. To extract the capacitance information, therefore, an amplitude-measuring method was necessary for ECT application. Hardware and software could both achieve the function. This section introduces hardware methods only.

Envelope Detector An envelope detector is a circuit whose output is proportional to the amplitude of a high frequency signal. A simple envelope detector is constructed using a diode, capacitor and resistor, which act as half-wave and full-wave rectifiers . Since an input sine is symmetric, both functions would have the same result in our application. A half-wave envelope detector was built and tested, a schematic of the circuit was shown in Figure 2.8. The principle of this circuit was to block negative signals and charge the capacitor when the voltage of the input signal its current charge. The design requirements for the envelope detector were shown in equation 2.5:

$$\frac{1}{f_c} \ll R_e C_e \ll \frac{1}{W} \quad , \tag{2.5}$$

where f_c is the signal frequency (Hz), R_e and C_e are resistor (Ω) and capacitor (f) of the envelope detector, and W is the bandwidth of the message (Hz).

When the period of the source signal is much smaller than the time constant of the envelope detector, the capacitor C_e has enough time to charge and maintain the output

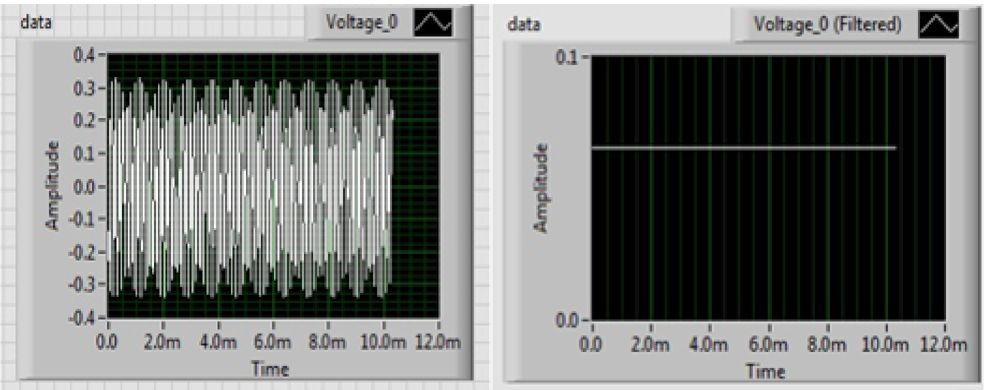

Figure 2.9: Original signal and envelope detector output.

voltage until arrival of the next peak of the input. Thus the output voltage can approximate the peak level of the input signal as seen in Figure 2.9. After applying a low-pass filter, the original AC signal is converted to a sTable and clean DC signal. A significant advantage of the envelope detector is to reduce the sampling rate of data acquisition circuit greatly. If sampling directly for a high frequency AC signal, e.g. 800 kHz sine wave in the experiment, at least 1.6 MHz sampling rate is the minimum (Nyquist) sampling frequency to approximate the original signal and calculate the amplitude. Direct sampling from a sine wave will increase the system cost and reduce the measuring efficiency. However, sampling from a sTable DC signal require a very low sample number, the average of which could represent the amplitude of the output sine signal from the capacitance to voltage circuit.

A test was carried out to verify the feasibility of using envelope detectors in the designed ECT system. Based on the rule for designing an envelope detector (equation 2.5), R_e and C_e were set to 480 kΩ and 2.0 nf, respectively, the R_eC_e of which was well located in the appropriate range $2 \times 10^{-6} \ll 9.6 \times 10^{-4} \ll 10^{-2}$. The modified circuit was shown in Figure 2.10.

Sensor response was measured for a variable amount of water placed inside the sensor in a plastic cup. The measurement circuit included the envelope detector and its performance was tested in two steps.

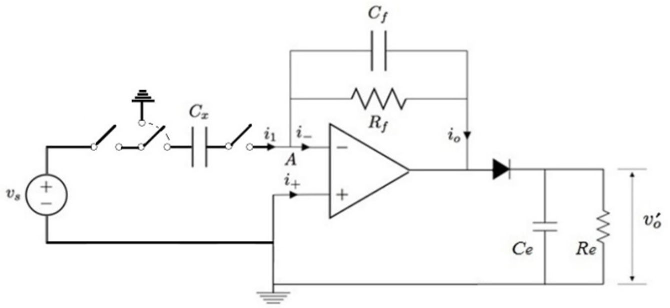

Figure 2.10: The sensor output circuit modified to include the envelope detector.

(1) Test in single pair of sensor electrodes. Two opposite electrodes were used to measure water volume between them. No switching action was included. The output of envelope detector V_o' was acquired directly using a device *NI 6361* (NI, Corp.). A digital low-pass filter was designed using LABVIEW 12.0 software (NI, Corp.) with a cut-off frequency of 100Hz. The signal was sampled at 10 kHz. 100 voltage measurements were averaged and saved to correlate with the volume of water, which was added into the plastic cup gradually from 0ml to 500ml. Result were listed in Figure 2.11 (blue). A good linear relationship was observed, suggesting that the envelope detector could extract the amplitude information accurately.

(2) Test in ECT. All electrodes and switches were used with the envelope detector. All 28 capacitances were saved and summed as the sensor output value. Other procedures and devices were the same as step 1. Results were as in Figure 2.11 (orange).

The envelope detector worked well for non-switching system. However, outliers were observed frequently for ECT (fully switched) mode, the cause of which were suspected to be the switching system itself. For example, when electrode 1 was used as source, electrode 8 was at high(er) potential. The capacitance of the envelope detector connected to electrode 8 was also charged, over some (relatively short) time, to a higher voltage. During the next measuring sequence, the source electrode was switched to 2, and one would expect the potential at electrode 8 to decrease (the distance between electrode 2 and 8 being greater

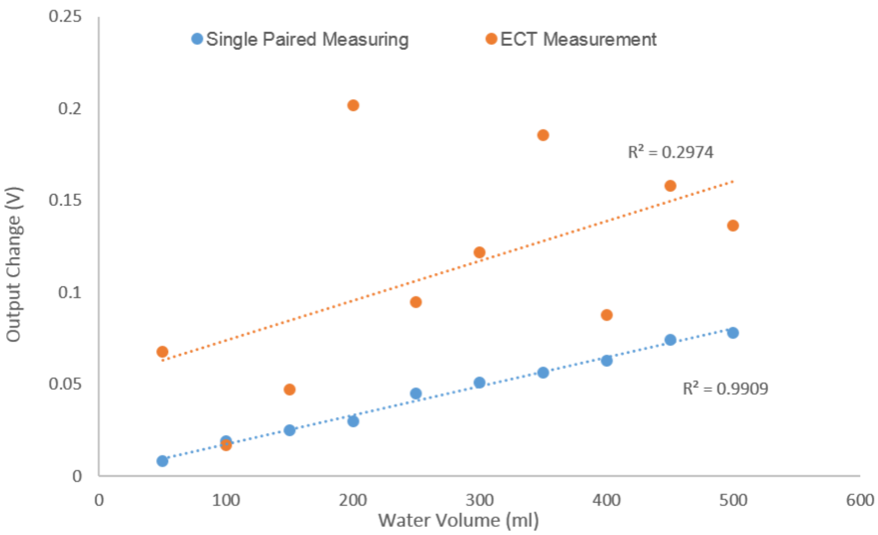

Figure 2.11: Output sensor voltages measured for the circuit configured as in Figure 2.7b and as in Figure 2.10. The results indicated the envelope detection hardware caused significant reduction in SNR.

than 1 and 8). However, the excess charge held on electrode 8 and its measurement circuit was still present and, because the electrode was now at lower potential, was discharged and tended to bias the new capacitance measurements, causing outliers. For this reason, this simple envelope detector circuit was not employed in the ECT system, although some extra design work might have been able to solve the problem.

AC/DC transducer Yang and York (1999) provided an AC to DC converting method to measure output signal amplitude. The system consisted of three parts: phase measuring and shifting device, signal multiplier, and low pass filter.

The method focused on the multiplier part. Suppose the input sine wave $V_s = A\sin(\omega t+\alpha)$ and output signal $V_o = AB\sin(\omega t+\beta)$, the multiplier is to correlate the output signal with input signal to create a new output:

$$V_o' = AB\sin(\omega t+\beta)\times A\sin(\omega t+\alpha) = \frac{A^2B}{2}\left(\cos(\beta-\alpha)-\cos(2\omega t+\alpha+\beta)\right) \quad , \qquad (2.6)$$

where A is the amplitude of exciting signal, B is the amplitude gain from the converting circuit as $-\frac{C_x}{C_f}$ in equation 2.5, α, β are the phase of input and converted signal. When the phase of the output signal is adjusted to match the source signal ($\alpha = \beta$), the equation 2.6 would become:

$$V_o' = \frac{A^2 B}{2} \left(1 - \cos\left(2\left(\omega t + \alpha\right)\right)\right) \quad . \tag{2.7}$$

The new output signal has two parts: DC, and high frequency AC. Applying a low-pass filter, the high frequency part was removed (e.g. if the input frequency was 800 kHz, the multiplied output frequency would be 1.6 MHz). The output signal would become a DC signal ($V = \frac{A^2 B}{2}$) only, which would be proportional to the capacitance being measured.

2.2.5 Power and Stabilization

The capacitance-to-voltage signal processing circuit contained two kinds of chips: AD844 Op-Amp and ADG419 switch, the working power of which were 15 V and 5 V respectively. A 5V regulator was used to convert the input 15 V to 5 V that supported ADG419.

To avoid any instability arising from very quick changes in power levels in the circuit (due to the switching network), multiple capacitors were installed into the ECT data acquisition circuits to act as charge pumps. When the power supply for the circuits pulsed, these capacitors could provide, or absorb, current to eliminate that specific source of measuring error. A large capacitor (47 μF) was installed near the power supply side, and a smaller capacitor (0.1 μF) was put as close as possible to the functional chips (Figure 2.12).

2.2.6 Grounded Shield

With all electrodes exposed directly to the air, a potential problem would be caused by outside signals or material. Although a strong external noise signal was not observed frequently, any nearby materials could alter the electric field inside the ECT enclosure and affect the capacitance measurements. A simple test was conducted to compare sensor responses

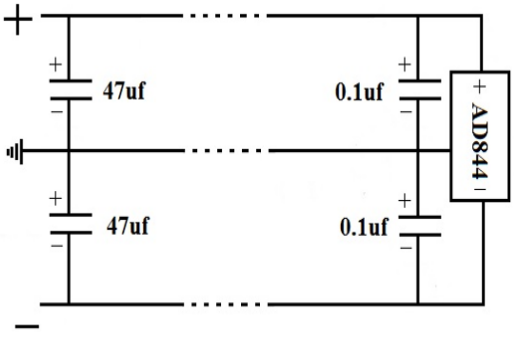

Figure 2.12: Power stabilization setup

with and without external influences. The introduced disturbance for the test was to use a grounded copper sheet, which was about one inch distance away from an electrode (electrode 1 was chosen in this test). Results of using electrode 1 as source and in combination with the shield were shown in Figure 2.13.

Without the shield, the measured capacitances (seen as voltages) were greatly decreased when a grounded material was placed close to any electrode as the object diverted some of the input energy to ground. The amplitude of this decrease was significant compared to permittivity changes inside the measuring enclosure and their presence in an online sensor would render it useless.

Wires or PCB boards nearby might create noise also. Since all PCBs were connected with the 800 kHz sine wave, though switches were designed to separate the strong input signal and detecting circuit completely in the circuit board, the penetrability of the high frequency signal would create noise from wires that might directly arrive at the data acquisition system. To avoid this potential problem, as well as nearby grounded materials, an earthed shield was applied to block external signals and the grounding effect of outside bodies. A copper sheet was chosen as the appropriate material to build the shield. The copper sheet was fixed surrounding the electrodes area, material between electrodes and shield was air (permittivity=1). Parameters were listed in Figure 2.14.

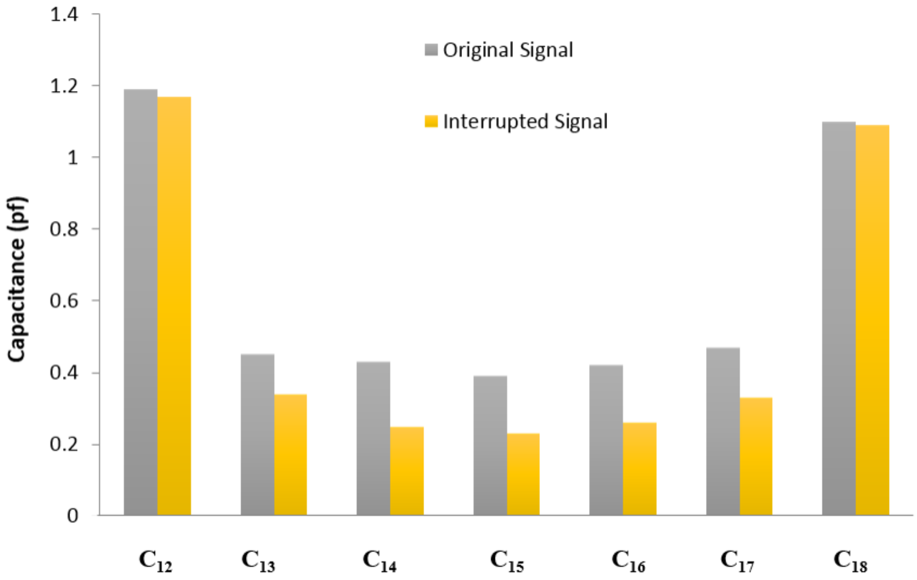

Figure 2.13: Capacitances with and without ground interruption. Ground interruption refers to the placement of a grounded object near the sensor electrode under test.

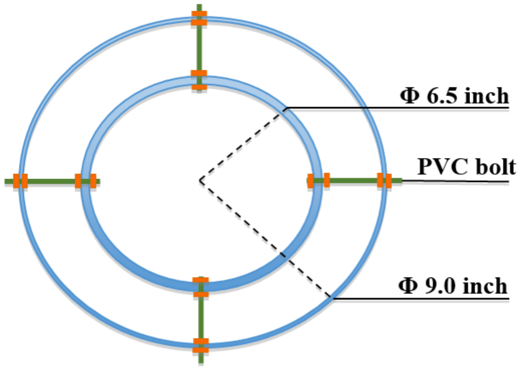

Figure 2.14: Dimensional parameters of the grounded shield.

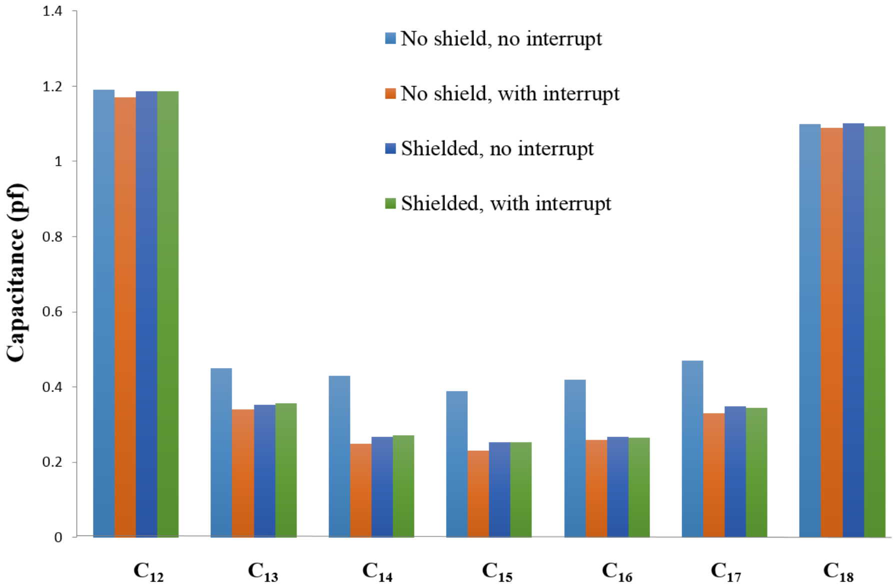

Figure 2.15: Example of the benefits of including the grounded shield (plus isolation ground switch) in the sensor output circuit.

With the protection of the copper shield, another experiment was done to verify its beneficial effect. Data were compared with and without the shield in place, as in Figure 2.15. The response indicated the grounded shield successfully protected the circuit signal from outside disturbances, which increased the sensor robustness. However, the responses of all electrode combinations were decreased significantly. This could be explained in the same way as any other grounding material being placed near an electrode. Though the shield was effectively another grounded sink for input charge, the advantage was, however, the fixed distance between shield and measuring electrodes. Thus the effect of the shield charge diversion was constant within the enclosure. This effect would, reduce the sensitivity of the measurements, but not increase the measuring error. In addition, all wires for signals were shielded to eliminate any stray capacitance between adjacent conductors. The ECT sensor, as it appeared with all modifications in place, was shown in Figure 2.16.

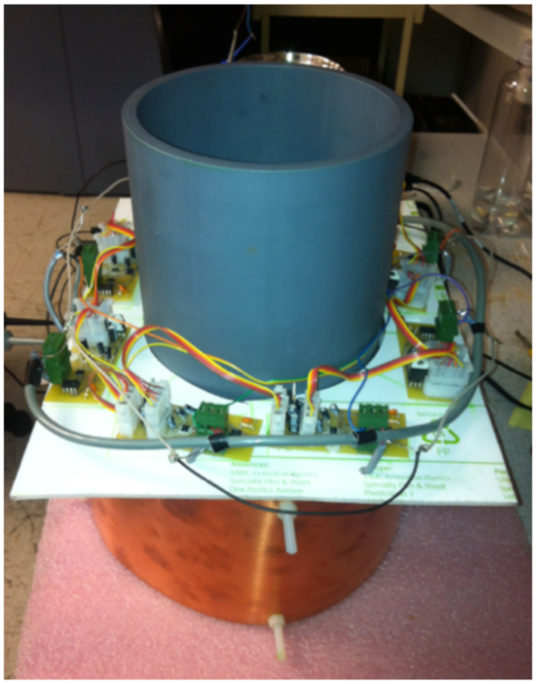

Figure 2.16: Prototype ECT sensor.

2.3 Software Design

The software of an ECT sensor may include data acquisition, switch control, and image reconstruction. Though the switching network could be easily controlled by a pulse signal that might not rely on software, this project used software to control it. The reason was: (1) Easy to modify for different switch combination tests, and (2) simple to make data acquisition match with switch actions. However, including the switch control function in data acquisition program would reduce the sampling frequency eventually.

2.3.1 Data Acquisition Program

Since the previous test in 2.2.4 was not encouraging for the inclusion of the envelope detector in the ECT system for AC to DC conversion, the original high frequency sine wave was directly collected using *NI 6361*. The device allowed sampling ECT outputs at 2 MHz. LABVIEW 12.0 software was chosen for implementing the data collection system. The software provided functions to read data from the USB port, display signals in plot or data

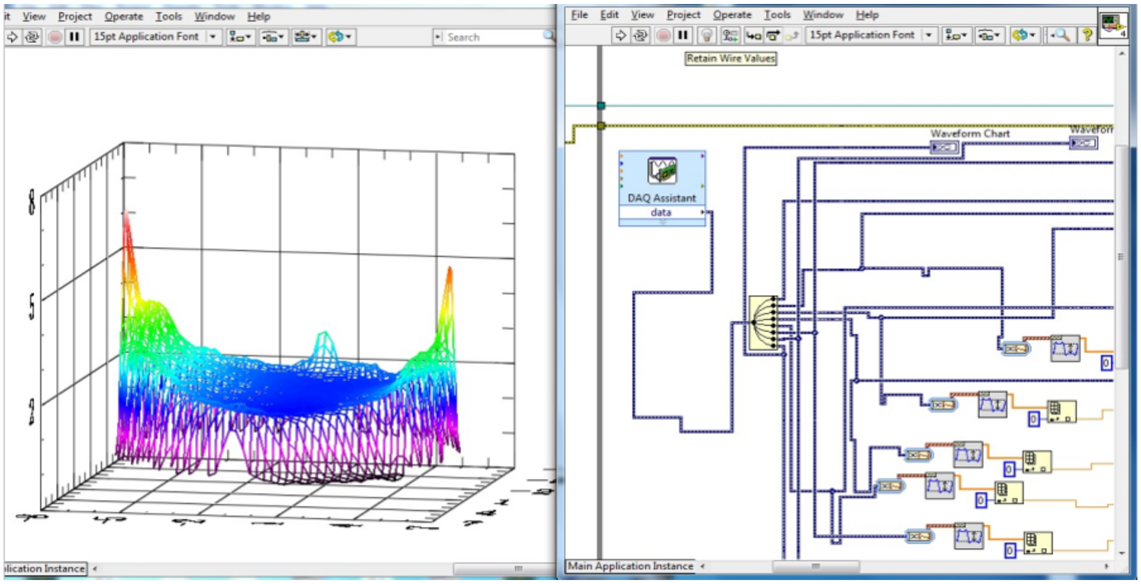

Figure 2.17: A screen capture of the LABVIEW block diagram and UI developed for the ECT system.

sequence, process data, and save it in a user-defined form. It is also possible to compile MATLAB® (The MathWork, Inc.) codes and reconstruct images in both 2D and 3D within LABVIEW. The user interface developed for the project was as Figure 2.17.

The data processing for this ECT system was to extract amplitude precisely from a high frequency AC signal. Multiple methods were embedded in LABVIEW to measure the amplitude of a signal, including time domain and frequency domain method.

Time domain amplitude measurement In time domain, the amplitude can be computed by either direct calculation from the signal or correlation of two signals.

Direct calculating methods in LABVIEW are peak-to-peak measuring, standard deviation (std) measuring, and root mean square (rms) computing. If a dataset is collected from a signal as: $X_1,\ X_2,\ \cdots,\ X_{N-1},\ X_N$, the peak-to-peak method was simply calculate the amplitude by subtracting the minimum value from the maximum of a signal with certain length, as the equation 2.8.

$$\text{Amplitude} = \max\left[X_1,\ X_2,\ \cdots,\ X_{N-1},\ X_N\right] - \min\left[X_1,\ X_2,\ \cdots,\ X_{N-1},\ X_N\right]\ . \quad (2.8)$$

The mean of the data sequence was: $\mu = \frac{X_1 +\ X_2 +\ \cdots +\ X_{N-1} +\ X_N}{N}$, and the standard deviation is calculated as $\sigma = \sqrt{\frac{1}{N}\sum_{i=1}^{N}\left(X_i - \mu\right)^2}$. Since the relationships between amplitude and std are fixed, the amplitude could be calculated by equations 2.9.

$$\text{Amplitude} = \begin{cases} 2\sigma & \text{Square wave} \\ 2\sqrt{2}\sigma & \text{Sine(Cosine) wave} \\ \sqrt{12}\sigma & \text{Triangular wave} \\ 6-8\ \sigma & \text{Random noise} \end{cases} \quad (2.9)$$

The rms of the signal, which is computed as: $X_{\text{rms}} = \sqrt{\frac{1}{N}\sum_{i=1}^{N} {X_i}^2}$, has the relationship with amplitude as below.

$$\text{Amplitude} = \begin{cases} 2X_{\text{rms}} & \text{Square wave} \\ \sqrt{2}X_{\text{rms}} & \text{Sine(Cosine) wave} \\ 2X_{\text{rms}}/\sqrt{3} & \text{Triangular wave} \\ 2X_{\text{rms}}/\sqrt{3} & \text{Sawtooth wave} \end{cases} \quad (2.10)$$

Both methods could be also done using an electrical circuit, such as AD 636 (True rms-to-DC converter).

Correlation is a common method to detect a known signal from a noisy measurement. It could also be applied to measure amplitude of an AC signal. The principle of this method is signal multiplication, as AC to DC transducer by (Yang and York 1999) stated before. LABVIEW could also be used to simulate the correlation process. Another approach could be to use auto-correlation. Multiplication of the two signals in that case becomes:

$$y_2^2 = B\sin(\omega t + \varphi_2) \cdot B\sin(\omega t + \varphi_2) = \frac{1}{2}B^2\left(1 - \cos\left(2\left(\omega t + \varphi_2\right)\right)\right) \quad . \tag{2.11}$$

y is the output of the capacitance to voltage transducer, B is the amplitude of y (in V), ω and φ_2 are the frequency and phase of y, respectively.

The advantage of the method was no phase detecting and adjusting processes were required, however, B was usually smaller than 1 and the squared signal would have much smaller amplitude (e.g. if B was 0.5 V, then the new amplitude would be 0.125 V).

Frequency domain method Fourier transform is a mathematical approach to convert a time domain signal to its frequency domain representation. According to the theory of Fourier transform, any continuously acquired signal could be represented as infinite superposition of sine wave at different frequencies (Bochner and Chandrasekharan 1949). A signal is usually considered to consist of useful information plus additive noise. The noise is usually thought to be present with some known frequency distribution. The amplitude of signal could be measured in the frequency domain if the frequency of source signal was known. As in this measurement, if using 800 kHz sine wave as input, the output frequency was an 800 kHz signal plus something that might be considered white noise. In time domain, signal and noise were compounded that might be difficult to measure the actual amplitude. But in frequency domain, the amplitude at 800 kHz was close to the real amplitude.

To find an appropriate method to acquire the amplitude of ECT outputs, four methods, including peak-to-peak amplitude (Amplitude and Level Measurements Express.VI), standard deviation, Fast Fourier transform (FFT.VI) and auto-correlation, were used to take measurements at same sample. Different amounts of water (from 10 – 50ml) were measured in a plastic cup. Since results from different methods were distinct, the measurements were converted to amplitude using the following techniques:

$$\text{Amplitude} = \begin{cases} a & \text{amp.vi} \\ 2a & \text{FFT} \\ 2\sqrt{2}a & \text{Correlation} \\ 2\sqrt{2}a & \text{Standard deviation} \end{cases} \tag{2.12}$$

Results were shown in Figure 2.18. Here the FFT and auto-correlation method showed relatively good performance in measuring permittivity change from the variation of water volumes inside the measuring enclosure. The peak-to-peak amplitude VI provided a relatively lower R^2 model compared to FFT and auto-correlation methods. However, the standard deviation method did not achieve results comparable to the other methods. The influence of noise was observed more significantly than in the other three methods. FFT and auto-correlation methods were more robust to system noise, as was expected. Considering the complexity of each method, auto-correlation was more time consuming to calculate than others. Given the goal of building an ECT system was to dynamically measure MC of biomass, it was preferable to use as high a sampling rate in acquiring data as possible. Based on the requirements of both accuracy and high sampling rate, the FFT and peak-to-peak amplitude approaches for estimating amplitude of the output signal were chosen for this work.

2.3.2 Switching Control and Related Measurements

The need for a switching network was introduced in 2.2.3. For this study, the connections between electrodes were controlled using digital outputs from the data acquisition system, *NI 6361*. The status' of electrodes (for switch arrangement to achieve these states see Figure 2.6) were controlled as in Table 2.3. Three different states of electrodes provided the capability to carry out different sampling methods, which could be summarized as:

- single source-single receiver mode,

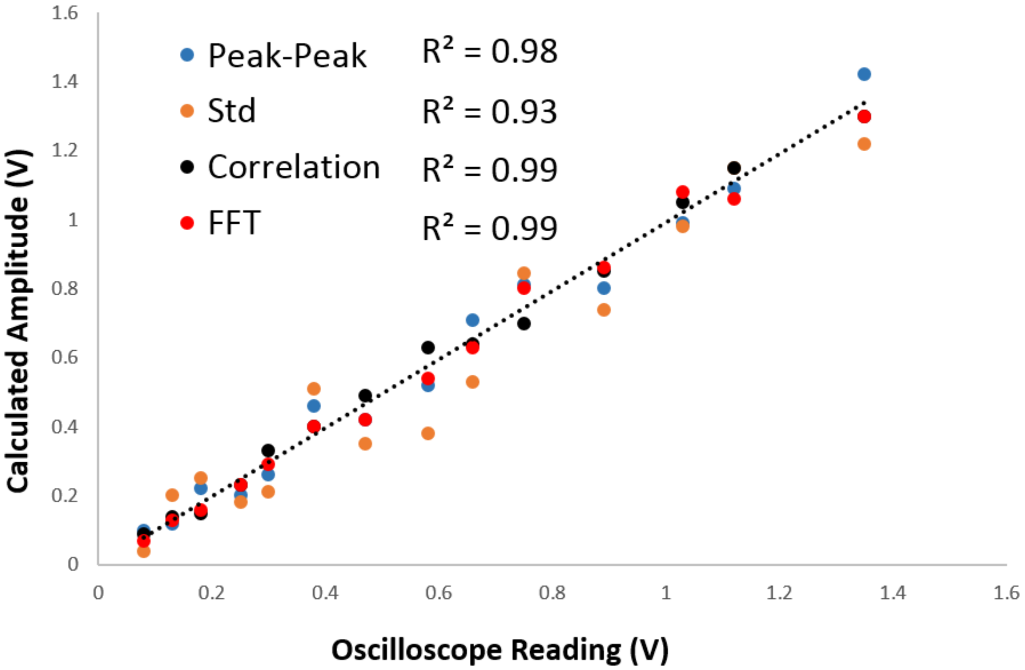

Figure 2.18: Regression results for tests comparing the different amplitude measurement techniques.

- single source-multiple receiver mode,
- multiple source-single receiver mode, and
- multiple source-multiple receiver mode.

The multiple source method was introduced in 1.2.3 and was due to Mohamad *et al.* (2011). The method required having two different frequency input signals but, due to limitations in available instrumentation, the approach could not be done for this study. This work implemented only the first two of these sampling options and therefore only they will be discussed. Single source-single receiver mode is straightforward, but single source-multiple receiver mode has some options, which are outlined below.

Table 2.3: Electrode state configurations possible with the switching network, and their relation ship to switch closures.

Switch #	**Source**		**Detection**		**Wait**	
	Logic Input	Switch Condition	Logic Input	Switch Condition	Logic Input	Switch Condition
S1	1	On	0	Off	0	Off
S1	0	Off	1	On	1	On
S1	1	On	0	Off	0	Off
S1	0	Off	1	On	0	Off

(1) Single sampling option. The method could be described as: when the source electrode was at k, take output measurements from k+1 to N simultaneously. Here k is the kth electrode excited by input signal, N is the total number of electrodes. For the designed 8 electrodes, N is equal to 8, and k counts from 1 to 7.

(2) No waiting option. The electric field between some electrode combinations was not able to cover the entire measuring area. If the residence time of an object within the sampling zone was shorter than the sampling period, then the ECT would not detect its presence. No electrode at wait status referred to the option of all electrodes having only two states: receiving or exciting. In this 8 electrode system, always 7 electrodes were taking data: when source electrode was at k, taking measurements from 1 to N except k'th electrode. The method also finished data collection in one traverse around the electrodes for each source chosen.

(3) No adjacent measurement option. Shao *et al.* (2003) found the contribution from adjacent measurements was small. For an 8-electrode ECT, the number of adjacent

measurements (side-by-side electrodes) was also 8, which exceeded one fourth of the total (28). Removing adjacent measurements would significantly improve the sampling rate. The large reading from adjacent electrodes was also reported to elicit side effects in image reconstruction. The method could be expressed as: when source electrode was at k, take measurements from k+2 to N; e.g. when the source electrode was 1, take measurements from 3 to 7 (skip electrodes 2 and 8)

All four methods were described in detail in Table 2.4. Though the no waiting method could capture all information of a fast-moving object, it required redesign of the switching network. Since the switching action was done very fast, when one electrode connected to the source signal switched to the detector state, that electrode remained briefly at high electric potential. As a result, part of that potential could be measured as sensor response, while the true reading was undetecTable. A work-around solution could be achieved by adding a ground connection during the transition between the exciting and detecting states. An extra switching action, however, would increase the measuring period.

The no adjacent option was faster than the other methods. In this research, however, it was not preferred. Because dynamic ECT measurements were greatly dependent on the precision of reconstructed images (details in Chapter 5), fewer capacitance combinations would reduce data available for reconstruction and possibly lead to poorer quality images. The remaining two methods (single source-single receiver, single source-multiple receiver) were therefore reserved for further use.

2.3.3 Image Reconstruction Program

The main advantage of the ECT system was its ability to create a 2-D image representation of a field variable from a finite number of 1-D measurements. The fundamentals of image reconstruction process are the result of a mathematic transformation named the Radon and inverse Radon transforms, after Johann Radon (Deans 1983). It was proposed in 1917 that any N-dimension object could be reconstructed by an infinite number of $N-1$

Table 2.4: Sampling methods summary.

Methods	**Source**	**Detection**	**Wait**	**Measurements**
One source, one receiver (28 actions[*])	1	(2) (3) (4) (5) (6) (7) (8)	Remaining 6 electrodes	1 1 1 1 1 1 1
	2	(3) (4) (5) (6) (7) (8)		1 1 1 1 1 1
	3	(4) (5) (6) (7) (8)		1 1 1 1 1
	4	(5) (6) (7) (8)		1 1 1 1
	5	(6) (7) (8)		1 1 1
	6	(7) (8)		1 1
	7	(8)		1
One source, multiple receivers (7 actions)	1	(2) (3) (4) (5) (6) (7) (8)	N/A	7
	2	(3) (4) (5) (6) (7) (8)	(1)	6
	3	(4) (5) (6) (7) (8)	(1,2)	5
	4	(5) (6) (7) (8)	(1,2,3)	4
	5	(6) (7) (8)	(1,2,3,4)	3
	6	(7) (8)	(1,2,3,4,5)	2
	7	(8)	(1,2,3,4,5,6)	1
One source, seven receivers (7 actions)	1	(2,3,4,5,6,7,8)	N/A	7
	2	(1,3,4,5,6,7,8)		7
	3	(1,2,4,5,6,7,8)		7
	4	(1,2,3,5,6,7,8)		7
	5	(1,2,3,4,6,7,8)		7
	6	(1,2,3,4,5,7,8)		7
	7	(1,2,3,4,5,6,7)		7
No adjacent measurement actions (6 actions)	1	(3,4,5,6,7,8)	(2,8)	5
	2	(4,5,6,7)	(1,3)	5
	3	(5,6,7,8)	(1,2,4)	4
	4	(6,7,8)	(1,2,3,5)	3
	5	(7,8)	(1,2,3,4,6)	2
	6	(8)	(1,2,3,4,5,7)	1

[*] Electrode(s) in the same bracket means they are read at the same time for the given arrangement. One ‘action’ means changing the status of switches once.

dimensional projections. For the two-dimensional situation, if $f(x, y)$ is a continuous and convergent function in plane Z, and there exists a line $p = x\cos\theta + y\sin\theta$, then the integral of $f(x, y)$ along line p is defined as the Radon transform. It can be expressed as:

$$R_f\left(p, \theta\right) = \int_{-\infty}^{+\infty} \int_{-\infty}^{+\infty} f\left(x, y\right) \delta\left(p - x\cos\theta - y\sin\theta\right) dx\, dy \tag{2.13}$$

where $\delta()$ is the Dirac delta function. Since the function of the line p is known, the Radon transform could be calculated from equation 2.13. The inverse Radon transform is used to calculate $f(x, y)$ with a known $R_f\left(p, \theta\right)$. The inverse formula can be written as:

$$f\left(r, \varphi\right) = -\frac{1}{4\pi^2} \int_{0}^{2\pi} \int_{-\infty}^{+\infty} \frac{\partial R_f(p, \varphi)}{\partial p} \cdot \frac{1}{p - r\cos(\varphi - \theta)} dp\, d\theta \tag{2.14}$$

where $r = \sqrt{x^2 + y^2}$, $\varphi = \tan^{-1}\frac{x}{y}$.

For an ECT system, the capacitance measurements were treated as known $R_f\left(p, \theta\right)$ and available to calculate the two-dimensional image $f(x, y)$. As Radon's theory described, infinite capacitance data were required to perfectly reconstruct the original image. However, the capacitance combinations were much fewer in number, 28 for the 8-electrode sensor. Though insufficient information would cause imprecision in the reconstructed image, the result, which could satisfy this study's requirement, has been widely used in ECT applications.

Mathematical Model for ECT system To solve the partial differential equation of the inverse Radon transform, knowledge of boundary conditions was crucial. There are three different normal boundary conditions applied, including Dirichlet boundary conditions, Neumann boundary conditions, and Robin boundary conditions. For an ECT system, the boundary condition is derived from excitation with a constant voltage signal, which is equivalent to Dirichlet boundary conditions. If no signal were applied to any electrode, the electric potential gradient could be described using the Poisson equation (Yang and Huang 2007):

$$\nabla\left[\varepsilon\left(x,y\right)\nabla\phi\left(x,y\right)\right]=0 \tag{2.15}$$

where $\varepsilon\left(x,y\right)$ and $\phi\left(x,y\right)$ were the permittivity and the electric potential at point (x,y), respectively. When an electrode, e.g. electrode i, was excited by a voltage signal V, the boundary conditions for an N-electrode ECT sensor were changed:

$$V=\begin{cases} V(x,y)\in s_i & i=1,2,\cdots,N \\ 0(x,y)\in s_j & j=1,2,\cdots,N\ j\neq i \end{cases} \tag{2.16}$$

where s_i is the surface of electrode i. The electric potential distribution $\phi\left(x,y\right)$ could be calculated from equations 2.15 and 2.16. The capacitance between electrodes i and j was computed as:

$$C_{i,j}=-\frac{1}{V}\oint\varepsilon\left(x,y\right)\nabla\left(x,y\right)\mathrm{ds} \tag{2.17}$$

Image reconstruction process An ECT system is used to describe the permittivity distribution at discrete points inside a measuring enclosure, which can be thought of as a vector each element of which is associated with some fixed location. The resulting permittivity distribution vector elements are used as the gray scale values for the reconstructed image (G). The integral relationship of equation 2.17 is usually simplified to a sum operation over $\binom{N}{2}$ electrodes, which corresponds to the matrix formulation:

$$C=SG \tag{2.18}$$

where C is the $N\times1$ capacitance matrix, G is the $M\times1$ gray level distribution image and S is a new concept called a sensitivity matrix $(N\times M)$. For any pixel k, its sensitivity corresponding to electrode i and j is defined as:

$$S_{i,j}\left(k\right)=\frac{\lambda_{i,j}\left(k\right)C_{i,j}\left(k\right)}{\varepsilon_{\text{high}}-\varepsilon_{\text{low}}} \tag{2.19}$$

where $\lambda_{i,j}(k)$ is the area factor of pixel k, $C_{i,j}(k)$ is the normalized capacitance between electrode i and j, $\varepsilon_{\text{high}}$ and ε_{low} are the permittivity of high and low dielectric materials, respectively (Pan and Wang 2004).

To obtain the gray scale image G, it is calculated by rearranging equation 2.18:

$$G=S^{-1}C \tag{2.20}$$

However, the dimension of the sensitivity matrix S is $N \times M$, which does not have a normal inverse unless $M=N$. Though there can exist a pseudo-inverse of S, for ECT applications the inverse is usually approximated as S^{T} to solve the ill-posed problem. The approach is known as the *Linear Back Projection* (LBP) method (Xie *et al.* 1992).

$$G=S^{\mathsf{T}}C \tag{2.21}$$

The key in computing the ECT image G is to obtain the sensitivity matrix S. Two ways could be applied to obtain S: experimentally, and software simulation (Guo *et al.* 2009). The experimental measurement approach has large calculating requirements and is usually not adopted. In this dissertation, ANSYS 13.0 (SAS IP, Inc.) was used to simulate the sensitivity matrix S. The main steps can be stated as follows:

(1) Select element (material) type, set appropriate permittivity,

(2) Draw the sensor with true dimensions,

(3) Mesh the sensing area into 225 nodes, using a triangle mesh element shape,

(4) Set the boundary conditions (apply voltage to electrodes),

(5) Compute the electric field distribution.

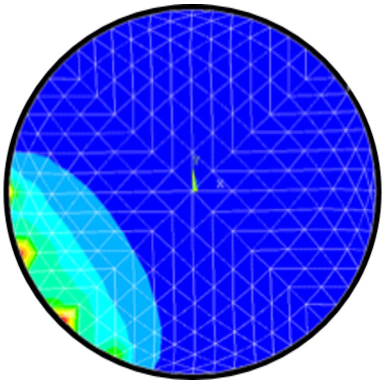

Figure 2.19: An example electric field distribution calculated using the ANSYS model. The example shows the field resulting from two adjacent electrodes, one providing excitation, the other as the ground (or receiver) side.

An example ANSYS output from above steps was shown in Figure 2.19. This example was built using the ECT in single source-single detector mode with two adjacent electrodes. An 8-electrode ECT sensor would require calculating 28 distinct sensitivity matrices, one for each electrode combination. An example sensitivity matrix is shown in Figure 2.19. Actually, however, it was not necessary to estimate 28 separate sensitivity matrices using ANSYS in all situations. For the single source-single detector mode, there were only four unique electric charge distributions (resulting electrode combinations 1-2, 1-3, 1-4, and 1-5, the source electrode being 1). Other combinations could be generated by rotating one of the four characteristic distributions.

As mentioned, the LBP approach using S^{T} as a substitute for S^{-1} would lead to image errors. A *Landweber* algorithm (Yang and York, 1999) was applied to improve the accuracy. The algorithm was used to iteratively improve estimates of G by minimizing the squared error term $\frac{1}{2}\left\|SG - C\right\|^2$. New estimates of G were calculated from equation 2.22.

$$G_{k+1} = G_k + \alpha S^T(C - SG_k) \tag{2.22}$$

where α is fixed and $\|\alpha S^T S_2\| < 2, k = 0, 1, 2, \cdots$. The algorithm is repeated either for a fixed number of iterations or until the difference $|C - SG_k|$ is less than a given threshold.

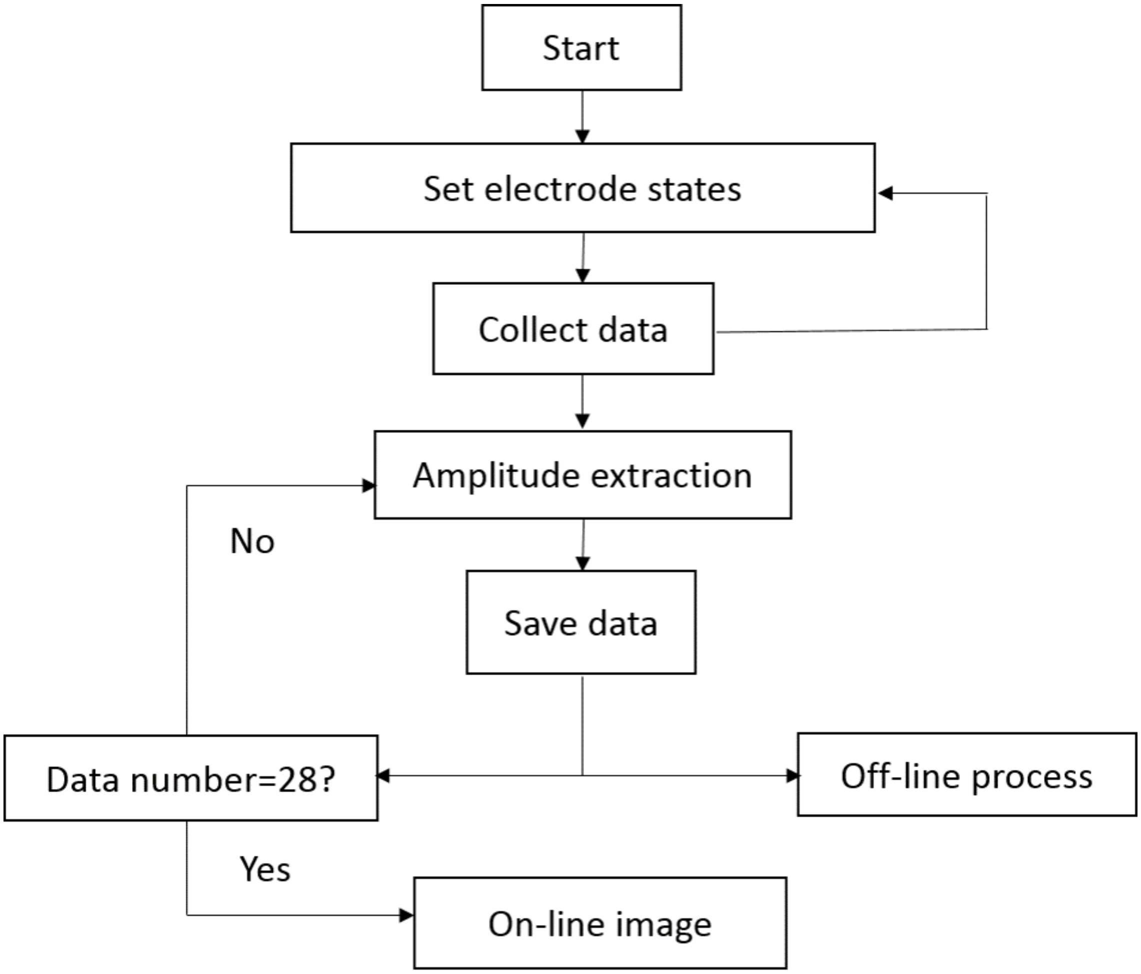

Figure 2.20: ECT flow diagram

2.4 Chapter Summary

The ECT system was designed with 8 electrodes surrounding a PVC tube, each electrode connected to a capacitance-to-voltage transducer. A switching network was embedded in all electrode circuits and used to control their state of operation. The AC output of each sensor was directly sampled using a commercial data acquisition system and the amplitude of the signal was calculated using various methods implemented in software (LABVIEW). The system had the capability to save resulting data, or reconstruct ECT images on-line. A flow diagram of the ECT system operation was shown in Figure 2.20.

Chapter 3

ECT SENSOR CHARACTERISTICS

An integrated ECT system was designed in Chapter 2. Before applying the sensor to measure MC for wood chips, its basic characteristics were tested and the results reported in this Chapter. Results were expected to provide information on the limits of performance of the sensor and be important to understand before pursuing more complicated experiments with the ECT system.

3.1 Hardware Features

To verify the design, capability, as well as limitations, of the sensor, the tests outlined in the following sections were carried out.

3.1.1 Functionality Test

Responses of the 28 different electrode combinations were collected to verify consistency in output. Since all electrodes and circuits were designed exactly the same, the single paired parallel plate capacitance measurements should provide the same result under the same conditions. Sources of variation that might have introduced errors could have been associated with size or placement differences between electrodes, or response variability between electronic components used in the sensor circuits. The following two assumptions were tested to evaluate how well the sensor approximated the ideal response.

(1) Any pair of measurements, if their detecting electrodes were separated at the same distance, e.g. C_{14} and C_{25}, should be the same theoretically.

Table 3.1: ECT readings when empty. Units of values are in pF.

Adjacent		**Separation 1**		**Separation 2**		**Separation 3**	
C_{12}	1.067	C_{13}	0.382	C_{14}	0.339	C_t15	0.311
C_{23}	0.933	C_{24}	0.384	C_{25}	0.345	C_{26}	0.325
C_{34}	0.847	C_{35}	0.380	C_{34}	0.339	C_{35}	0.322
C_{45}	0.876	C_{46}	0.371	C_{47}	0.349	C_{48}	0.317
C_{56}	0.914	C_{57}	0.395	C_{58}	0.914		
C_{67}	0.958	C_{68}	0.376	C_{16}	0.332		
C_{78}	0.976	C_{17}	0.390	C_{27}	0.346		
C_{18}	0.965	C_{28}	0.381	C_{38}	0.331		
Average	0.942	**Average**	0.382	**Average**	0.341	**Average**	0.319

(2) Capacitance values should decrease when the separation between two electrodes increase ($C_{12} > C_{13} > C_{14} > C_{15}$).

The experiment was done in two steps. The first step was to collect data in an empty state (nothing but dry air in the sensing area). The input signal used in the tests was an 800 kHz sine with 10V amplitude. Data were sampled using the one source/one detector mode at 1.99 MHz. Peak-to-peak amplitude was measured with 5 replications and the values were averaged. Results were listed in Table 3.1 (separation 1, 2 and 3 refer to the number of other electrode(s) between the pair of electrodes under test). According to the assumption (1) above, the capacitance readings for each column should be the same. However, both location of electrodes and noise from capacitance-to-voltage transducers would add error and result in capacitance variation. Fortunately, these variations were relatively small and within an acceptable range. Assumption (2) was supported by all individual and average values very well since values measured at different separations were significantly different from each other.

The second part of the test was to repeat the above experiment with the sensor in a full state, meaning the measuring area was fully occupied by a test material. The objective in building the ECT system was to measure moisture content of wood chips, thus green chips (MC around 80%) were chosen as the test material. To avoid unnecessary air gaps between

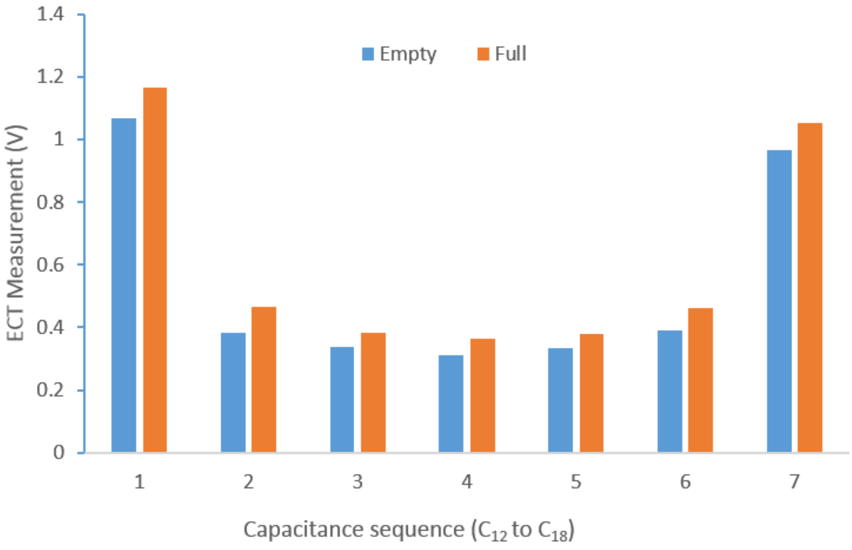

Figure 3.1: Readings from electrode 8 as captured during excitation from the other 7 electrodes. The horizontal axis refers to the exciting electrode, and empty and full refer to the absence, or presence, of chips within the sensor enclosure.

individual particles, large chips (wet weight > 10.0g) were excluded. Results were shown in Table 3.2, with values displayed in this case being actual capacitance (rather than summed voltages), in pF. The same trends were observed as in the empty state. Though absolute ECT readings were different from other data reported in the literature, as, for example, in Yang and York (1999), the trend was exactly the same.

The data from tables 3.1 and 3.2 were also shown graphically in Figure 3.1, but this time in terms of raw sensor output (volts). The graph highlights the consistency in sensor response for the various combinations of excitation/response electrodes and between the empty and full states. The ratio of sensor outputs for the full and empty states for a given electrode was uniform regardless of the separation from the excitation signal. This result strongly suggested the arrangement of electrodes and the data processing circuits were correctly designed and adequately built. The ratio of four different separations in empty state was 2.95:1.20:1.07:1, while 2.85:1.25:1.05:1 in full state. The capacitance values increased with similar ratios, example of electrode 1 was plotted as .

Table 3.2: ECT readings when full. Units of values are in pF.

Adjacent		**Separation 1**		**Separation 2**		**Separation 3**	
C_{12}	1.164	C_{13}	0.467	C_{14}	0.383	C_{15}	0.364
C_{23}	1.059	C_{24}	0.469	C_{25}	0.397	C_{26}	0.367
C_{34}	0.961	C_{35}	0.453	C_{34}	0.379	C_{35}	0.370
C_{45}	0.971	C_{46}	0.438	C_{47}	0.394	C_{48}	0.360
C_{56}	1.002	C_{57}	0.461	C_{58}	0.377		
C_{67}	1.036	C_{68}	0.445	C_{16}	0.380		
C_{78}	1.079	C_{17}	0.463	C_{27}	0.394		
C_{18}	1.051	C_{28}	0.462	C_{38}	0.371		
Average	1.040	**Average**	0.457	**Average**	0.384	**Average**	0.365

3.1.2 Repeatability Test

A test of the repeatability of the sensor was also undertaken. Before the test, all output circuits were fixed on a PVC board to eliminate undesirable variation resulting from non-constant stray interaction between the individual elements. The board was attached outside and perpendicular to the axial direction of the measuring vessel (Figure 3.2). The location was relatively far from electrodes to avoid excessive stray capacitance between circuits and electrodes. The length of lead wires between test circuits and electrodes was also fixed and uniform.

The repeatability tests were done in the same manner as the functionality tests outlined above: background measurements with the sensor enclosure empty, and a second reading when filled with a test material. Tests were carried out in a lab environment where air humidity and temperature were relatively stable. The background measurement was repeated three times a day for three consecutive days. The location of the experimental setup remained fixed. 50 groups of data (28 capacitances per group) were collected for each measurement, and the total measurements contained 450 groups (12,600 data points), using one-source-multiple-receiver sampling mode. Material under test was chosen to be dry wood chips. The dry chips were placed in the same envelopment with ECT system for two weeks,

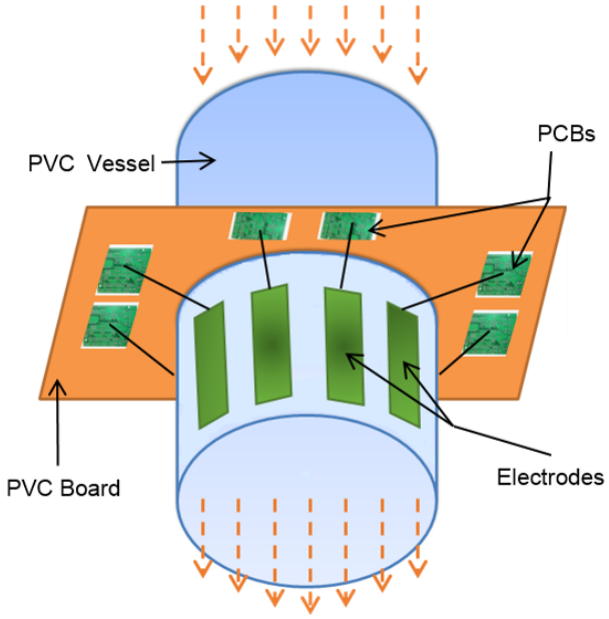

Figure 3.2: PVC board to fix PCBs

so that the water inside would come to equilibrium with air humidity. Methods used for ECT measurements were the same as in the background test. The MC of the sample was assumed constant during the three-day test, which was also the reason for not using green chips. The chips were not disturbed during the test. Data were processed by combinations. Distributions in sum are shown in Figure 3.3 Analysis methods were as follows:

(1) Sort the data by combination of receiving and emitting electrode. Each capacitance combination C_{xy} had 450 repeats, where x=1, 2,...,7, and y=2, 3,...,8 represented the index of the electrode. The data were rearranged into a matrix as:

$$\begin{bmatrix} C_{12}^{1} & \cdots & C_{12}^{450} \\ \vdots & \ddots & \vdots \\ C_{78}^{1} & \cdots & C_{78}^{450} \end{bmatrix}_{28\times 450}$$

(2) Calculate the mean (μ) of each row of the matrix. The signal-to-noise ratio (SNR) was computed as equation 3.1 (Lu *et al.* 2004).

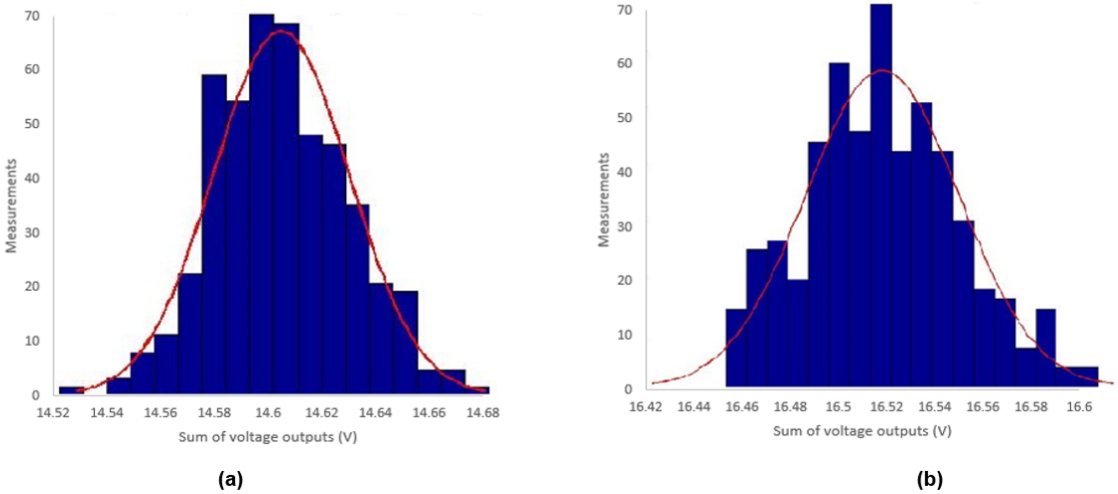

Figure 3.3: Plot of the distribution in observation counts falling within the indicated summed output voltage range. Plots are shown for (a) background and (b) dry wood chips as the material under test. The normality of the plots indicated sensor measurements were predictably repeatable with a known variance in response.

$$\mathrm{SNR} = 20 \log |\frac{\mu}{C}| \tag{3.1}$$

where $\mu = \frac{1}{N}\sum_{i=1}^{N} C_i$, and $C = \frac{1}{N}\sum_{i=1}^{N} |C_i - \mu|$, N=450.

(3) Calculated the sum of each column. Equation 3.1 was also calculated for the summed result, referring to the overall SNR when using the sum as sensor response.

Result of both empty and full states were shown in Table 3.3. The minimum SNR was observed from C_{15} (36.56 dB) in the full state. It was possibly because the separation between electrode number 1 and 5 was the biggest and had a greater chance of undesirable variations appearing. If choosing electrode 1 and its combinations as an example, the SNRs decreased when the separation increased. For the capacitances C_{12} and C_{18}, the materials between the electrodes were PVC tube, wood chips, and air. Since the PVC tube was constant and occupied a larger ratio of sensing area than any other non-adjacent electrode combinations, the probability of variation would be reduced. Overall, even the minimum SNR, was large enough to support the conclusion that the ECT sensor as built was a stable and low noise system. The variation in summed capacitances was significantly smaller than any single capacitance. It was, therefore, reasonable to use the capacitance (or voltage) sum as the sensor output predicting overall average permittivity within the entire sensing area. This implied the use of the multiple-electrode system was equivalent to a single-paired-plate capacitance sensor, but perhaps provided greater stability in the presence of variability in the material under test.

3.1.3 Sensitivity Test

Based on Gauss's law, any permittivity change within the ECT sensor's measuring area should be observable as a capacitance change, and therefore as a change in its output voltage. In the previous section, system noise levels in the sensor output were shown to be small relative to the effect of permittivity variation, but it was not zero and should affect the sensitivity of the system. Experiments were undertaken to identify the minimum quantity of a material that could be observed using the ECT sensor in the presence of typical noise levels The material under measurement for the tests was pine chips, which for the purposes of these experiments was considered to be composed of a mixture of two phases: dry wood and water. Sensitivity of the sensor to both phases was estimated.

Water Test

This test was to establish the minimum quantity of water observable using the sensor. It was not possible to accumulate only water inside the sensor, therefore a clean and dry plastic container was used to hold it. The container was placed at two different positions in the sensing area: on the edge near the enclosure wall, and in the center. The empty container was used as the reference data (background) for the test. Water samples were directly acquired from the faucet and added into the container a drop at a time using a plastic transfer pipette, which had the capability to hold 3 ml water in total. A single drop of water was about 0.04 ml. Each test consisted of adding two drops of water, taking the

Table 3.3: Results of the sensitivity test showing SNR (in dB) measured for each electrode combination for the listed materials under test.

Test Material	**Electrode Combination**							
	C_{12}	C_{13}	C_{14}	C_{15}	C_{16}	C_{17}	C_{18}	C_{23}
Bkgd	47.97	40.50	38.55	37.28	37.15	38.15	47.71	47.95
Wood	47.77	40.03	38.85	36.56	37.09	37.81	46.03	47.06
	C_{24}	C_{25}	C_{26}	C_{27}	C_{28}	C_{34}	C_{35}	C_{36}
Bkgd	38.90	37.97	37.88	38.05	37.18	40.29	38.09	38.00
Wood	38.59	36.74	37.00	37.62	36.51	44.80	37.92	37.46
	C_{37}	C_{38}	C_{45}	C_{46}	C_{47}	C_{48}	C_{56}	C_{57}
Bkgd	38.01	39.02	45.37	38.78	38.59	39.17	46.37	38.98
Wood	37.49	37.91	44.64	37.80	38.20	38.32	44.81	37.95
	C_{58}	C_{67}	C_{68}	C_{78}		**Sum of 28 capacitances**		
Bkgd	37.65	43.94	37.90	43.53		59.08		
Wood	37.65	44.73	37.05	45.04		58.77		

capacitance measurement (sum of 28 voltages), and repeating. This experiment was repeated 10 times. Student's *t-test* was used to check if a sensor reading was significantly different from the reference level at a 95% confidence level. Once identified, that volume of water significantly different from a background reading was defined as the system resolution, or minimum sensible amount, for water. Part of the results were shown in table 3.4.

The minimum detectable water volumes were 24 drops (0.96ml) and 56 drops (2.24ml) for edge and central areas, respectively. A consistent phenomenon was observed such that the sensitivities of edge and center locations were different, and this result will be discussed more thoroughly in the next section.

The sensitivity in the central portion of the sensor was lower than the edge and around 2.24 ml of water. The total volume of the measuring area within the sensor was about 1824 ml, which meant a 0.12% volume change from air to moisture would have a more significant effect on measured capacitance than noise.

Table 3.4: Results of the sensitivity test showing SNR (in dB) measured for each electrode combination as the listed number of drops of water were added to the sensor.

Edge Area

Drops	0	4	8	12	16	20	24	28	32
Mean	14.843	14.846	14.854	14.862	14.869	14.860	14.877	14.879	14.879
P	1	0.7053	0.2428	0.0792	0.0249	0.11	0.0018	< 0.001	0.0031

Drops	36	40	44	48	52	56	60	64	68
Mean	14.874	14.887	14.891	14.894	14.897	14.890	14.892	14.919	14.925
P	0.0038	0.0016	< 0.001	< 0.001	< 0.001	< 0.001	< 0.001	< 0.001	< 0.001

Central Area

Drops	0	10	20	30	36	40	44	48	52
Mean	14.806	14.819	14.822	14.822	14.825	14.825	14.821	14.824	14.827
P	1	0.9687	0.3777	0.9454	0.1732	0.2580	0.2478	0.3489	0.6593

Drops	56	60	64	68	72	76	80	84	88
Mean	14.834	14.847	14.851	14.854	14.857	14.850	14.852	14.869	14.885
P	0.0038	0.0016	< 0.001	< 0.001	< 0.001	< 0.001	< 0.001	< 0.001	< 0.001

Wood Sensitivity Test

Chips were in two states, bone dry and green. Single pieces of wood (individual chips) were measured to avoid location and air gap influences.

Dry chips, dried in an oven for 24 hours, were selected for the experiment based on their weight. A total of 30 dry chips were selected with weights ranging from 1.73g to 28.31g. Green chips were stored in -20°C refrigerator for a week. All chips were in a frozen state during the measurements. As in the dry wood test, 30 green chips were selected with weights ranging from 1.01g to 18.33g. The bottom edge of the ECT electrodes were about one inch above the bottom of the PVC tube. To keep the chips within the measuring area, the same container was used to hold the chips as used in the water sensitivity experiment. Since the sensitivity was known to be different in edge and central areas, both locations were measured with the same chip samples. Background data were also taken with the container

Table 3.5: Summary of wood chip sensitivity results.

Dry	Edge	Weight (g)	0	1.73	3.44	5.77	8.01	11.48
		Mean	14.845	14.856	14.855	14.852	14.865	14.866
		P	1	0.3766	0.2592	0.1603	0.0286	0.0211
		Weight	13.45	15.82	19.75	23.85	26.62	28.31
		Mean	14.876	14.871	14.880	14.899	14.902	14.913
		P	< 0.001	0.0047	< 0.001	< 0.001	< 0.001	< 0.001
	Center	Weight (g)	0	1.73	3.44	5.77	8.01	11.48
		Mean	14.809	14.813	14.812	14.819	14.819	14.827
		P	1	0.3766	0.2592	0.1603	0.0286	0.0211
		Weight	13.45	15.82	19.75	23.85	26.62	28.31
		Mean	14.876	14.871	14.880	14.899	14.902	14.913
		P	< 0.001	0.0047	< 0.001	< 0.001	< 0.001	< 0.001
Green	Edge	Weight (g)	0	1.01	1.81	2.17	3.67	4.19
		Mean	14.849	14.855	14.863	14.872	14.889	14.892
		P	1	0.1083	0.0837	0.0101	< 0.001	< 0.001
		Weight	5.65	6.29	7.40	8.68	9.02	10.87
		Mean	14.882	14.909	14.887	14.937	14.926	14.945
		P	0.0012	< 0.001	0.0013	< 0.001	< 0.001	< 0.001
	Center	Weight (g)	0	1.61	2.17	3.67	4.19	5.65
		Mean	14.807	14.810	14.809	14.815	14.812	14.819
		P	1	0.6701	0.8045	0.2681	0.3845	0.0887
		Weight	6.29	7.40	8.68	9.02	10.87	12.77
		Mean	14.827	14.825	14.837	14.846	14.865	14.884
		P	0.0424	0.0430	0.0014	< 0.001	< 0.001	< 0.001

at empty status (but including the holding container). Individually, the dielectric constant of air ($\varepsilon_r = 1$), dry wood (3-5), and water (80) are quite different (Norimoto 1976). The weight increment of wood to be detectable should be much bigger than water. Data analysis methods were exactly as in the water test. Part of the results were shown in Table 3.5.

The minimum measurable sizes of dry pine chips were 8.01g and 15.82g for edge and central locations, respectively. The first observation with $P < 0.05$ (H_o: summed capacitance equal to background data) for center measurement was at dry weight of 11.48g. However, the following measurement at 13.45g did not have a statistically significant difference from background at 95% confidence interval. It would be inappropriate to conclude that the

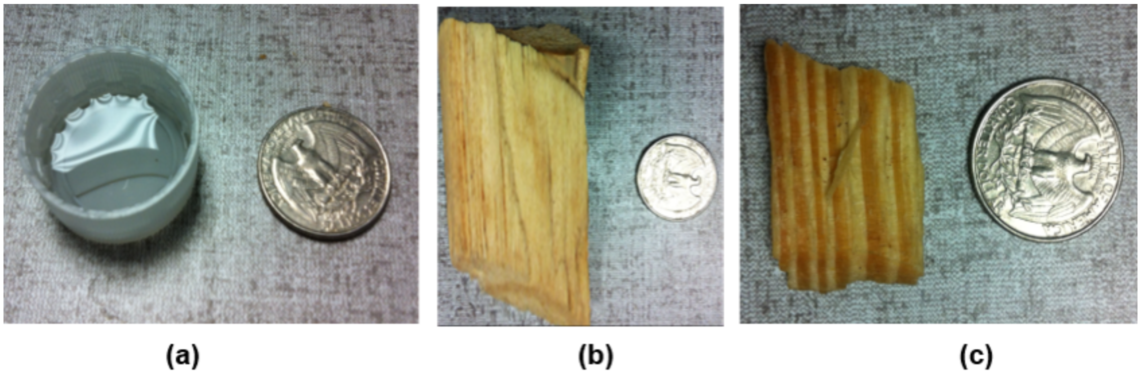

Figure 3.4: Minimum detectable size of (a) water (0.96ml, at edge), (b) dry chip (15.82g, at center), and (c) green chip (2.17g at edge).

system minimum background sensitivity was 13.45g of dry wood and the smallest amount of detectable dry wood was 15.82g. For green wood, the minimum measurable amounts were 2.17g and 6.29g for edge and center locations, respectively. The water inside a green wood chip exists in two forms: bound water and free water. Bound water exists as a component of cell walls; free water is in the lumen parts and may be liquid or vapor moving freely in cavities (Reeb 1995). The permittivity of bound water and free water are different (Boyarskii *et al.* 2002). However, the difference has been reported as being small. From the dry wood chip measurements, we knew that 2.17g and 6.29g dry wood could not be sensed using this ECT system. Thus the contribution to capacitance was mainly from water in the green chips. The MC of the green chips was around 75% normally, 2.17g and 6.29g green chips were therefore carrying about 0.93 ml and 2.70 ml water, which were close to the minimum volumes of water detectable in previous experiments (0.96ml and 2.24ml). Based on this result, it was concluded the measurement of a composite material (wood and water) could be successfully viewed as the sum of individual measurements on its two components, or that the sensor response was linear to these two materials.

Photos of the minimum detectable amounts of water (a), dry (b) and green wood chip (c) at edge or central areas were shown in Figure 3.4, compared with a US quarter dollar.

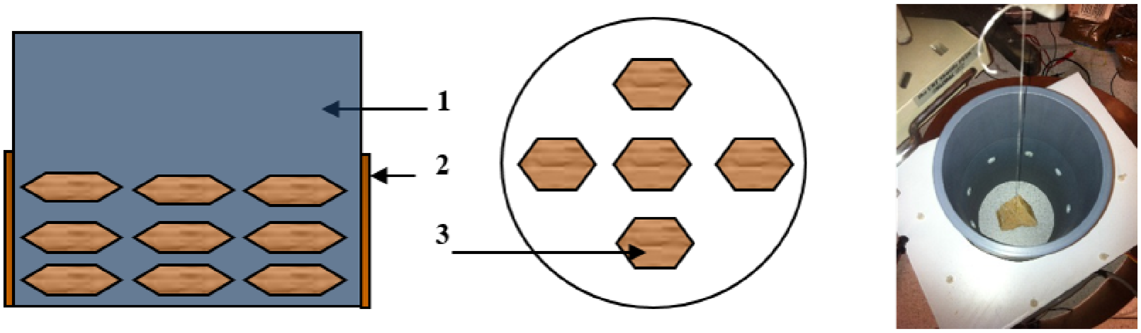

Figure 3.5: Illustration of location tests. (1) Measuring vessel, (2) electrodes, and (3) suspended wood chip.

3.1.4 Location Test

In the previous section, it was noted the sensor response was different for the same sample placed at varying locations within a plane normal to the PVC tube's central axis. Water and wood samples tested in section 3.1.3 were also only at the bottom of the sensor, therefore the effect of the vertical location was unknown. These variabilities were further tested in these experiments. The measuring volume within the sensor was about 182.4 $cm^2 \times 10.0$ cm (H) and was divided into 15 test volumes: 5 locations in a horizontal plane (4 at the sensor edge at cardinal points, and 1 in the center), and 3 levels in the vertical direction, as in Figure 3.5. Capacitance measurements were made as in the sensitivity tests for individual chips, but the tested sample was a single large, green chip (36.5g). A piece of fishing line, whose permittivity was examined and found to be ignorable, was used to hang the sample at the 15 different locations. This arrangement was also illustrated in Figure 3.5.

Each location was measured statically and sampling repeated 10 times. The sum of 28 capacitances was used the sensor response. An analysis of variance (one-way ANOVA) was carried out to evaluate differences in sensor response by height at the 5 locations. Results were summarized in Table 3.6 which listed P-values for the null hypothesis H_o: the readings within a location (x, y) were the same. The P-values all exceeded 0.8, indicating no statistically significant differences between the bottom, middle and top of sensing area within a single x, y location.

Table 3.6: ANOVA test results for vertical direction

Location				
Central	Edge 1	Edge 2	Edge 3	Edge 4
0.9831	0.8444	0.9346	0.9373	0.9037

Another ANOVA test was run for all 15 position data, to test H_o: all position means within a plane were the same. The P-value was 0.0706, which suggested all means were the same at 95% confidence interval, however, the sensor response at the central location tended to be smaller than the edge locations for the same object. The effect would reduce sensor accuracy, e.g. 70% MC wood chip at an edge location might have the same sum with a 73% MC chip at the center.

A normalization process was developed to eliminate variations in sensor output resulting from nonlinearities observed in the previous experiments. The process covered two error sources.

(1) Design error. From assumption (1) in 3.1.1, capacitances with the same separation should be the same. However, measurements in Table 3.1 showed small differences between them. This error between theory and real design was referred as design error, and it could be reduced using a normalization process.

(2) Unequal sensitivity error. This error referred to the different sensitivity at central and edge locations.

The normalization algorithm was done in two steps:

(1) Basic calculation. From 3.1.1, the sensor responses for each electrode from excitation by a given electrode were found to be increasing with almost the same ratio, if the measuring volume was completely filled and air gaps distributed uniformly. Based on this, a ratio normalization method was used. In this dissertation, wood chips would be the material to test. Thus the data for full and empty states in 3.1.1 could be used

as the upper and lower limit for the sensor readings. The normalized sensor response (V) was calculated as equation 3.2:

$$V_{n\ (i,j)} = \frac{V_{(i.j)} - V_{e(i,j)}}{V_{f(i,j)} - V_{e(i,j)}} \tag{3.2}$$

where$V_{(i,j)}$was the direct reading between electrode i and j, $V_{e(i,j)}$ and $V_{f(i,j)}$ were measurements from paired electrode i and j at empty and full states, respectively.

From equation 2.3, the amplitude of the output signal was proportional to the measured capacitance. Suppose the ratio was a constant k, such that

$$V_{n\ (i,j)} = \frac{V_{(i.j)} - V_{e(i,j)}}{V_{f(i,j)} - V_{e(i,j)}} = \frac{kC_{(i.j)} - kC_{e(i,j)}}{kC_{f(i,j)} - kc_{e(i,j)}} = \frac{C_{(i.j)} - C_{e(i,j)}}{C_{f(i,j)} - c_{e(i,j)}} = C_{n(i,j)} \tag{3.3}$$

The normalized sensor output would therefore be the normalized capacitance.

(2) Outlier removing. Normalized capacitance should be in the range from 0 to 1. However, because C_n was possibly varying outside that range due to system and measuring noise, a threshold operation was used to limit this kind of error, as shown in equation 3.4.

$$f\left(C_n\right) = \begin{cases} 0 & C_n < 0 \\ C_n & 0 \leq C_n \leq 1 \\ 1 & C_n > 1 \end{cases} \tag{3.4}$$

An ANOVA test was performed for normalized data taken in the location tests described previously, again with H_o: all location means were the same. The P-value after normalizing was 0.4438, compared with P=0.0706 for the original ANOVA data. Though the normalized data from the center region always tended to remain a little bit smaller than edge readings, the difference was greatly reduced. The conclusion was made that the ECT sensor was robust to sample location variation because its variability was known.

3.1.5 Particle Size Test

A particle size test was another way to evaluate the location issue. Wood chips include three material phases: air, water and wood. For dry chips, it would become two phases: air and wood. When samples having the same weight, but different chip size distributions, were placed in the ECT enclosure, the result would be segregation vertically based on size: small chips would tend to migrate to the bottom of the sensor, which would tend to leave air space at the top. Moderately-sized chips would create some gaps, and large chips would leave bigger empty spaces. The difference among these situations would be the location of wood and air. A test was designed to evaluate this effect of particle size distribution. Three samples with different size distributions were measured in the test: wood powder, small (<2.0g per piece) and large wood chips (>4.0g per piece). The total weight for each sample was 200.0g. All samples were fully dried. Figure 3.6 shows the conceptual argument for performing the tests (varying air/wood distribution for the same sample), as well as photos of the material tested in the experiment.

The sum of 28 capacitances was again used as the ECT response. Each wood sample was measured 10 times. An ANOVA test was applied to check if the three data groups had the same mean. The resulting P-value was 0.5624, suggesting the particle size would not affect the ECT output. Since the particle sizes vary for different industrial conversion processes, the ECT sensor could be effective in process control applications across conversion methods, provided the feedstock densities do not vary greatly.

3.2 Image Reconstruction Test

Image reconstruction algorithm was introduced in 2.3.3, the method was mainly from the literature, e.g. Chen *et al.* (2007). Though the algorithm has been widely used in ECT applications, imaging of wood chips has never been tested. In this part, the LBP method and Landweber iteration will be tested on chips and other materials.

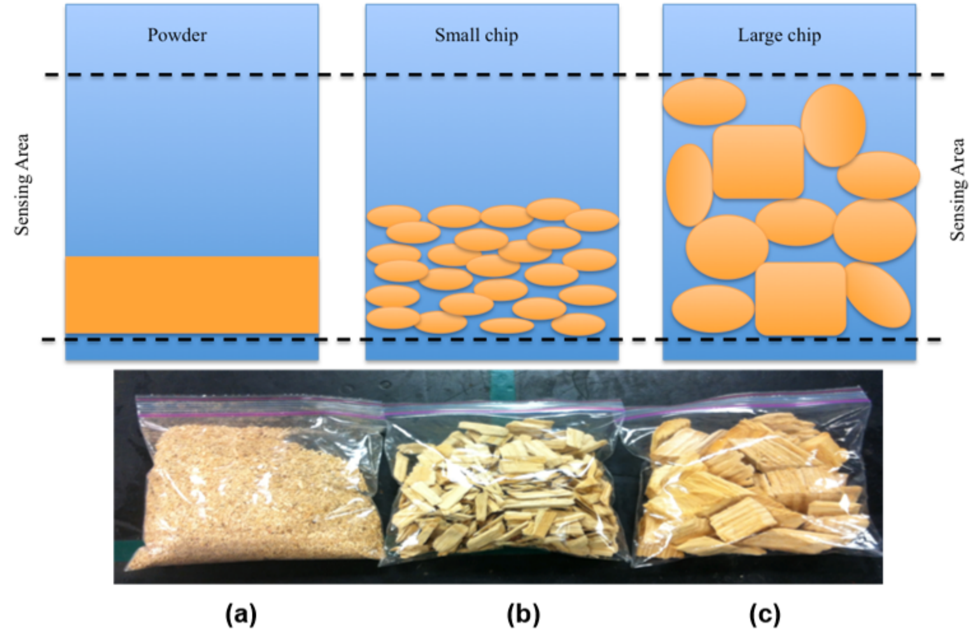

Figure 3.6: Illustration of samples for particle size tests. (a) Wood powder, (b) small particle wood chips, and (3) large chip samples

3.2.1 Electric Field Distribution of Electrode Combinations

In a high energy measuring system, such as X-ray scanning, the probe signal would transmit straight from the emitter to the receiver, without any bending and the area under measurement for any electrode pair would be obvious. An electric field established between two capacitance electrodes, however, is not so simple and can be highly variable in its distribution, depending on what other conductive materials are nearby and the nature of the dielectric material itself. It is necessary to know the electric field distribution for this particular sensor in order to successfully apply the tomographic image reconstruction algorithm. Since it is hard to view the true electric field, software ANSYS 13.0 was selected to simulate the electric field using a finite element approach with the measurement area meshed with triangular elements, and the node number equal to 225.

According to 2.3.2, two sampling methods were reserved for further experiment: single source-single receiver (denoted here as One-One) and single source-multiple receiver (One-N). The measuring areas, which would be different for the two sampling methods, were simulated using ANSYS 13.0. For One-One mode, boundary conditions in the simulation were set as source equal to 10 V, and detector electrode to 0 V. The other (unused) electrodes did not apply any voltage. And, for One-N mode, the source electrode voltage applied was 10 V, and the N measuring electrodes were set to 0 V. Simulations results were shown in Figure 3.7. The color blue indicated low electric potential and red was high electric potential. The central part was always in a low energy state, which could explain the low sensitivity discussed in the 3.1.4 location test. As mentioned in 2.3.3, the electric field distribution of One-One mode only had 4 unique states. Because the system was symmetric, e.g. 1-2 equal to 1-8 equal 2-3, the electric field distribution of the other combinations would be the same but shifted. For the One-N mode, there were 7 different electric field distributions, which were created by different detector numbers from 7 to 1.

The simulation results also provided the sensitivity matrices crucial to image reconstruction. The matrices for the two methods were computed as follows:

1. One-One mode. Suppose electric field distributions of O1 to O4 were V_1 to V_4 (225x1 vector), then the transposed sensitivity matrix would be:

   $$S_1^T = [V_1, V_2, V_3, V_4, \cdots, V_k, \cdots, V_{28}] \quad . \tag{3.5}$$

   For $4 < k \leq 28$, any V_k could be calculated from V_1 to V_4.

2. One-N mode. If electric field distributions of N1 to N7 were V_1' to V_7' (225x1 vector), the sensitivity matrix was:

   $$S_2^T = [V_1', \cdots, V_1', V_2', \cdots, V_2', V_3', \cdots, V_3', V_4', \cdots,'_4, V_5', V_5', V_5', V_6', V_6', V_7'] \quad . \tag{3.6}$$

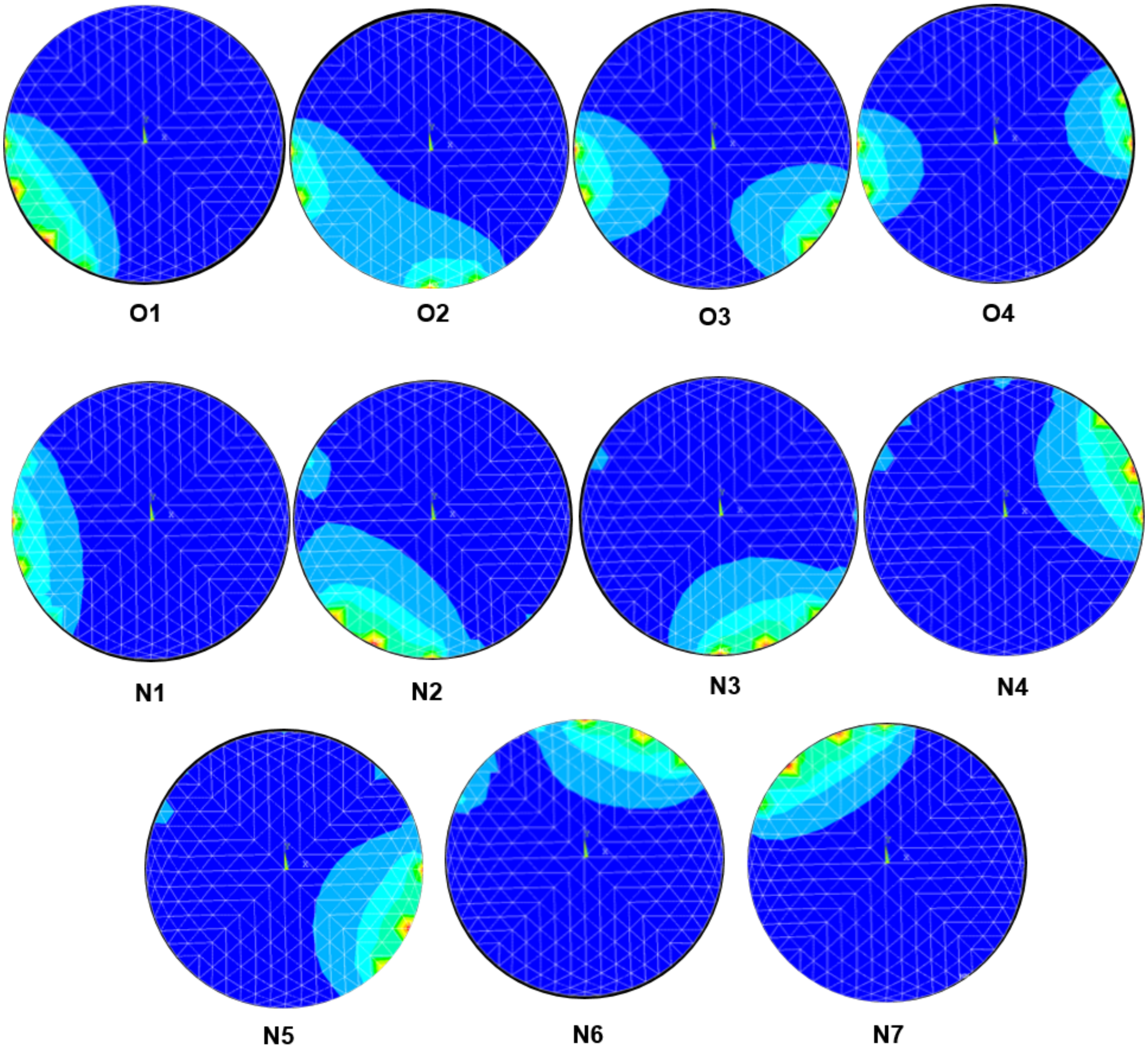

Figure 3.7: Electric field distribution in two measuring modes. O: One-One mode. Oi: electrode 1 and i (=2,3,4). N: One-N mode. Nj: electrode j source, and (8-j) receivers.

When electrode j (1, 2,.., 7) was used as source, (8-j) measurements were taken. So the number of E_j in sensitivity matrix S_s was equal to (8-j).

3.2.2 Post-Processing Image Reconstruction

Given the image reconstruction methods and sensitivity matrices were implemented as introduced in sections 2.3.3 and 3.2.1, an estimated permittivity distribution image based on ECT sensor readings could be computed using the LBP method. According to equation 2.18, the resulting image, G, was actually a 225×1 vector, rather than an image, but the coordinates of the 225 node points were known from the electric field distributions calculated in the sensitivity matrix simulations. The vector-based G estimates were converted to images using an interpolation scheme written in PYTHON^{TM} 2.7 (PYTHON Software Foundation) and employing the `SmoothBivariateSpline` routine from `scipy.interpolate`.

A standard material was used to test the imaging system. A PVC rod was reported in the literature to be a detectable material (Steiner *et al.* 2005), and was also used in this test. In addition, an alternative sensitivity matrix free method (SMF) for calculating the permittivity nodes was applied to compare with the LBP method. The SMF method was carried out in two steps:

(1) Analyze the coverage for each pair of electrodes, such as the area in Figure 3.7.

(2) Take the smallest normalized capacitance value as the gray scale for all covered pixels. For example, if pixel $k(i, j)$ is involved in the coverage of pair 1-5, 2-6 and 3-7, the gray value $G_{k(i,j)} = \min\{C_{1-5}, C_{2-6}, C_{3-7}\}$.

The SMF method, although perhaps less precise, could be used to speed up imaging calculations in real-time applications.

The PVC samples were tested using One-One mode, with excitation input 800 kHz, 20V peak-to-peak sine wave. Data were sampled at 2 MHz and collected for 10 repeats. The average of 10 measurements was used to reconstruct an image. Since it was not possible to measure a sensor-full background state for the PVC material, the data were only compared with empty state (air background). Another normalization method was required to for situations in which no background measurement could be acquired, as was the case for later tests using PVC targets. In this alternate approach, the image was rescaled to use the maximum and minimum value of the calculated gray scale vector G, as:

$$G_n = \frac{G - G_{\min}}{G_{\max} - G_{\min}} \quad , \tag{3.7}$$

where G was the data from the un-normalized capacitance, $G_{\min}$ and $G_{\max}$ were the minimum and maximum value in vector G. After normalizing, the gray scale was limited to the range [0-1]. The process might be inaccurate for some outliers observed in original G. However, averaging from 10 repeated measurements would greatly reduce the effect of extreme values.

Results of both methods were shown in Figure 3.8. The true area percentage of the test PVC rod was 6.25% (1.5 inch diameter PVC rod in 6 inch inner diameter sampling space). The measured area estimates were 5.80% and 19.11% for SMF and LBP separately. Both images indicated the appropriate location and area and the results supported the conclusion it was possible to reconstruct ECT images with some accuracy. The total effective pixels of the two methods were 293 and 225. Better resolution and accuracy were achieved using the SMF method. Another advantage of using the SMF method was faster image processing. Since the method was based on calculating outputs from single paired electrodes separately, fewer computations were necessary after the 28th reading was collected compared to LBP. However, an image reset function was necessary to initialize the image for the next 28 readings. If calculating the image for every paired-electrode capacitance reading, the process would have lots of repetitions and that would decrease the effective sampling rate. If implemented the method after all 28 readings were acquired, the method took a longer time to reconstruct as opposed a simple matrix multiplication. Since the sampling rate would be the first consideration for an ECT application in dynamic situations (moving contents), the

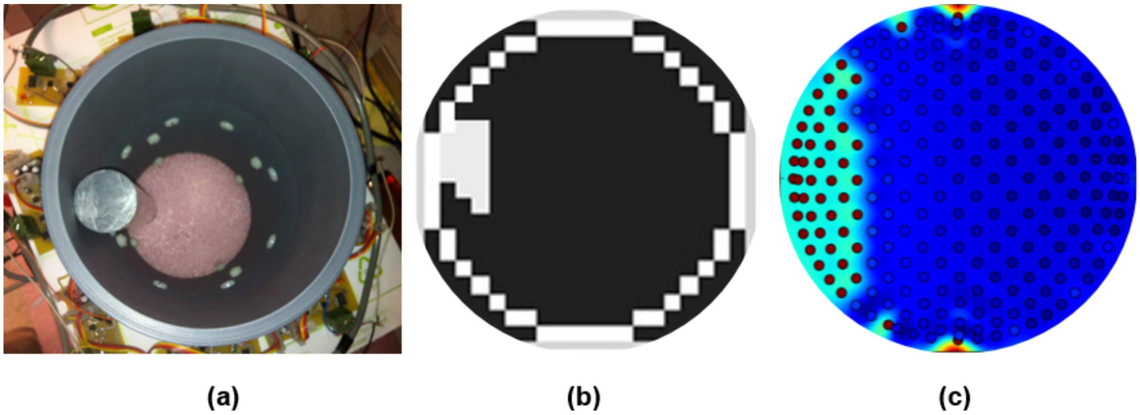
(a) (b) (c)

Figure 3.8: Image reconstruction result of the arrangement in (a) using (b) SMF and (c) LBP method image reconstruction methods.

LBP method, the accuracy of which could be improved by other mathematical approaches, was chosen to measure wood chips.

The ECT image was expected not only to detect the area and location of wood chips, but also the MC, or, at a minimum, tell the difference between wood chips with high and low MC. To test this ability, green and dry wood chips were selected as a sample to be measured, and the same measurement procedures used in the standard material (PVC rod) test were applied, except reference measurements and normalization processes were possible. For these tests, paper sheets were used to separate green chips from dry, or from empty space. The full state used in the normalization calculations was sensor response for the tube filled with green chips and the capacitance readings were normalized, as in 3.1.4. Resulted images were shown in Figure 3.9. Two capabilities of the ECT imaging system could be concluded from results in Figure 3.9:

(1) ECT could show an accurate area in an image occupied by certain materials, e.g. wood chips, air;

(2) MC information could be extracted from the color in the image. In figure 3.9b, yellow referred to MC = 0%, and red referred to green chips, e.g. 75% MC; for Figure 3.9d, blue was at 0%.

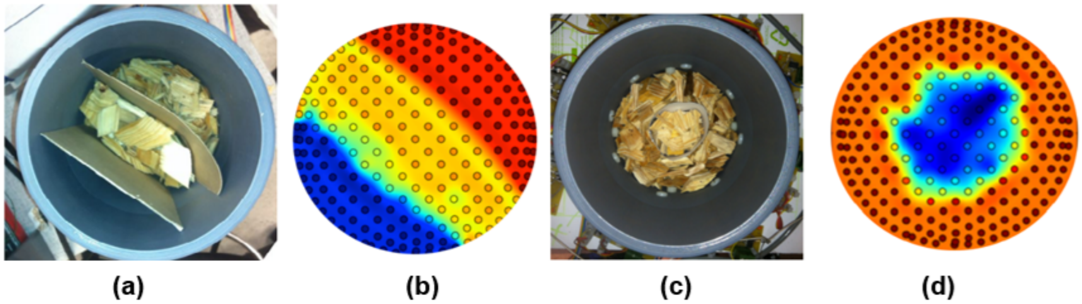

Figure 3.9: Example images generated using the sensor in tomographic mode for varying arrangements of green and dry chips. (a) Image of green chips, dry chips, and empty separated by cardboard partitions, (b) reconstructed image of (a); (c) Green chips surrounding dry chips, again separated by a paper partition; (d) Reconstructed image of (c).

3.2.3 Error Source and Improvement

Though the LBP method was simple and easy to compute, the accuracy of spatial estimates based on its results was worrisome. The image error came mainly from two sources.

One is algorithm error. From the equations 2.18 and 2.21 in 2.3.2, the LBP algorithm used S^T as a substitute for S^{-1} to calculate G. However, the two equations were not equal:

$$C \neq SG = SS^T C \quad . \tag{3.8}$$

The difference between the true and computed images was a major error source of the ECT system. To reduce this type of error, the crucial problem was to reduce the difference between C and SG. The *Landweber* iteration method introduced in equation 2.22 was a good approach to accomplish this. The algorithm was: $G_{k+1} = G_k + \alpha S^T(C - SG_k)$; when C was bigger than SG_k, a positive value would be added to G_k and become the next G_{k+1}. The next SG_{k+1} would be bigger than SG_k, and was closer to the measured C. When C was smaller than SG_k, the Gk would be reduced by the factor $\alpha S^T(C - SG_k)$. Thus whatever the initial situation was, by running the iteration with a correct α that made the iteration convergent, the difference between C and SG would be minimized. The method was tested using the PVC rod data from 3.2.2, the result for 10 and 20 iterations of the algorithm

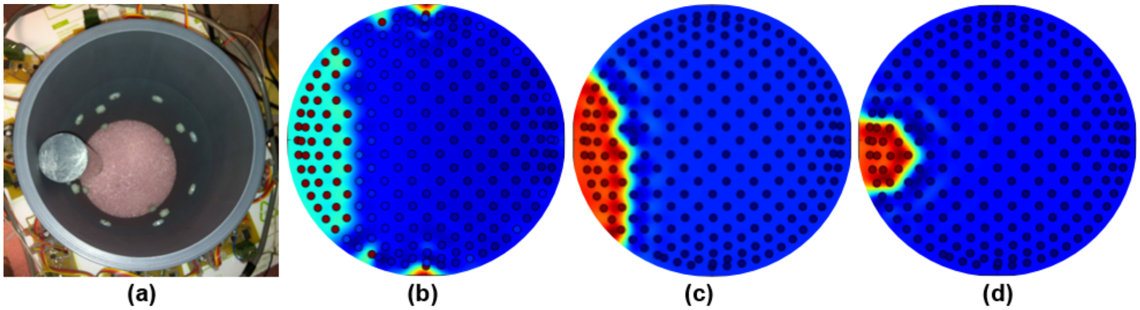

Figure 3.10: Application of the Landweber algorithm in improving ECT images. (a) The actual test arrangement; (b) The initial LBP-reconstructed image; (c) LBP image after 10 Landweber iterations, and (d) after 20 iterations.

were shown in Figure 3.10. The estimated area ratio of the rod was reduced from 19.11% to 13.33% and 6.67% for 10 and 20 iterations, respectively. The relative difference from the true area ratio was decreased from 12.86% to 7.08% and 0.42%. Compared with the SMF accuracy (0.45% error), the LBP-*Landweber* method was proven to be as rapid and accurate. However, higher accuracy could take an indeterminate number of iterations and that could, in some situations, reduce the sampling rate. The iteration number used needed to be carefully selected based on the specific measuring requirements.

Another error source was from the nonlinearity of the electric field, meaning the electric field would be affected by the material under test. When a dielectric material is placed in an electric field, it causes the field to twist and changes the distribution of charge density. In addition to this effect, a dielectric material would become polarized in an electric field and create its own internal electric field. This electric field would also affect the initial field applied by the input high frequency signal. These two influences made the electric field change with different materials, different sizes, and different locations. According to the changes in electric field, the sensitivity matrix should be changed for every unique combination materials being probed. However, for the LBP method, the sensitivity matrix was fixed to the sensor empty state. The assumption of LBP was the sensitivity matrix only related to the structure and material of ECT system itself, and was immune to changes with measuring material. This contradictory assumption has become known as the ‘soft field’ property (Yan *et al.* 1999, Elmy and Omar 2011). The phenomenon has been identified as an important but unsolved problem limiting the accuracy of ECT systems using the sensitivity matrix approach.

3.2.4 Online Image Test

Before analyzing the real-time imaging system, it was necessary to understand the dynamic measurement procedures. Two disparate sampling methods were available to collect analog sample data in LABVIEW software (or voltage measurements in ECT): N-sample and continuous sample. The N-sample method acquired N data points on demand, while continuous sampling read data continuously. To achieve the highest frame rate in implementing the imaging system for this study, it was necessary to use the continuous sampling method, which could take measurements resulting in about 80 image frames generated per second. If using the N-sample approach, 10 frames per second was the highest that could be achieved.

The continuous sampling method, however, read from all channels simultaneously and saved the data in a buffer. These data were incompatible with the electrode switching actions and resulted in numerous outliers (previously excited electrodes discharging while reading another). This was an unavoidable limitation of using LABVIEW for the ECT control and data acquisition program.

Another parameter affecting effective sampling rate was data acquisition mode. For experiments using LABVIEW, One-One mode required 28 iterations of a measurement loop to complete, but only 7 iterations of the same loop for One-N mode. However, if measuring from 7 channels simultaneously using the *NI 6361*, as in One-N mode, the effective device sampling rate would be divided by 7, which for these tests was 286 kHz. This was much lower than necessary to detect peak amplitude values in the electrode outputs.

For an input 800 kHz sine wave, the period is $1.25{\times}10^{-6}$s. and the peaks in amplitude will appear at $3.125{\times}10^{-7}$ and $9.375{\times}10^{-7}$s after a rising transition in voltage above 0V. With an incorrect, low sampling rate, e.g. 200 kHz, the measured points will capture a peak only if somehow the phase of sampling and the signal are either matched, or the shift is otherwise a multiple of the sampling rate. Given that the sampling period is $3.59375{\times}10^{-6}$s, the first point measured would be at $1.09375{\times}10^{-6}$s ($3.59375{\times}10^{-6} - 2 \times 1.25^{-6}$), the second and seventh points at $9.375{\times}10^{-7}$s and $3.125{\times}10^{-7}$s, respectively. These calculations suggest if sampling rate ($1/3.59375{\times}10^{-6}$s) were 278.26 kHz, the amplitude could be obtained in 7 readings, provided the sampling and signals are in phase. Though in actuality there exists some phase shifting between the two, the shift is constant and, if enough data were taken, measured voltages at specific time intervals should be at least proportional to the peak value sought.

Figure 3.11 is an example image generated in real time using all the above methods to speed the calculations. The target was a plastic bottle containing water. With an input 800 kHz sine wave, 300 samples were taken at 278 kHz for any single capacitances estimate (peak detection), and the imaging algorithm was implemented in LABVIEW. With this approach, the imaging system could generate 10 frames per second in real time.

3.3 Conclusions

In this Chapter, basic features and capabilities of the ECT sensor were tested, including electrode response, system stability for background and test material measurements, sensitivities of the system to materials with different permittivity, location, and particle size difference, and off-line and real-time image generation. The system sampling rate was also analyzed in a simple fashion. In summary, tests in this Chapter suggested:

(1) The designed ECT sensor was stable and and its output was sensitive to materials across a range of permittivity. The system could, therefore, be used to detect moisture content in woody biomass.

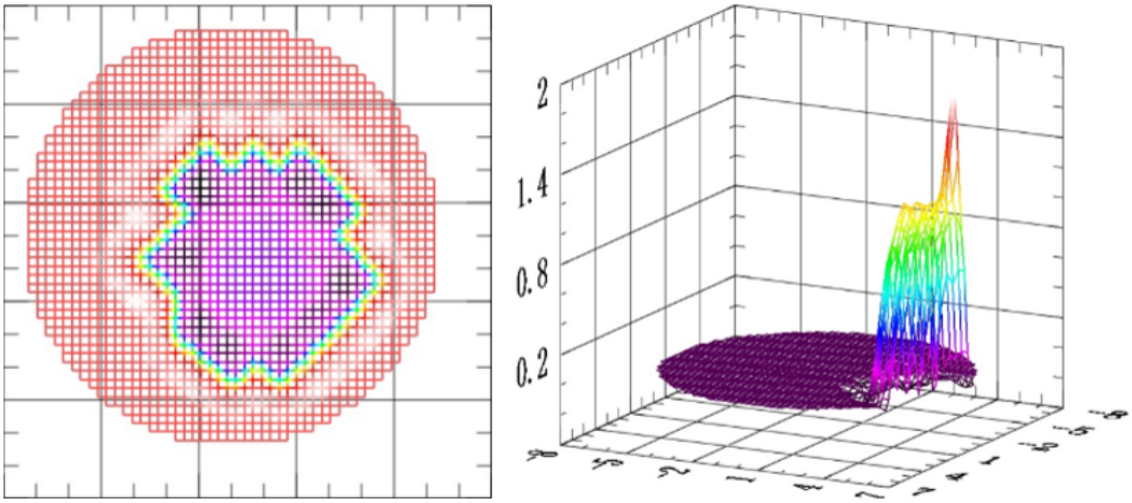

(a) (b)

Figure 3.11: ECT images reconstructed in real time using a LABVIEW program. The image (a) is a 2D version of the image, and (b) a 3D image. Either could be constructed in real time (10 fps).

(2) The image reconstruction algorithm could provide accurately the location and cross-sectional area of different materials, e.g. wood, air, water, PVC.

(3) The system has the capability to measure MC of wood chips both statically (not moving) and dynamically (moving through the sensor enclosure while measuring).

Chapter 4

STATIC MOISTURE MEASUREMENT FOR WOOD CHIPS

In the previous Chapter, the ECT sensor built for this study was verified as being sensitive to both wood and water. Since determining the MC of wood chips required measuring the relative amounts of water and wood, this ECT sensor should have the capability to sense variation in MC. This sensitivity was shown to be exploitable in two manners, or modes, listed below.

(1) Parallel-plate (or summation) mode. The ECT sensor included 8 individual electrodes, any pair of which could be used to detect permittivity of a test material. This single-measurement-single-response method was exactly equivalent to that in a single paired parallel plate capacitance sensor, but the ECT sensor, with multiple pairs, could more completely probe the material housed within the measurement enclosure and might, therefore, give higher accuracy in its readings. In this case, the summed value of all capacitances should be proportional to the average permittivity of the material under test.

(2) Tomography mode. In this approach, capacitances for each pair of electrodes were used individually to to compute an image representing the 2-D variation within the measurement enclosure. The image provided location plus quantity/volume of objects in its field of view.

For static (non-moving sample) MC measurement, the summation mode was the principal method applied and its application was the focus of the experiments reported in this Chapter.

4.1 MC Prediction Model Study

The key in building a MC prediction model was to establish a relationship between ECT readings and the MC of mixed-phase materials. For the MC to be calculated as the ratio between water and wood as a percentage, it was necessary to know the relationships between ECT output and water/wood quantity.

4.1.1 Wood Test

The purpose of this test was to understand the relationship between ECT readings and wood weight. To exclude the effect of water, dry wood chips were used in the test. The objective was to characterize the sensor response to varying amounts of dry wood. The experimental procedures were as follows.

(1) Set the input signal to 800 kHz, 20V peak-to-peak amplitude sine wave. The data acquisition method applied was One-One mode (see sec. 3.2.1 in the previous Chapter, basically referred to the sequencing approach taken to cycle through the measurements), sampling at 2 MHz for 10 iterations of all paired-plate combinations (28 each iteration, 280 measurements total). The average of the 10 summed voltage readings was recorded as sensor response.

(2) Measure reference (background) values in the above manner for the sensor in an empty state.

(3) Wood data collection. The minimum sensible quantity of dry wood was around 8 g (3.1.3), so the starting quantity tested was 10 g. More wood chips were added to those already in the sensor between readings. Response was measured for 18 different chip quantities.

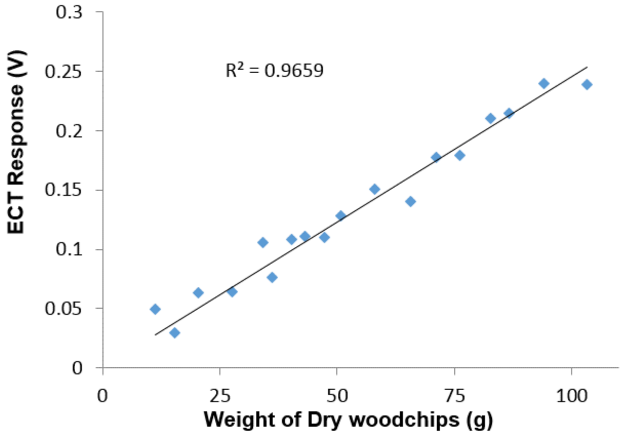

Figure 4.1: Result of the test evaluating ECT response as a function of sample mass (dry wood chips).

Chips were obtained from a single source in Alabama, US, dry densities of which were varied over a small range. According to the parallel electrode capacitance calculating method:

$$C = \frac{\mathrm{KA}}{4\pi d} \tag{4.1}$$

where C is capacitance, A the area of the electrode plate surface, K the permittivity of the material between electrodes, and d the distance between two plates. With A and d fixed, the capacitance should have been proportional to the permittivity of sensing area. Adding chips was equivalent to replacing some volume of air with wood, increasing the overall permittivity. If the chip density was constant, increasing chip mass should increase the capacitance linearly.

The difference between chip and reference data was plotted with wood chip weights, as shown in Figure 4.1. Sensor response was significant ($\mathrm{P} < 0.001$) and, as expected, linear with dry wood mass ($\mathrm{R}^2 = 0.97$).

4.1.2 Water Test

Given there was a linear relationship between wood quantity and capacitance, the next step was to test sensor output with water as the test material. According to the capacitance relationship in eq. 4.1, response of water should be similar to wood, with a different slope (permittivity of water is 80, dry wood is 3-5: Norimoto 1976). However, the effect of water inside chips was unknown. To explore the issue, a test using a fixed quantity of dry material with varying amounts of water was performed. Several samples of pine chips (around 100g dry weight each) were dried, weighed, and then measured using the ECT sensor. This process was repeated on the samples over the entire expected range of moisture content. Since the same chip sample was repeatedly dried to create the water difference, no wood quantity variation was involved. A parallel experiment was to test water held in a plastic container. Sampling, calibrating and modeling methods were the same as in the dry wood test above. Results of both water tests were shown in Figure 4.2. A highly correlated ($P < 0.001$ for both) linear relationship between sensor output and water quantity in both tests matched the capacitance theory and dry wood test very well. For the test with samples consisting of water and wood, referenced to an empty sensor, the intercept was found to be the capacitance resulting from dry wood for the sample quantity tested (100 g), as it should have been. The slopes of the two regression results, though significantly bigger than dry wood, were statistically different ($\alpha = 0.1$). The reason for the difference was the two water forms existing in wood chips, as mentioned before. Bound water has a smaller permittivity than free water and that decreased the slope a bit. The difference being small, however, this effect could be ignored, and was in further tests.

4.1.3 MC Prediction Model

From the last two tests, it was known that capacitance contributions from water and wood were both positive and linear, which fit the theory of capacitance theory. It was

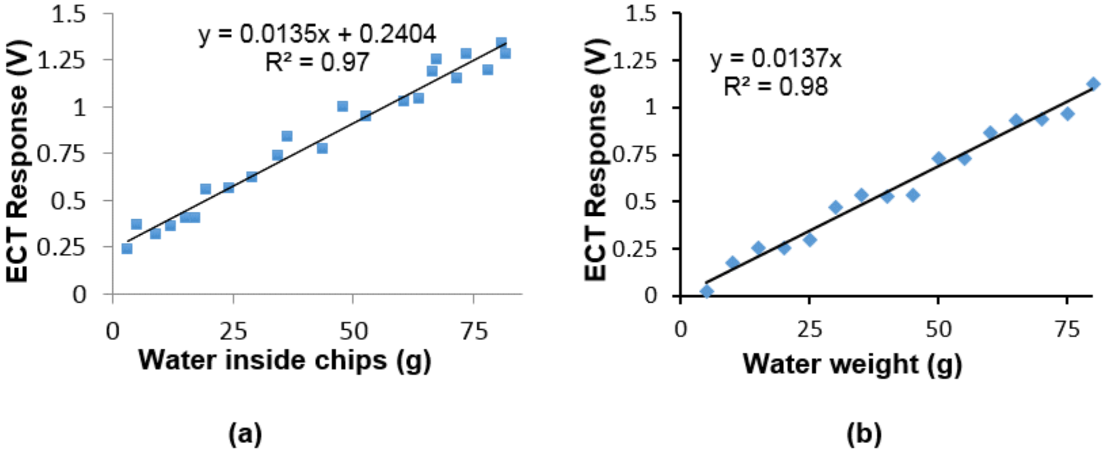

Figure 4.2: Measured ECT response with samples of green chips (mixed water and wood) (a) or (b) water alone held in a plastic container.

surmised, therefore, the relationship among capacitance, water and wood quantity for mixed test samples could be modeled as in equation 4.2.

$$V = \alpha_0 W_1 + \beta_0 W_2 + \gamma W_1 W_2 + \varepsilon_0 \quad , \tag{4.2}$$

where V was the change in ECT output voltage (sum), W_1 and W_2 were the weight of dry wood and water respectively, α_0, β_0, γ, and ε_0 were constant coefficients. To test this supposition, a validation test was done with chips at different MC.

A large quantity of loblolly pine chips were collected from a local mill (south Alabama, US). Chip samples were randomly selected from the population and divided into 35 groups. Each group contained 40-80 individual chips. Four groups of chips were kept in a green state, another 31 groups were dried in a 105°C oven for varying lengths of time to develop a range of moisture content among the samples. Wet weights of sample after the pre-drying process were from 167.2 g to 273.4 g. The chip samples were measured using ECT with methods as described in 4.1.1. The chips were placed with a uniform depth to avoid the location effect, thus no normalization was necessary to calibrate the data. Moisture content of individual chips within a sample were considered uniform. After ECT data were acquired,

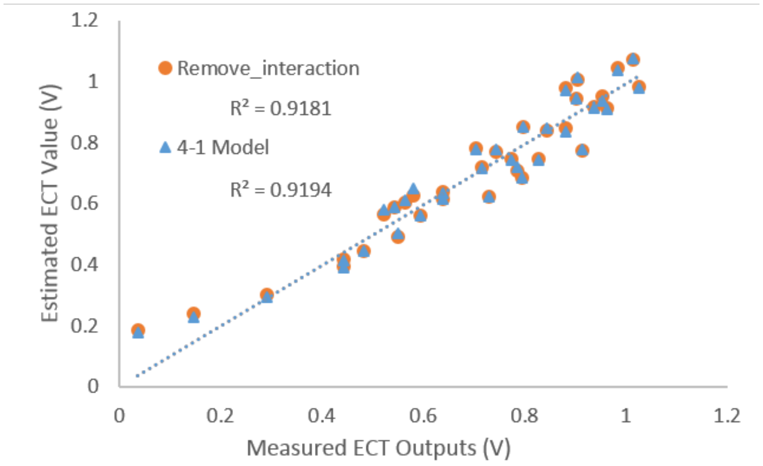

Figure 4.3: A graph showing measured and predicted moisture content for green chip samples. The line represents a 1:1. Prediction models were built based on equation 4.2 (blue), or equation 4.3 (orange, no interaction term).

the chip samples were dried in an oven for 24 hours and dry weights ranged from 119.3 g to 163.7 g. Sample MC was calculated from wet and dry weights. The range was from 8.3% to 83.5%. The calibration model 4.2 was fit, as in Figure 4.3 (blue points). The statistical analysis showed P-values for water and wood weight coefficients were < 0.001 ($\mathrm{R}^2 = 0.92$), which again proved the significant influence on capacitance from both materials, and that they were individually discernible when mixed. However, the P-value for the interaction term, indicated as W_1W_2 in equation 4.2, was 0.1019, and was therefore concluded as being insignificant in estimating capacitance. After removing the interaction effect, both water and wood remained significantly related to the ECT output (Table 4.1), and estimated values without the term were shown in Figure 4.3 using orange markers. Based on these results, the relationship among capacitance, water and wood weight was revised to:

$$V = \alpha_0 W_1 + \beta_0 W_2 + \varepsilon_0 \quad . \tag{4.3}$$

Since the wet weight of wood W was simply the sum of its constituents, $W_1 + W_2$, equation 4.3 could be rewritten as:

Table 4.1: P-values of the coefficients for the given factors in both moisture content prediction models.

Model 1 (eq. 4.2) Factor	Model 1 (eq. 4.2) $\Pr(>\lvert t\rvert)$	Model 2 (eq. 4.3) Factor	Model 2 (eq. 4.3) $\Pr(>\lvert t\rvert)$
Intercept	< 0.001	Intercept	< 0.001
W_1	< 0.001	W_{1r}	< 0.001
W_2	< 0.001	W_2	< 0.001
$W_1 \cdot W_2$	0.4053		

$$V = \alpha_0 W_1 + \beta_0 (W - W_1) + \varepsilon_0 \quad . \tag{4.4}$$

If we define $\alpha_1 = \alpha_0 - \beta_0$, then equation 4.4 becomes:

$$V = \alpha_1 W_1 + \beta_0 W + \varepsilon_0 \quad . \tag{4.5}$$

Dividing the wet weight W from both sides, and rearranging, equation 4.4 will be:

$$\frac{V}{W} = \alpha_1 \frac{W_1}{W} + \beta_0 + \frac{\varepsilon_0}{W} \tag{4.6}$$

$$\frac{W_1}{W} = \frac{1}{\alpha_1}\frac{V}{W} - \frac{\varepsilon_0}{\alpha_1}\frac{1}{W} - \frac{\beta_0}{\alpha_1} \quad . \tag{4.7}$$

The term $\frac{W_1}{W} = \frac{1}{\mathrm{MC}+1}$, and substituting the following variables in equation 4.6, $\alpha = \frac{1}{\alpha_1}$, $\beta = -\frac{\varepsilon_0}{\alpha_1}$, and $\varepsilon = -\frac{\beta_0}{\alpha_1}$, the final moisture content prediction equation becomes:

$$\frac{1}{\mathrm{MC}+1} = \alpha \frac{V}{W} + \beta \frac{1}{W} + \varepsilon \quad . \tag{4.8}$$

Knowing the wet weight of a sample W, and the sum of 28 capacitance readings V, MC could be estimated using equation 4.8.

4.2 Moisture Content Prediction

It was established in the tests outlined in the previous section that, given a wet sample weight, the ECT sensor could provide an estimate of MC. The accuracy of those measurements relative to another approach was tested and was reported in this section. The reference method chosen was near infrared spectroscopy (NIR) because it has been applied successfully in measuring moisture content in wood (Axrup *et al.* 2000).

The comparison with NIR was made on samples of two types: individual pine chips, and bulk estimation for larger groups of chips. It was hypothesized that NIR measurements, because they were independent of sample size, should be more accurate on small quantities, but ECT should have an advantage in accuracy for larger amounts.

4.2.1 Chip Samples

Chips were selected from six batches of loblolly pine pulp-type chips obtained from three local sources (Alabama, US, two batches per source). Four of the batches were fresh and green (marked as batches 1-4, 1 and 2 were from the same local mill, 3 and 4 were from another). Two of the batches had been stored for about six months, one had been air-dried in a thin layer for about two months (Batch 5, MC ranging from 7%-12%), and another was piled green outdoors (Batch 6, MC $>$ 100%). It had been raining for three days before batch 6 was collected and the chips were in an extremely wet condition. Their surface of which was dusty when compared to the other samples. One of the fresh batches (Batch 1) was used to calibrate a prediction model for moisture content and samples from it and the remaining five were used for validation.

4.2.2 Testing Procedures

Assessment of the difference in the two methods began with measurements of moisture content in individual wood chips. The ECT sensor as used in this study could not reliably detect quantities of wood less than about 8 grams dry weight (at edge) , so samples were screened to separate larger chips and the ones used in the model calibration and validation were randomly selected from among the remaining larger ones.

Individual chips were dried in a 105°C oven for varying lengths of time to develop a range of MC among the samples, as in the model validation test. After drying, chips were assessed using the NIR system followed immediately by ECT measurements on the same samples. After measurement using sensors (ECT and NIR), chips were dried for another 24 hours to obtain the dry weight. The MC could be calculated by wet and dry weight, the result of which could be used to estimate coefficients of equation 4.8. Calibrations between sensor outputs and moisture content were built using 50 individual chips (from batch 1) and validated using another 34 samples. The validation set used 10 chips from batch 2. Part of the 10 chips were also dried in a 105°C oven for different lengths of time to create a moisture gradient among the samples. Another 24 were from the remaining 4 batches (6 chips each) at their original condition: batch 3 and 4 were green, batch 5 was at a relatively low MC state, and batch 6 was at very high MC.

Measurements on bulk samples were made on subsamples of 40-80 chips from single batches. The chips were assembled into groups from the quantity available and each group sample was dried for a varying period of time then weighed. This process resulted in bulk samples ranging in average moisture content from near bone dry to about 110% (dry basis). A total of 30 groups were used for calibration and 18 for validation. 6 groups of validation set, which were from batch 2, were dried to develop MC difference. Another 12 from batch 3-6 were not processed (3 groups each).

NIR Measurements

A *PerkinElmer Spectrum 100N FT-NIR spectrometer* (PerkinElmer, Inc.) equipped with a fiber-optic probe was used to collect woodchip spectra. The range of the spectrometer was from 1000 nm to 2439 nm, which covers two major absorption bands of water.

NIR measurements are derived from interactions between incident light and the material under test, but these interactions are confined to very small volumes. All NIR measurements, therefore, were made on individual chips, even those used in testing its ability to predict the bulk moisture content. For each chip tested, NIR spectra were taken from two randomly selected points, one on each large side. The test was measured at the full range of the spectrometer. The data interval was 2.00 wave numbers. Each spectrum was an average of 16 samples taken consecutively. The software *Spectrum Quant+ 4.6.0* (PerkinElmer, Inc.) was used to baseline correct and smooth the spectra. The final spectrum used to represent a single chip was the average of those processed spectra taken from both sides.

For bulk measurements, all chips within the sample were individually sampled in the exact same manner as in the single chip tests. Calibration models predicting bulk moisture content of the entire sample were built using random subsets of the sampled data with increasing proportions of the individual chips included in the assessment. Validation tests were done using the same approach, also being repeated using increasing proportions of the sample included in the measurement set representing the bulk characteristic.

The spectral data were processed using the following methods:

(1) Following baseline correction, smoothing and averaging, the NIR spectra were exported into EXCEL (Office 2013, Microsoft, Corp.) within which raw spectra from batch tests were assembled into groups.

(2) Principle component analysis (PCA) was used to extract linearly independent variables (principle components, PCs) from the spectral data. PCA is an efficient and common approach to reduce the dimension of large data sets. A single spectrum in this test had 2951 individual frequency variables and PCA facilitated identifying only those frequencies that contributed most of the variability in the observations. After running PCA, the 20 largest loadings could account for over 99.9% of the data variation. These loadings became the dependent variables that were correlated with MC.

(3) Used multiple stepwise regression, $\alpha = 95\%$, to identify the PC loadings most highly predictive of MC (Via *et al.* 2003).

ECT Measurements

ECT measurements for individual chips were made with the chip placed on a PVC support located on the edge of the space surrounded by sensor electrodes. Bulk measurements were made with the sample simply poured into the sensor enclosure to a uniform depth. The bottom of the sensing area was fully covered for those tests. A single measurement consisted of the sum of all unique combinations of sensor outputs from electrode pairs with the sample in place minus the observed output for the pair without the sample. The location of the PVC container was fixed. Every sample was measured with 10 replications, using One-One mode. The average value of 10 measurements was recorded as the final ECT response of the specific sample.

4.3 Results and Discussion

Results for the tests outlined above assessing the response of the ECT sensor relative to NIR in individual wood chip and bulk samples were reported in this section. The advantages and disadvantages of both methods were also discussed.

4.3.1 Individual Chips

Predictions of moisture content of individual chips were generally more accurate using NIR than ECT sensors. Figure 4.4 shows the measured and estimated moisture contents, Figure 4.4a for NIR and 4.4b for ECT. Each plot includes the calibration set data (from a single batch), plus predicted results for chips from all five batches. The coefficients of determination shown were for the combined data (calibration plus prediction). Table 4-2 lists standard errors of prediction for the calibration (RMSEC) and prediction (RMSEP) sets by sensor and sampling method. The calculating method for RMSE was:

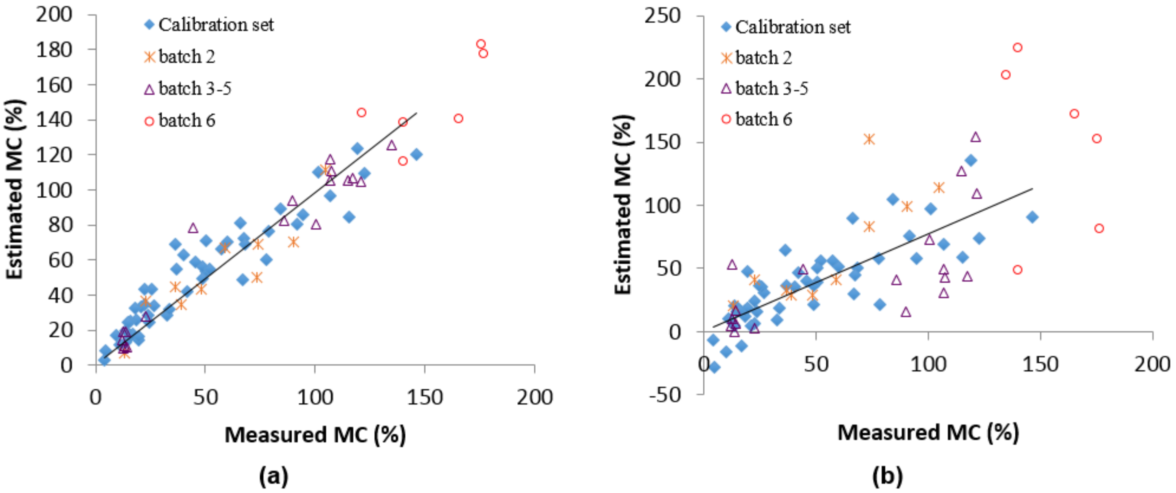

Figure 4.4: Moisture content of individual wood chips, estimated and measured using oven drying, for the two sensors. (a) is from NIR (R^2=0.84) and (b) is based on ECT (R^2=0.67). Plots are combined prediction and calibration datasets.

$$RMSE = \sqrt{\frac{1}{N}\sum_{i=1}^{N}(V_{\text{measured}} - V_{\text{estimated}})^2} \tag{4.9}$$

The overall prediction errors for individual chips using the ECT sensor were about 3 times that of NIR. The largest contribution to this error level was from the chips that had been stored outdoors for six months (batch 6). These chips were less homogenous in nature than the fresh batches (larger amounts of dirt and contaminants) and also tended to be very wet, typically wet to the touch. Their moisture content was also outside the range observed in the calibration set and this could have explained at least some of the extra variability observed. Without considering batch 6, the RMSEP of ECT was about 2.6 times that of NIR.

The relatively poor results using ECT were likely due to the sensor operating near its detection threshold for samples as small in mass as a single chip. Such small quantities of material in the sensor produced output signals only marginally larger than background noise (SNR $<$ 4 dB). This result indicated the difficulty in designing an ECT sensor to work efficiently across a broad range of sample quantity for materials consisting of two distinct

Table 4.2: Root mean square error of the calibration (RMSEC) and prediction (RMSEP) data sets for MC estimates for individual chips.

Sampling	**Sensor**	**RMSEC (%)**	**RMSEP (%)**				
			All Samples	Batch			
				2	3 & 4	5	6
Individual	NIR	12.40	13.80	11.90	13.88	4.16	21.0
	ECT	23.20	41.30	27.80	34.07	18.02	75.7

phases (wood and water, in this case) because of its mass dependency. NIR spectroscopy has a strong response at frequencies corresponding to hydroxyl bonds as found in water. Hydroxyl bonds are also present in biomass in significant numbers and would represent a source of error in moisture content measurements, but the NIR response of these non-water bonds should be relatively constant between individual samples of the same type of biomass. This bias can be easily removed using regression techniques, but it also illustrates the calibration problem inherent in NIR measurements. Accuracy of NIR in measuring moisture content is only as good as the calibration used in its prediction, and that calibration tends to be specific to a single form of biomass. ECT could hold an advantage if one were trying to predict moisture content in, for example, mixed hardwood and pine chips because its output is not tied as explicitly to the chemical composition of the material being sensed.

4.3.2 Bulk Measurements

ECT measurements of moisture content on bulk samples of chips were generally accurate, with mean RMSEP equal to 10.9% (Table 4-3) based on a calibration set from a single batch of chips (batch 1).

The RMSEP values for single batches were less than 9% in all cases except batch 6, which was, as in the individual chip results, more than twice as large. Again, batch 6 moisture contents were outside the range of calibration and this fact may have helped explain the poor performance of the ECT system for that material. However, the RMSEP of batch 6

Table 4.3: Root mean square error of the calibration (RMSEC) and prediction (RMSEP) for MC estimates in bulk samples.

Sampling	**Sensor**	**RMSEC (%)**	**RMSEP (%)**				
			All Samples	Batch			
				2	3 & 4	5	6
Bulk	NIR	8.48	13.25	7.27	9.71	7.57	26.50
	ECT	6.54	10.88	6.36	8.87	4.34	21.30

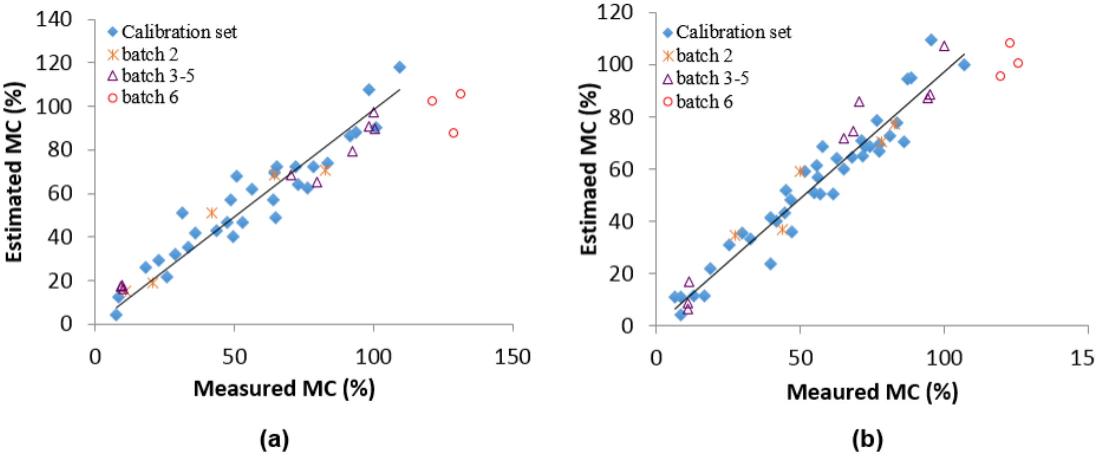

Figure 4.5: Calibration and prediction of moisture content for bulk samples using the two sensors. (a) is from NIR (R^2=0.90) and (b) is based on ECT (R^2=0.93).

for ECT measurements was greatly reduced in bulk samples, compared to those for a single chip. The improvement in RMSEP also proved that the error of ECT in a single chip test was mainly from size limitations (referred to as system sensitivity Chapter 3).

Figure 4.5 shows the performance of NIR and ECT predictions of moisture content for bulk samples. The α, β, and γ in equation 4.8 were determined as -69.1843, 65.6807 and 0.5807, respectively. The NIR response shown in the figure resulted from a 100% sampling of the chips in the group under test, i.e., spectra were collected from all chips in the bulk sample and then averaged. Results of the NIR testing with 100% sampling were very comparable to ECT predictions, but were slightly better for ECT across all samples and for those in specific batches (as seen in Table 4.3).

Table 4.4: RMSEC and RMSEP of MC estimates for bulk samples. In this test, all sample batches (sample source) were included in the calibration set, rather than only batch 1.

Sensor	**RMSEC (%)**	**RMSEP (%)**					
		All Samples	Batch				
			1	2	3 & 4	5	6
ECT	7.65	8.42	8.02	8.13	8.57	3.97	14.31

An alternative method was to build the calibration model using samples from all batches (1-6), rather than a single batch. A test using this approach was in which the prediction set also included samples from all batches. This test was only done in bulk measurement. The calibration set consisted of 20 groups of chips from batch 1, and 10 groups from the other five batches (2 group per batch). The validation set was 10 groups from batch 1, 4 from batch 2, and another 4 from batches 3-6 (one each). Results were presented in Table 4.4. By including data from all batches, the prediction accuracies increased for all samples, especially for batch 6, for which the prediction error was reduced more than 30%. For batch 2, which was from the same population as batch 1, the RMSEP actually increased, but only slightly. The correlation coefficient and RMSE of the calibration model, however, was not as good as when calibrating with only a single batch. This result suggested it would be advantageous to include as varied a wood sample as possible (in our case, from multiple locations) if the model was built for general use. However, a general model would have less accurate than a specific model for some certain species or origin of samples.

Using less than 100% of the individual chips in the NIR measurements to calibrate the bulk moisture content model resulted, as one would expect, in a greater amount of variability in the validation samples. Table 4.5 shows RMSEP values when spectra from a varying percentage of chips in the bulk samples were used to develop the calibration models. Chips were randomly selected from each bulk sample for inclusion in both the calibration and validation data sets. Errors increased when fewer chips from a bulk sample were used in

Table 4.5: RMSEP values of MC estimates based on NIR spectra from a varying percentage of individual chips used to predict the average value for the entire sample.

	Batch	**Percent Sampled**				
		100%	80%	60%	40%	20%
RMSEC (%)	1	8.48	10.88	12.05	14.66	17.05
	2	7.27	9.57	10.88	15.34	20.09
RMSEP (%)	3&4	9.71	11.29	16.90	19.22	22.43
	5	7.57	8.17	8.64	8.56	9.43
	6	26.50	30.07	34.37	38.78	52.36

calibration, and using a 40% sampling rate more than doubled the RMSEP relative to 100% sampling for most batches.

4.3.3 Sensor Discussion

For predicting MC of small quantities of biomass, basically amounts that could be considered to have uniform water content, the NIR method was superior. With more spectral averaging on single chips (multiple spectra collection points per side, for example), the difference in performance relative to ECT could have been even greater. The advantage of ECT, that the sensor responded to cumulative changes in dielectric regardless of how the sample was positioned within its confines, was also its limiting factor in tests on individual chips. Single chips having small mass resulted in changes in sensor output that were near the minimum resolution of the instrument and this meant higher errors when predicting MCs.

Both methods suffered when the assumption of uniform moisture content was violated, as seen in the results for batch 6, those chips having been stored for a long period outdoors. Batch 6 chips often had significant amounts of free water present on their surface, the result of heavy rains just prior to sample collection. The extra water was difficult to account for in the calibration process used and prediction errors were several times that observed in other batches for both sensors. In NIR measurements, the free water errors could have been compounded by variations in surface roughness, or the proportions of early and late wood sampled at a particular spot. Both of those variations might have been compensated for somewhat by greater sampling density over the surface of the chip.

ECT predictions of MC in individual chips should have been less sensitive to the presence of surface moisture because it should have responded to the total mass of water and dry wood placed in the sensor. Besides the sensitivity issue, there could have been some additional variation in batch 6 measurements, however, because of the different amounts of free and bound water between it and the other samples, although the literature indicates this effect should have been small.

NIR predictions of bulk samples composed of individual chips having variable weight and moisture contents would be expected to have higher errors unless these factors were controlled. In this study, spectrum estimates from each chip included in the bulk sample were combined without regard to chip dry weight and, without compensating for that combined mass/moisture variation, the NIR sensor errors were greater than those observed with ECT. The ECT predictions, on the other hand, should have been immune to variation in individual chip mass because the sensor responds to the cumulative quantities of water and dry wood rather than an estimate of their relative proportions, as in NIR.

Both sensors should be useful in situations where moisture content of larger populations of chipped, or otherwise comminuted, biomass were predicted using subsampling. The ECT approach, however, would be simpler since it more reliably predicts bulk MC on a bulk sample, rather than necessitating the combined size/moisture content variation in the material being quantified as is required with NIR. Given a relatively uniform distribution in those parameters, however, NIR should be feasible if results from averaged measurements on smaller quantities were sufficient. The ECT sensor had the additional advantage of being a simple and rapid measurement technique. With the ECT system used in this study, less than 1 second per reading was required to make a MC determination regardless of sample quantity up to the amount that could be placed within the sensor itself. However, to achieve equivalent accuracy as ECT measurement for bulk sample, such as 50 pieces, NIR method

Table 4.6: NIR and ECT system summary

Method	**NIR**	**ECT**
Advantage	Independent with mass, Accurate for small sample	Robust to surface condition and moisture gradient, rapid, capability to reconstruct image
Disadvantage	Spot and surface measurement, sensitive to surface condition, less efficient for bulk measurement	Low sensitivity, chip weight required to make the estimation

needed to acquire 100 spectra. Excluded data processing steps, only spectra collection would take more than 10 minutes to scan. The advantage and disadvantage were summarized in Table 4.6.

All discussion on ECT for small samples, e.g. pine chips with weight around 10 g or less, were concluded from applying the ECT system as built, the sensing area of which was 6 inches in diameter. In other words, the volume of a single chip was less than 1% that of the sensor itself. If the sensor enclosure were reduced to a suitable size, such as perhaps a 2 inch diameter, MC of a 10 gram chip could possibly be measured accurately. In that case, the imaging system could be used to estimate the volume of the chip, which directly related to the dry matter. That system, however, was not the objective of designing an ECT system. As the goal was to measure MC for a large quantity of biomass, only the bulk measuring method was focused on in this dissertation.

4.4 Mass-Free MC Determination Methods

Based on the bulk results reported above, MC of static samples could be measured accurately if the weight of the bulk sample was known, e.g. by locating the ECT sensor on a scale. That method, however, might not be appropriate in all situations. A mass free MC detecting method was necessary to ensure the ECT system was applicable in any situation.

Two feasible approaches were developed for static (non-moving) biomass, in particular for wood chips.

4.4.1 Known Volume Approach

The known volume method was exactly that of the paired parallel-plate mode except for the requirement that the volume of the sample being measured filled the sensor enclosure. Since the ECT sensing area was fixed, overloading it with chips would not be detected by simply measuring the original output signal. Given pine chips were of a uniform size distribution and density, total dry weight of sample in the completely filled enclosure should be relatively uniform. Variation in the the sensor response between samples, therefore, should only reflect the difference in the amount of water present, and therefore the MC. To test this premise, 20 groups of pine chips were selected that exhibited similar depth when placed in the sensor. The chip samples were dried to different MCs. The ECT response was tested directly with MC and dry weight using a linear model, $C = \alpha W_d + \beta \mathrm{MC} + \gamma$, where C was capacitance, W_d was dry weight, and MC was moisture content. The variation of dry weight of tested samples was from 130.1 g to 146.8 g, and MC ranged from 15.0% to 93.4%. The P-values for intercept and MC were < 0.001, however, for dry weight (W_d) it was 0.853. The result supported very well the assumption that filling the enclosure removed the effect of dry matter mass on the sensor output.

These procedures were repeated using the same samples as described in 4.2.1 to verify the result of the overloading method. To make a direct comparison, 30 calibration set samples were also selected from batch 1, and 15 validation sets were from the other four batches. Batch 6 was excluded in this and further experiments. ECT data were acquired in the same manner with all static measurements: One-One mode and 10 repetitions. Results were listed in Table 4.7 and Figure 4.6. Without knowledge of the state of the chips in these tests (dry or wet weight not known), the accuracy was reduced, as expected. The reduced accuracy, however, was in an acceptable range. Without measuring any weight, the

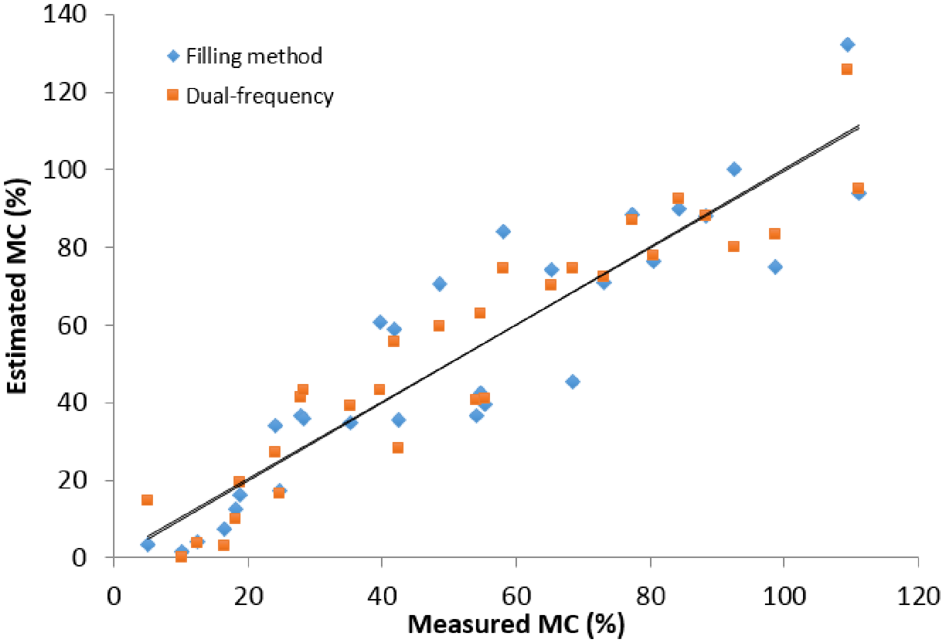

Figure 4.6: Measured and predicted MC of bulk samples using the known volume method (R^2=0.84, blue) and dual-frequency (R^2=0.89, orange).

measuring efficiency was improved. A practical dynamic application could be potentially be designed that accumulated samples within the sensing area for a fixed time, filling it as described above. This would give dynamic measurements without knowledge of the sample mass, at the expense of controlling flow in and out of the system.

4.4.2 Dual Frequency Approach

As described in papers by Kandala & Sundaram (2010) and Kandala & Puppala (2012), a dual frequency method could also be used in an ECT system. According to the theory outlined in the cited papers, the difference in measurements at two distinct frequencies should only be related to moisture content, and independent of sample density, weight, and location. This assertion provided another means of measuring material MC without any *a priori* knowledge of weight.

Table 4.7: Measuring errors (RMSEC and RMSEP) of mass-free MC prediction methods.

Method		**RMSEC (%)**	**RMSEP (%)**			
			All Samples	Batch		
				2	3 & 4	5
Known Volume		12.57	12.95	13.51	14.68	6.47
Dual Frequency	Fixed Quantity	10.66	10.93	11.07	12.73	5.32
	Random Quantity	11.15	12.04	12.45	13.50	7.11
Known Mass		6.54	7.17	6.36	8.87	4.34

The method was tested in parallel with the known volume experiment in 4.4.1. ECT measurements at a second excitation frequency, 500 kHz, were taken after the regular measurements at 800 kHz. Readings at both 500 kHz and 800 kHz were processed in the same manner as other tests in this Chapter. Instead of using a single point averaged from the ECT data sum, the dual frequency result was calculated as the average response at 800 kHz minus that at 500 kHz. Calibration and prediction sets were the same as in the known volume test above. Results were listed along with those from the known volume method in Table 4.7 and shown in Figure 4.6.

Since the dual frequency approach was described as a mass free method, another experiment was carried out using random quantities of wood chips, amounts that represented a varying percentage of the volume occupied in the sensor enclosure. The wet weights of the samples varyied from 68.0 g to 533.7g. Calibration and validation sets were as in the previous tests. Results were also included in Table 4.7.

4.4.3 Mass-Free Method Discussion

Two distinct MC measuring methods were provided as solutions to avoid the mass acquisition step. From the experimental results in Table 4.7, both RMSEC and RMSEP for all batches were increased significantly. The error source was mainly the variable air gaps present in the individual samples. For the known volume method, more air gaps indicated

Table 4.8: Mass free methods summary.

Method	**Single Frequency**	**Dual Frequency**
Advantages	Fast.	Quantity independent, accurate.
Shortcomings	Sample quantity exceeding sensing area. Less accurate.	Doubled measuring time and data.

less wood in the measuring volume. Since the wood was chipped to random shapes, it was impossible to make the bulk density of the samples, and their associated air gaps, constant. These uncontrollable influences were the main contributors to the relatively low accuracy when compared with the known mass model. The method should be more suitable for materials with relatively uniform shape and particle size, such as grain, corn, wheat, etc. For the dual frequency method, according to the paper by (Kandala & Puppala 2012), the presence of varying quantities of air gaps should also cause errors. Phase angle and impedance data were reported as a way to compensate for this error. It was reported to work well for a single paired plate capacitance sensor in the cited paper, however, the method could not be applied to our ECT system directly. The sum mode was a method to simulate the single paired plate sensor by calculating the sum of 28 different capacitances. If measuring the phase angle, the ECT system would have 28 different values, which would have made no sense to be summed as a single data observation. Thus no further study on this topic was pursued in this dissertation.

Though the accuracies for both mass free MC estimation methods were not comparative to the mass-included model, the results were still relatively close to true values, just somewhat less precise. Especially in cases where rapid determination of MC was required the mass free methods had advantages compared to any mass included method. Advantages and shortcomings were list in Table 4.8. Even for the dual frequency measurement, though the ECT scanning time was doubled (less than 2s), the time cost was shorter than independently acquiring the weight of a sample using, for example, a scale. As a result, no conclusion could be made about which was the best method in determining MC of a static sample. Different options would have different applications that depended on the specific requirements of that measurement.

4.5 Conclusions

In this Chapter, relationships between ECT readings and materials (water and wood) were studied. Pine chips under test were from three different locations, and in three distinct states. A mass-based MC prediction model was built, the accuracy of which was compared with a traditional NIR method, which worked well in predicting MC for small quantities of biomass, or for samples exhibiting uniform water distribution within a single sample (chip, in this case). However, due to its surface and spot scanning properties, the accuracy could be compromised if measuring a bulk sample or sampling chips with non-uniform moisture distribution. Comparatively, ECT was more robust in its response to particulate biomass exhibiting a large moisture gradient. Additionally, the measuring speed of ECT, which was independent of sample quantity (up to the volume of the measuring enclosure), was much faster than NIR for bulk samples. However, MC of small samples (e.g. total weight of chip(s) < 10.0g) was not reliably predicted because of the sensitivity limitation of the particular ECT system.

Two mass-free methods of applying the ECT sensor in measuring MC of static samples were also tested. One relied on completely filling the sensor volume, the purpose of which was to control the variation in dry weight of measured chips. If the dry matter could be approximated as constant, the sensor output was only related to the moisture content. Another was to use two excitation frequencies and the difference in their outputs as the MC predictor. Given that the goal of designing the ECT moisture sensor was to measure a large quantity of biomass, the mass free methods were only verified in bulk measurements. Though the two methods did not achieve an equivalent accuracy as when mass was accounted for independently, the faster measuring speed was a distinct advantage.

Based on the results, the following suggestions could be made for MC measurements across the full range of biomass quantity: for very small samples (e.g. less than 10 pine chips), use NIR; for medium quantity (chip volume larger, but less than sensing volume), use ECT & mass model; for large quantity (exceeding the measuring volume), use mass free models with two options – faster (known volume) or more accurate (dual frequency).

Both ECT and NIR sensors should also have utility in on-line measurement of moisture content in flow applications, but both have limitations as well. For NIR, simultaneous variation in chip size and moisture content would limit its accuracy in situations where this effect could not be averaged out over time. ECT measurement accuracy would also be limited unless simultaneous estimates of mass flow were available. The imaging capabilities of the system may provide an acceptable estimate of mass flow, but the accuracy of the method was not verified yet. The ECT combined mass/physical property measurement approach has been tested by others (Arko *et al.* 1999, Sun *et al.* 2008) on different multi-phase materials, however, and found to be feasible.

Chapter 5

DYNAMIC MC DETERMINATION METHOD

The principle of dynamic MC measurement is the same as that for static tests covered in Chapter 4. The ECT readings are, again, mainly affected by the two biomass phases: water and wood, but these two effects were linear and could be separated. As the dry mass and moving velocity could be expressed together as mass flow rate, the moisture content of dynamic materials might be estimated from capacitance and an independently-known mass flow rate. The capacitance in this case is referring to the overall permittivity, the value of which is calculated using the sum mode (single paired parallel-plate mode), as it was investigated in Chapter 4. The capacitance sum is easy to collect if the sampling rate is high enough to finish the required 28 measurements while the the biomass to be measured resides within the sensor. The key issue for dynamic MC measurement, therefore, is to focus on the mass flow determination and the speed of sampling in the ECT system. In this Chapter, two different methods were discussed to measure the mass flow for pine chips, as well as simultaneously determine their MC.

5.1 Dynamic System Setup

A dynamic MC system requires a different approach than static measurement. It should have two additional features: (1) feed chips into ECT continuously, and (2) not accumulate them in the sensing region. Modifications to the measurement system were developed to meet these two requirements, but the sensor itself remained the same.

Feeding system To feed particulate material like chips into the ECT sensor, a conveyor belt was thought to be a good choice and also easy to build. An ideal conveyor belt should be

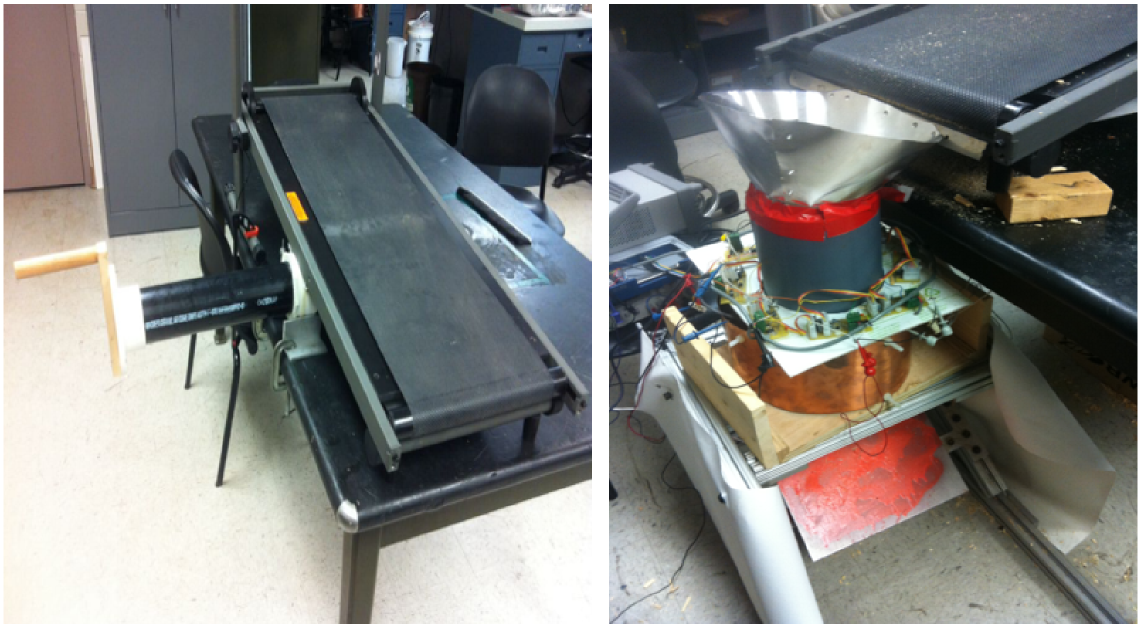

Figure 5.1: Photos of the dynamic ECT measuring system as used in this study. On the left is the conveyor system built to carry chip samples to the sensor. On the right is the sensor itself mounted in place. Chips dropped off the conveyor into the sensor and fell onto the impact force measurement transducer (orange) at the bottom.

capable of being driven at constant speeds and be controlled in real-time. Such a conveyor, however, usually costs several thousand dollars. To reduce the cost, a mechanical treadmill was used as the conveyor system, and is shown in Figure 5.1. The end of the treadmill was placed right above the ECT sensor. A plastic pipe was placed under the conveyor belt to drive it manually. Because it was driven manually, however, the control aspect was lost and this could be a serious difficulty in assessing accuracy of the ECT mass flow measurement capabilities. It also limited the speed of conveyance to about 30-40 cm/s, reducing the range over which mass flow could be assessed. An aluminum hopper was placed between the ECT tube and the conveyor belt to collect chip samples as they fell from the treadmill belt.

Support system A wooden base with a central hole was made to support the ECT tube. The diameter of the hole was about 16.00 cm, which was slightly larger than the inside diameter of the measuring tube (15.24 cm) and smaller than the outside (16.51 cm). When biomass was fed into the sensor, it would pass through without any contact with the support base.

5.2 Mass Flow Measuring Method Summary

Mass flow rate is defined as the weight of matter passing per unit time. It is an important factor in multiple industries that could be used to (1) describe the capacity of a production line, (2) map the yield of a bio-product, (3) or control the ratio of feedstocks in some process, etc. Because of its importance, multiple mass flow sensors have been developed and applied in industries and our daily life. Their application field includes gas flows (Birchall *et al.* 1970, Kupnik *et al.* 2004), gas/liquid two phase flow (Han and Dong 2009), liquid/liquid two phase flow (Tan *et al.* 2013), and solid (Yan 1996) and gas/solid systems (Xu *et al.* 2000). Different methods and technologies were used in these applications, such as a differential pressure meter (Han and Dong 2009, Tan *et al.* 2013), ultrasonic transit-time meter (Kupnik *et al.* 2004, Van Deventer 2005), vortex flowmeter (Huang *et al.* 2003), surface acoustic wave sensor (Brace *et al.* 1989), thermal mass flow sensors (Jacobs *et al.* 2007), Coriolis force based sensor (Enoksson *et al.* 1996), dual-plane electrical-resistance-tomography (ERT) system (Dong *et al.* 2006), capacitance sensor (Xu *et al.* 2000), and ECT system (Young *et al.* 1996, Sun *et al.* 2008). This dissertation was aimed at developing a moisture sensor for particulate biomass in motion, which also required knowing the material mass flow rate.

5.2.1 Mass Flow Measurement Technology

Mass flow sensors are common on agricultural combines for a variety of applications. Many use an impact method of sensing flow rate. In this approach, the stream of material is directed onto a force transducer that senses a change in momentum as it impacts a plate. The resulting force is used to predict mass flow. The impact force of grain was found highly correlated ($R^2 = 0.993$) with the accumulated yield (Birrell *et al.* 1996). The method was compared with a volumetric yield sensor which was applied simultaneously to monitor the total yield weight. The result showed signal with higher quality from the impact method than the volumetric yield monitor. The impact based mass flow monitor was described as being more closely approximating a continuous sampling method than the volumetric sensor. The smaller calculation error supported the impact method to be a good crop yield mapping technique. Principle and parameters of the impact based method were studied by Jiang and Qiu (2011) in which the system was simulated using a discrete element method.

Microwave systems were described as a way to measure MC of biomass in Chapter 1. The method was sensitive to the moisture both in material and air. Since a single frequency sensor was not able to separate the moisture variation with mass, a composite Right/Left handed transmission line resonator which included two measuring frequencies was used to measure mass flow and moisture content in published reports (Penirschke *et al.* 2010, Penirschke and Jakoby 2010). If only measuring the mass flow of a particular solid, the result was independent of MC, which was determined from changes in complex resonance frequencies. The designed system was concluded to be more sensitive compared to a conventional microwave mass flow detector (Angelovski *et al.* 2011).

An electrostatic sensor is a system measuring electric charge, the effect of which is based on surface area. The output of an electrostatic sensor also carries information related to particle mass flow rate (Xu *et al.* 2005). In that work, both time and frequency domain signals were analyzed. PCA was used to reduce the number of variables. The reduced variables (PCs) were modeled using a Neural Network method. The standard deviation of the relative error in predicting mass flow was less than 11.5%. The electrostatic sensor was also combined with a digital imaging sensor to measure mass flow rate and particle size (Carter and Yan 2005). The velocity of materials was measured using paired electrostatic sensors, and the volumetric concentration, as well as particle size information, were determined using an imaging sensor. The two measurements were carried simultaneously. The error source was from overlapping of particles in the images when the concentration was higher than a threshold value. However, in the measuring range, the system obtained accurate results (error around ± 4%).

Capacitance based sensors also have the capability to measure mass flow for different forms of materials. A parallel-plate capacitance sensor was introduced by Xu and others (2000) to measure flow of solid materials with low mass concentration. This permittivity determining method achieved a good result. However, the result was based on a uniform particle sized material. If the particle size was not fixed, their effects on permittivity would decrease the measuring accuracy. The system was also reported as an off-line method, since the baseline would drift with external factors, such as temperature, humidity and pressure. An ECT system, which consists of multiple capacitance sensors, would be insensitive to the particle size problem. Young and others (1996) developed an ECT system to measure flow of polyethylene and polypropylene nibs. The designed sensor provided 2-3 frames of cross sectional images per second. The maximum capability of measuring mass flow was 100,000 kg/h, the accuracy of which was within ± 2%. Another improved system was introduced by (Sun *et al.* 2008) and involved two parallel plate capacitance sensors. The principle was to measure material volumetric concentration with the imaging function of ECT using LBP and Landweber method (see Chapters 2 and 3), and determine the velocity of material by correlating the two signal sequences from two parallel plate capacitance sensors. For known distance between the two capacitance sensors, the time difference between the output signals could be converted to the velocity of material passing through. The data acquisition time for every frame was 0.00425s.

To select an appropriate way to determine the mass flow of wood chips, the impact and capacitance sensor would fit the goal of the project that required a low cost system. According to the analysis of the mass free methods in Chapter 4, the accuracy of mass prediction was not necessary to be very high. Based on the errors of both methods reported in the literature, the two methods should meet the requirement adequately. Considering both system cost and accuracy, the impact and ECT methods were selected and tested in this dissertation as described in the following sections. The results could be compared to make final a decision of an integrated MC and mass flow measuring system for pine chips.

5.3 MC Determination Based on Impact Method

The MC determination principle was to measure mass flow of wood chips using an impact sensor, and to simultaneously measure the relative quantities of the water and wood constituents using a capacitance sensor. Combining the two independent sensor measurements, the wood and water mass flow rates was separated. The accuracy of the impact method in determining mass flow was crucial, and validation tests of the method were done in both field and laboratory settings.

5.3.1 Field Mass Flow Test With Load Cell

A preliminary field test was done using a chipper system to verify the method was applicable in the intended application. A hinged element was added to the end of a chipper (3084 WTC, Precision Husky, Corp.) chute as shown in Figure 5.2a. A fixture mounted between the fixed and movable portions of the chute held a dynamic force sensor (DLC101-50, Omega Engineering, Inc.) that was loaded in compression when chips impacted the hinged plate (Figure 5.2b). The output from the sensor was a voltage signal proportional to force and was read using a USB-6210 data acquisition module (NI, Corp.). The data were sampled at 10 kHz and recorded using a program written in LABVIEW.

No independent measure of wood chip mass flow was found to be practically feasible, so experiments were instead conducted to correlate sensor output with tree diameter at breast height (DBH), which is a standard method of describing the size of a tree. The densities and standing heights of trees with the same age are similar. The square of a tree's DBH should be proportional to its weight. Data collected by partners in the study consortium indicated DBH^2 and weight were highly correlated for the types of stands being harvested, specifically, relatively young loblolly pine plantations. Figure 5.3 is a plot of the relationship between

Figure 5.2: Hinged element as used in measuring impact force of chips ejected from a chipper. The left image shows the modified chute in place, and on the right a close-up view of the sensing element.

weight and DBH^2 for a range of typical tree sizes found in the stands. The tree weights were measured using a scale suspended from a crane. A linear regression of DBH^2 on weight was found to be significant ($p < 0.001$) with R^2 in excess of 0.9.

Experiments consisted of measuring sensor output over the entire duration of a single tree being chipped. The time period used (33 seconds) was fixed. Figure 5.4 shows a plot of the typical force response while chipping a single stem. The 33s duration was sufficient, in most cases, to record force while the entire stem was chipped (chipping time for example plot 5.4 was less than 20 seconds). Problems with sampling the entire tree were sometimes encountered when, for example, the stem became hung in the debarker prior to entering the chipper. Stems in groups of about 10 were laid out on the logging deck near the chipper and measured for DBH and total height. Stems were then fed individually into the debarker and the chipper. Force response was measured and stored for each stem. Valid data for a total of 98 stems were measured sampling in this manner.

Two types of measures were calculated on each force record for correlation with tree DBH. These measures consisted of the following:

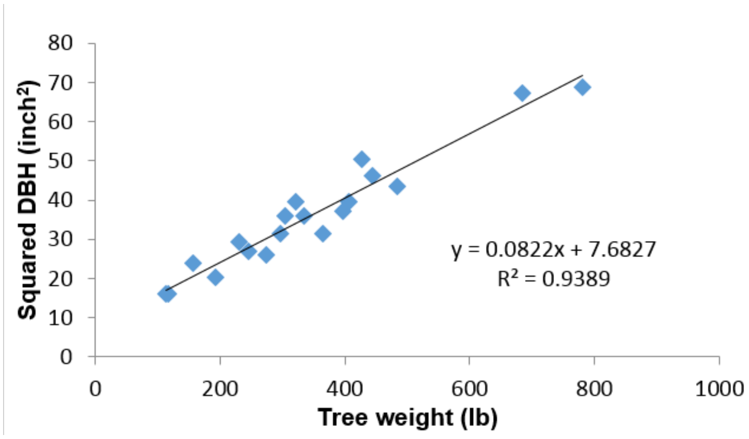

Figure 5.3: Results of a calibration between DBH^2 and weight of pine trees used in the mass flow measurement study.

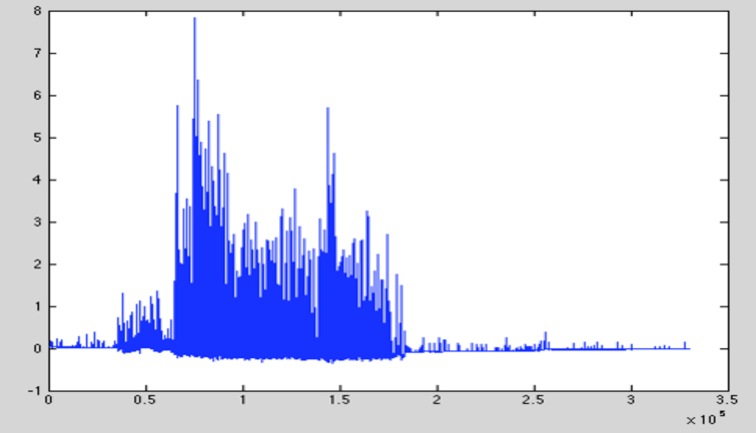

Figure 5.4: Force response example for a single stem as measured during chipping. On the horizontal axis is measuring sequence (time), and on the vertical, the sensor output (V, proportional to force).

1. Response sum. This was simply a sum of all force observations from beginning to end of the sampling period.

2. Power spectral density (PSD). The power spectrum of a signal describes the power per unit frequency it carries. PSD were calculated for each force response in MATLAB using the Welch method with Hanning windows of length 4096. This resulted in a relative power value at numerous (4096) discrete frequencies, only some of which were assumed related to size of the tree.

   A principle components analysis (PCA) was used to determine smaller groups of frequencies most closely correlated with tree size (frequency domain data from measuring method 2). The ten principal components (PCs) which explained most of data variance were selected and used in a stepwise regression analysis to determine the smallest set of values most closely predicting tree size. A random selection of eight force records was reserved and the prediction model built from the remaining 90 observations. Finally, predictions for the eight reserved trees based on the completed model were compared to actual DBH measurements.

Results and Discussion

There was no correlation observed between the summed force response and tree DBH^2. Figure 5.5 shows a graph of DBH^2 versus force sum for the 90 observations. It was originally supposed that a larger tree would produce a bigger force over the same length of time since the chipper fed at a constant rate and the trees were about the same height regardless of diameter. The sum should, therefore, have been greater for a larger tree, but this was not the case.

The PSD approach, however, proved more effective at capturing diameter information. The stepwise regression process resulted in a model having five total independent variables, four of which had P-values < 0.002, the fifth with $P < 0.1$. Though the relationship between DBH^2 and mass was linear theoretically, it was based on the assumption of uniform density

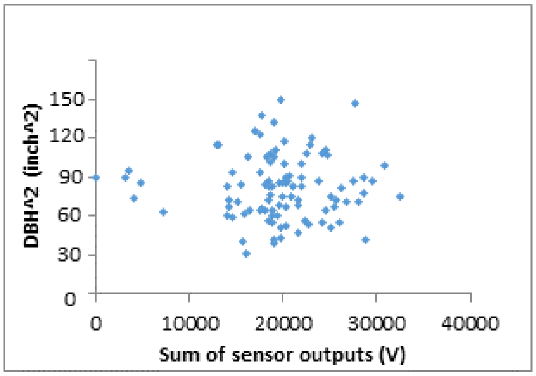

Figure 5.5: Plot of summed force (in units of volts) and DBH^2.

and standing height. However, variations in both density and height would affect the accuracy of the model if using DBH^2. A log-transformation was applied to the regression data to reduce this effect. With the transform, the linearity relationship between DBH^x and weight was improved (for any x, $\log(DBH^x) = x\log(DBH)$). Using this data processing method, the relationship between predicted and actual DBH was as seen in figure 5.6. The R^2 value in this case was 0.81. This result perhaps indicated that, although the chips were striking the impact plate as they exited the chute, their path was not changed a great deal and, therefore, force measurements were relatively low. This was intentional in that we did not want to alter the flow of chips into the van and cause problems filling its volume. Though the magnitude of the impact force of chips was not altogether different for larger trees, the rate at which they struck the plate seemed to be changed and this put higher frequency variations into the force signal. These higher frequency components were more pronounced for larger trees, indicating a more rapid rate of chip impact, and this was detected in the spectral analysis of the signal.

The eight reserved trees were also tested using the log-transformed model and results were listed in Table 5.1. The log-transformation method achieved a high accuracy in measuring DBH of pine trees. The RMSEP was 0.52 inch, for the sample with average DBH 7.90 inch. The relative prediction error was 6.61% (= RMSEP / mean (DBH) × 100%). This accuracy was calculated for each individual tree. If the eight trees were treated as a single

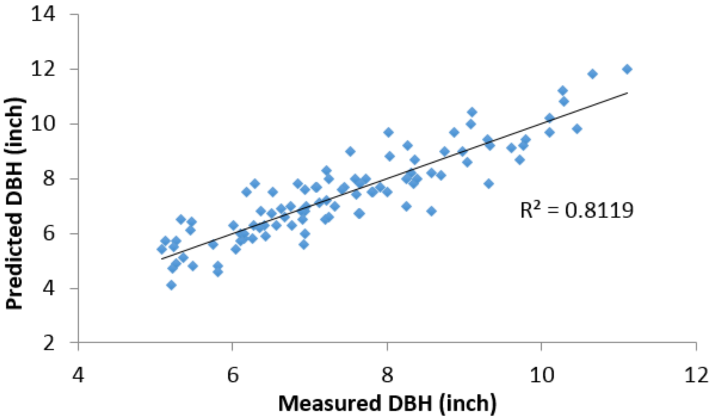

Figure 5.6: DBH prediction result using the approach outlined in the text. The method involved transformation of time-based force data to the frequency domain, calculation of principal components from spectral data, and application of the prediction model.

Table 5.1: DBH prediction results using impact force measurements transformed to the frequency domain. Values shown are for 8 stems reserved for validation of the prediction model built using data from 90 other stems.

Value (inch)	**Tree Number**								
	1	2	3	4	5	6	7	8	Average
Prediction	10.7	7.3	10.3	8.5	5.2	7.6	6.2	7.8	7.95
True DBH	11.8	7.0	10.8	8.2	4.7	7.4	5.8	7.5	7.9
Error	-1.1	0.3	-0.5	0.3	0.5	0.2	-0.4	0.3	0.05

sample, the relative error was less than 1%. The result implied the impact-based sensor was an accurate approach to measure mass of pine chips in real-time. The error sources were possibly from the following three factors: (a) non-uniform impact angle, (b) different impacting locations, and (c) only part of chips impacting the measuring plate.

An experiment was conducted to test if these results calculated for individual trees might be applicable in a production situation in which multiple stems were moving through the chipper on a continuous basis. Fundamental to this analysis was the assumption that the same force response would be seen whether a single stem, or multiple stems, were being chipped as long as the total tree cross-sectional area being fed through the chipper over time were the same. The difference in the two scenarios was the lack of knowledge about when a stem might begin or end its trip through the chipper. In our original tests, data were captured while the entire tree was chipped. In a production setting, the beginning and ending points would vary for each of many stems going through at any one time and it would not be possible to calculate the PSD and subsequent prediction based on the entire, individual-stem force signal. It was felt a discontinuous sampling strategy would be most practical in this scenario, that is, making estimates of mass flow over short bursts of time and accumulating them to predict total mass flow.

Four different sampling strategies were evaluated in these experiments. For each one, the sampling process was applied to the continuous data collected for individual stems, and the resulting DBH calculated using the PC regression model for the (shorter) periods of time covered. All these DBH estimates were then averaged and compared to the global average DBH for all stems. The four sampling strategies were as follows.

1. Continuous sampling over short periods

    a. Two second intervals

    b. Five second intervals

2. Discontinuous sampling

a. Sampling every other second

b. Sampling two seconds, then waiting three seconds

Results were listed in Table 5.2. For continuous sampling (strategies 1a. and 1b. above), all data were contained in the PSD computation and, as might be expected, the global DBH estimate was closer to the true value, differing by less than about 0.3%. For the partial sampling strategies (2a. and 2b. above), there was some loss in accuracy with global DBH estimates differing by about 1.8%, or less, from the true value. The correct approach to use in creating a production mass flow sensor would be related to the practicalities involved in developing the system itself. If the PSD calculations could be done in real time, the continuous strategy would most likely be more accurate in predicting DBH. If it were necessary to store data in order to make the PSD calculation, then the discontinuous approach would perhaps be more suitable with only a slight decrease in total accuracy.

Method Summary

An approach to measure mass flow rate of chips exiting a chipper was presented. The method used a force measurement over time to estimate mass flow. Data were correlated to tree size (and therefore weight) using a prediction model based on the force signal power spectrum. Results showed good agreement between measured and predicted individual tree DBH for the conditions used in these tests. Other experiments indicated the approach would be applicable for continuous measurement of mass flow from multiple stems, but this was not verified in practice. The test also confirmed the method to be feasible for on-line MC sensor.

5.3.2 Combination of Force Sensor and ECT for MC Determination

The impact method successfully measured mass flow for pine chips, therefore a similar system was built with an ECT sensor included for dynamic moisture content estimation. The same 50 lb load sensor was used as in the chipper tests, the sensitivity of which was

Table 5.2: DBH predictions resulting from different subsampling methods. These methods were tested as alternatives to sampling the entire force response for a single tree.

Sampling Methods	**Predicted DBH on Average (inch)**	**True DBH (inch)**
Two second intervals	7.41	7.43
Five second intervals	7.42	
Sampling every other second	7.36	
Sampling 2s then waiting 3s	7.30	

high enough for detecting a single chip. The schematic diagram was as shown in Figure 5.7. The load sensor was attached to a triangular holder below the ECT sensor. When a stream of chips passed through the ECT pipe and hit the sensing metal surface, the capacitance and impact data could be recorded. Since the height between the impact surface and electrode was known, the time delay could be set to make the two sensor data streams (impact and ECT) match. The slope of the impact surface would slightly affect the potential energy of the chips and could introduce some inaccuracies into the force measurements. However, if the surface is placed horizontal or with small slope, the chips would accumulate on the plate and cause even larger errors. The threshold of the angle to prevent this accumulation was about 30 degrees. In the field test, the direction of the chip stream was crucial to fill the truck. The angle of impact surface was designed to be very small so the momentum change did not alter the chip direction much. In this test, the impact angle was about 35 degrees, which resulted in much stronger impact signals.

Sample Preparation

In the following discussion, the term ‘batch’ refers to the batch of chips as discussed in the experiments in Chapter 4. A total of 109 groups of green pine chips were selected randomly, 30 were from batch 2, 10 were from batch 3 and 4, another 60 were newly collected from the same source as batch 3 and 4, and 9 were from batch 5. All samples were prepared in the same manner as in the static sensor measurements, which included being dried in a

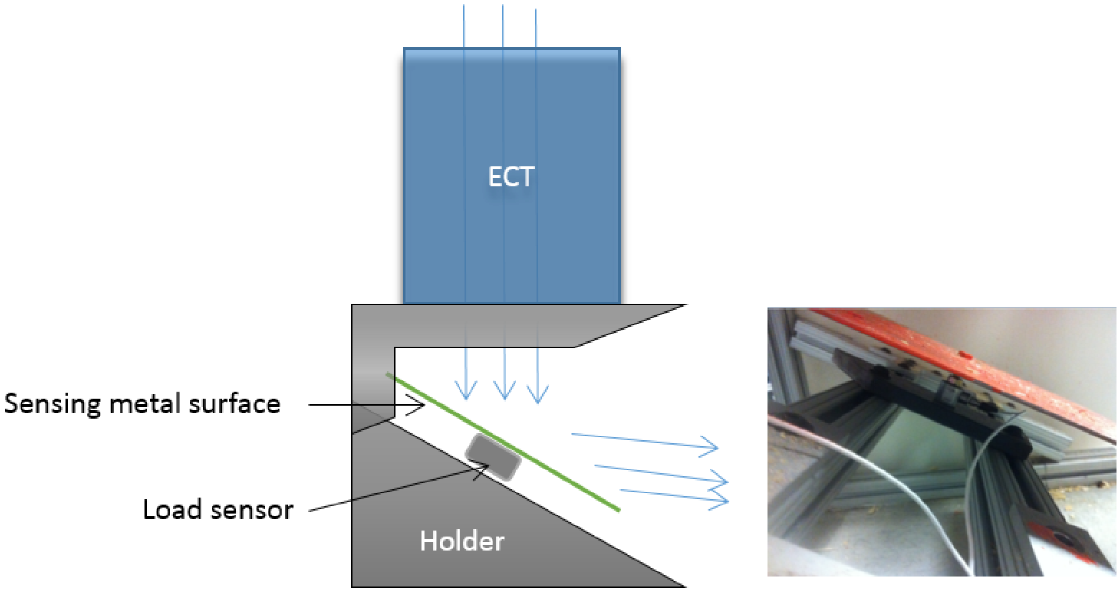

Figure 5.7: Diagram of the force sensor used in predicting mass flow rate, and its relative position to the ECT system.

105°C oven for varying lengths of time to develop a range of MC among the samples (final range was 14.0%-120.0%). Their wet weights were distributed in a wide range (from 267.6 g to 1084.3 g). A total of 60 groups were randomly selected for calibration, and the rest (49) were used in the validation set.

Data Acquisition Methods

Important information which was necessary to know for the test included: weights at both wet and dry states, ECT data, and load cell outputs. The steps in the data acquisition process were listed below.

1. Measured the wet weight of a bulk sample with scale.
2. Placed the chip sample on the conveyor belt arranged in a pile with constant length and width (about 35 cm (L) × 20 cm (W)). The height of sample depended on the chip quantity. For a single bulk sample, the piled height was uniform.

3. Set a fixed time delay between two sensors. Both impact responses and ECT readings were collected with a LABVIEW program. Though a single program could acquire and save data from both load cell and capacitance sensors, the sampling rate of the ECT system would be decreased when added an extra data acquisition task (force measurement) in the measurement loop. Using the same device (NI 6361 for ECT data collection) to sample the signal from the force transducer would also reduce the sampling frequency of the ECT system. For these reasons, a separate LABVIEW program was used to read data from the load cell. The sampling efficiency was improved about 20% using two programs, compared to integration of the two sensors in a single program. The ECT sampling rate was almost the same as when the load cell was not applied. However, two independent programs would have a synchronization problem. The measuring time for both sensors was necessary for data matching. In a single program, they were running concurrently and no time synchronization was necessary, while for two different program it was difficult to match acquitsition times. Thus a fixed time delay was set to control the starting time of both sensors. The data acquisition system for load sensor was run one second prior to that for ECT.

4. Program specifics. As discussed in Chapter 3 (Figure 3.7), a single paired electrode was most sensitive in only a portion of its volume, particularly near the edge. Information for a single chip would be reduced or missed if the sampling rate were low. To collect material information as much as possible, the switching network used One-N mode to sample ECT outputs. The sampling rate was 278.26 kHz (according to the calculation in 3.2.4), sample number was 200 points, and sampling method was N samples (limitation of another faster method were discussed in 3.2.4). The dynamic force sensor was sampled at 10 kHz as in the field tests.

5. Measurement. Procedures were (a) starting two data acquisition programs, (b) turning the handle to drive the conveyor belt with a somewhat constant speed, (c) stop the program and put measured chips back into the oven.
6. MC calculation. Another drying period was about 24 hours after the bulk sample measurements were taken. The dry weight was measured using a scale accurate to 0.01g.

Data Processing Methods

The force data was processed in the same manner as the field test, which included power spectrum calculation (*pwelch* function in MATLAB), PCA (*princomp* function in MATLAB) and stepwise regression (*stepwise* function in MATLAB). 50 PCs, instead of 10 as in the preliminary test, were analyzed using stepwise regression. A total of 5 PCs were selected as being highly correlated with mass at $\alpha = 0.05$. The multiple linear regression (MLR) method was applied to build models between selected PCs and the bulk weight.

The capacitance data was processed using sum mode, to show the combined effect of water and wood. The empty state of ECT was measured as reference data. The difference in sum between bulk and reference data was used as ECT response.

Results and Discussion

Mass flow measuring result. The length of the chip sample piled on the conveyor belt did not vary among measurements (fixed around 35 cm). When the conveyor belt travel rate was constant, the time of the total sample's passage through the sensing area would be the same. In that case, the sample mass would be proportional to the mass flow rate (assuming uniform density of material on the belt). For these experiments, both assumptions were made and only the total sample mass was used as the parameter representing mass flow for any calculation. Figure 5.8 shows the result for calibration and validation data. The RMSEC and RMSEP for the impact mass flow measuring method were 58.15 and 71.17

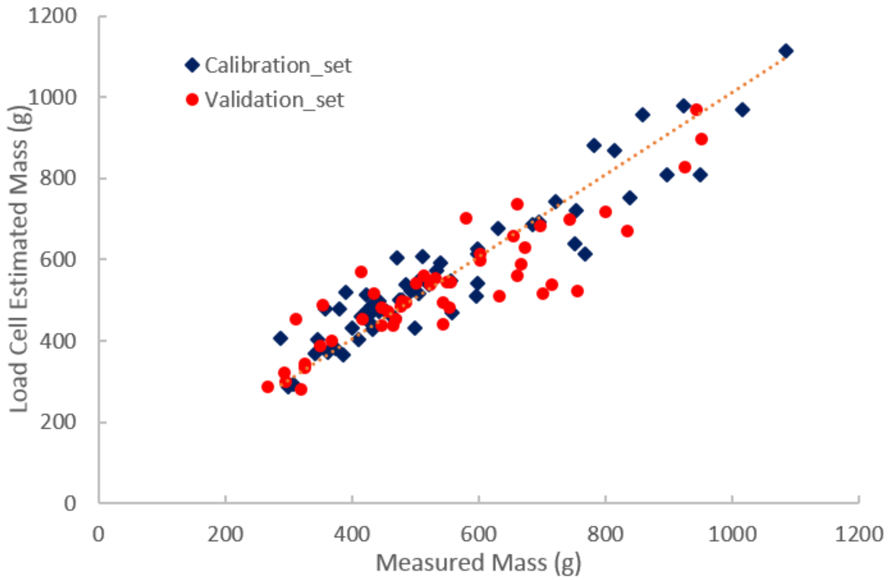

Figure 5.8: Calibration (R^2= 0.86) and validation (R^2=0.72) result of measuring chip mass using the impact method.

grams, respectively. The average weights of calibration and validation sets were 566.13 and 530.46 grams. The relative RMSEC and RMSEP, calculated as RMSE divided by the sample mean, were 10.27 % and 13.42 %, respectively. Both RMSEC and RMSEP increased, compared to the field test, RMSEP of which was 6.61%. Error sources were probably from four factors.

1. Different impact locations for a chip could create significantly different responses. When the chip number was large, e.g.10,000 pieces for a tree as in the field test, the distribution of impact points would be more normal than in small quantity tests, as done here.

2. The slope of impact surface. Though the impact angle in the field test was much bigger than in laboratory, the major source of impact energy was different. As chips exited the chipper, the energy along the moving direction was from a high speed spinning disc inside of the chipper, and the energy imparted to chips, and lost in travel to the spout, would be relatively uniform among all particles. However, the energy of chips

in the laboratory test was mainly from potential energy of the chips falling in the gravitational field. Different falling heights caused by the slope of the impact surface would have more influence than impact location in the field test.

3. Non-uniform feeding rate. The dynamic ECT system was driven manually, causing variation in feeding rate and affecting the energy carried by chips as they impacted the plate, leading to error.

4. Impact surface oscillation. The impact surface used in laboratory tests was a metal sheet. After a chip hit the plate, the signal would have a short ringing period that took some time to disappear.

Dynamic MC Determination Results An ideal real-time moisture sensor would have the capability to show the MC for a short period, such as every second. However, it was difficult to calibrate the MC of a chip stream every second. An appropriate way to test dynamic MC was to use the average of a bulk sample as a single measurement.

Based on equation 4.8 in Chapter 4.1.3, the dynamic MC could be calculated if the weight were known and the response of the ECT system was consistent. One source of inconsistency that could potentially affect readings was thought to be different relative velocity of particles. Because the electric field in the sensor was affected by the distribution of material inside, individual particles moving at non-uniform velocities might change the field sufficiently to introduce variability. The effect of velocity on ECT readings was therefore tested. A small bag of wood powder was measured statically and dynamically, the result of which showed a larger response for dynamic response in sum mode than static measurement. However, in this test, the particle velocity could be assumed constant (as free falling particles). Since the capacitance readings contained the influence of a uniformly moving sample, no extra velocity data was used in the MC measuring model.

Table 5.3: MC prediction results using the dynamic force sensor to estimate mass flow rate.

Method	R^2		RMSEC		RMSEP	
	Calibration	Prediction	Absolute	Relative	Absolute	Relative
True mass	0.82	0.73	10.81%	16.75%	11.07%	15.5%
Estimated mass	0.81	0.71	11.25%	17.43%	11.86%	16.61%

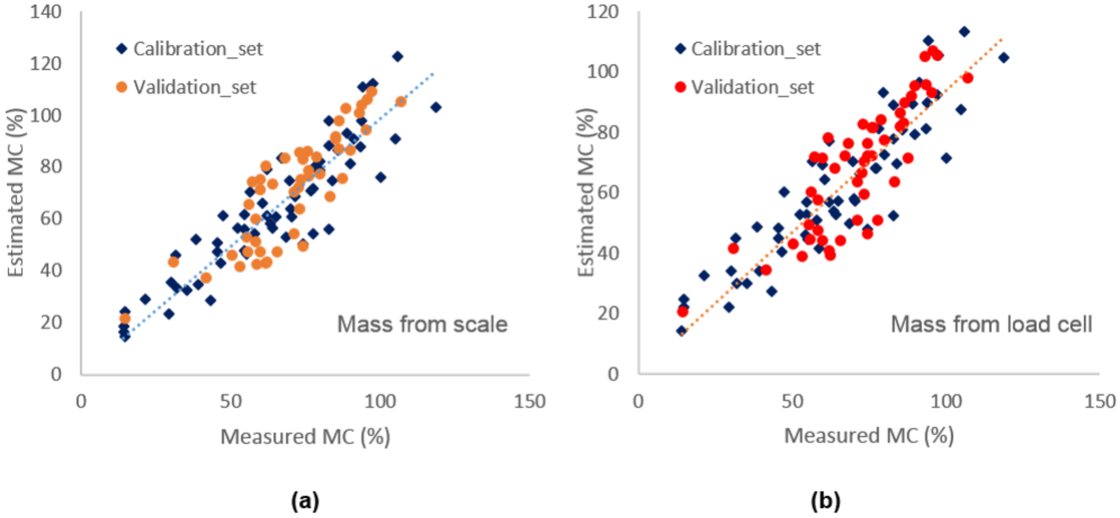

Figure 5.9: Calibration and validation results of MC predictions using mass determined with (a) scale and (b) impact method.

In Figure 5.9, two moisture measuring results were compared, Figure 5.9a using the scale measured weights, and Figure 5.9b included the load cell estimated mass. Results were summarized in Table 5.3.

Though the mass predicted by the force transducer was not extremely accurate, the final MC estimating result was close to the method using a scale to measure the true mass. The difference in error between them was less than 1%. Figure 5.9 directly compared the two methods of both calibration and validation sets, no significant difference was observed between these two datasets. The P-value in Table 5.3 also suggested the two methods had equivalent performance in predicting dynamic MC.

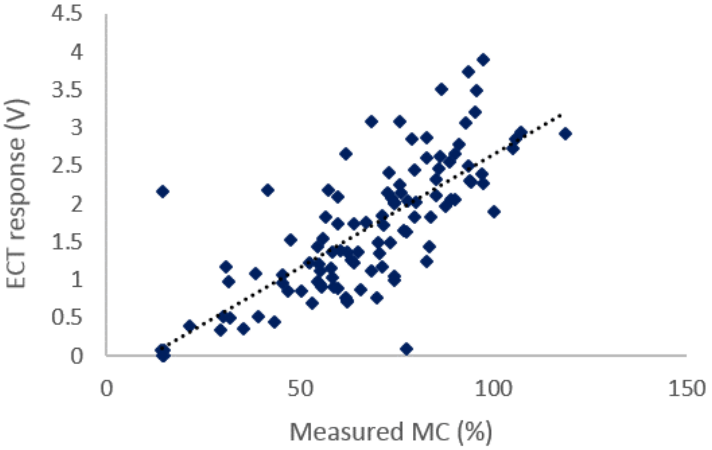

Figure 5.10: Regression result between MC and ECT without any knowledge of the sample weight (R^2=0.56).

Simply based on this result, it was insufficient to conclude that the impact method was useful in predicting MC for pine chips in motion. The mass might have no significant effect on the MC if the stream of chips moving through the sensor were uniform. For the MC prediction model (equation 4.8), statistical analysis showed P-values for V/W and $1/W$ were less than 0.001. The P-value indicated a strong relationship between MC and the mass. If the mass were removed as a factor, the regression plot between MC and ECT reading was as shown in Figure 5.10. RMSEP in that case would exceed 24%.

Based on these results, an impact mass flow combined with capacitance sensing was concluded to be a feasible approach to measure both dynamic mass flow and MC for chips. The impact method has been tested in an actual wood chipping machine, the results of which were better than laboratory experiments. Rather than using the tomographic function, the ECT was employed as a single paired plate capacitance sensor. However, the process still included unnecessary ECT operations, especially the switching network. While measuring different combinations among electrodes, some data was missed due to the slow N-sample method. If replacing the ECT system with a simple capacitance sensor, the sampling method could be made continuous, which could be expected to improve the moisture measuring accuracy. The ECT sensor could also be switched to a simple capacitance mode. Controlling the switching network to excite the electrodes 1-4 as source, and receive data from electrodes 5-8, the ECT system could be approximated as a single paired capacitor. Since no switching action was required, the continuous sampling method could also be applied, which in this case allowed greater than 1 kHz sampling rate (10 Hz for N sample ECT mode). A sensor constructed in this fashion could match the project objective very well.

5.4 ECT MC Measuring Method

Knowledge of the mass flow rate was proven to be a crucial component of dynamic MC measurement. For a practical MC measuring system, a mass flow sensor, such as the force transducer introduced in 5.3, would be a necessary precursor. However, all these possible ways of using an ECT system to measure MC statically or dynamically were merely using its single paired capacitance function, rather than using the full capabilities of ECT, its tomographic mode. In static MC measurement, the quantity of chips under test was normally big enough to cover the entire cross-sectional area of the ECT sensing volume. The image in that case could not provide any useful information related to either MC or mass, except perhaps variation within a vertical column of chips, which would be of dubious value. The sensor applied in this fashion could not separate moisture variation from mass variation. Using imaging, however, the water distribution (or at least between-chip MC distribution) could be observed. In dynamic tests, however, chips occupied only part of the sensing volume at any instant in time. When the velocity of chips was constant, the accumulation of cross sectional area associated with biomass material in tomographic images could possibly be used to represent the total volume of chips passing through, and that be converted to mass using density. Different wood types or different parts of a stem, such as juvenile wood and mature wood, early wood and late wood, tops and stems, inner veneers and outer, have different density. However, the most significant effect on density is moisture content, the dry densities do not vary much. Trees are usually harvested at a fixed age, their

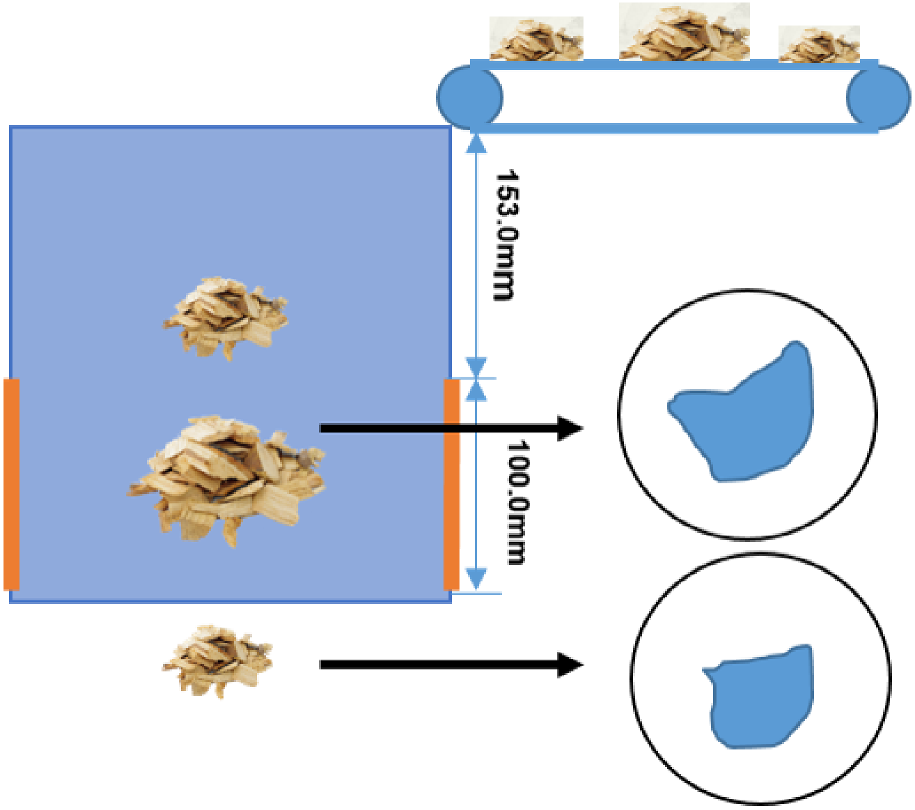

Figure 5.11: ECT mass flow measuring principle.

densities should be relatively uniform, on average. The volume of chipped material in that case could be approximated as their mass. Under this assumption, an ECT sensor would have the capability to measure mass flow and moisture content at the same time, without including any extra device. The schematic diagram of such a system was shown as Figure 5.11. More chips would occupy a larger cross section of the measuring area and this should be observable in an ECT image.

Two essential requirements for measuring mass flow using cross sectional imaging were: (a) high sampling rate to capture images of all flowing material, and (b) images revealed something about the mass currently in the sensor. To understand the requirement of ECT sampling rate, the measuring time for an object was calculated. Suppose the initial velocity was v_0, the distance between conveyor belt and electrodes was h_1, the length of electrode was h_0, then the residence time for wood chips passing through the sensing area could be calculated as equation 5.1.

$$\Delta t = \frac{1}{g}\left(\sqrt{v_0^2 + 2g\left(h_1 + h_0\right)} - \sqrt{v_0^2 + 2gh_1}\right) \tag{5.1}$$

In this experiment, the moving speed of the conveyor belt was slow (about 0.1 m/s), the square of which was significantly smaller than $2gh_1$ (around 3). Equation 5.1 could be approximated as:

$$\Delta t = \frac{1}{g}\left(\sqrt{2g\left(h_1 + h_0\right)} - \sqrt{2gh_1}\right) \tag{5.2}$$

For the designed ECT system, chips would reside in the sensing area for about 0.05 second. The minimum imaging rate of the ECT system should therefore necessarily exceed 20 Hz.

5.4.1 Image Calibration

To calculate the area covered by chips, the easiest way was to convert gray scale images to binary form, consisting of values 0 and 1 representing the presence, or absence, of wood in that portion of the sensor. The summation of all pixels would represent the area, and hence volume, of wood. Image processing procedures used to generate these types of images were as the following.

1. Compute the raw gray scale image from the sensitivity matrix. Use Landweber iteration for a fixed number of times to reduce the pseudo-inverse error.

2. Rescale the gray values of the image. For wood chips under test having different MC, high moisture chips would bend the (soft) electric field more than dryer chips. In order to convert gray scale images to binary, a fixed threshold was required to process all images uniformly and automatically. This conversion forced the need to calibrate images to some scale that could use a constant threshold not affected by moisture significantly. The calibration was done the same way as normalization: acquiring the

maximum and minimum value of the gray scale matrix marked as $G_{\max}$ and $G_{\min}$, the normalized value was:

$$G_n = \frac{G_n - G_{\min}}{G_{\max} - G_{\min}} \tag{5.3}$$

3. Binarization. Applied a fixed threshold (G_t) to all images, as:

$$G_n = \begin{cases} 0 & G_n < G_t \\ 1 & G_n \geq G_t \end{cases} \tag{5.4}$$

4. Sum up all pixels in the binary image. The summation of a single binary image represented the quantity of chips passing through the sensor at that moment. Accumulation of the sum during a period of time, e.g. 1 second, could be used as the mass flow rate.

The remaining problem of the above area determination method was to select an appropriate threshold for the third step. An image calibration method was applied to estimate the unknown threshold. A digital camera was used to record videos of chips falling through the ECT sensor. The basic idea was to find a threshold that made the reconstructed image as close to the real situation as possible.

Five location options for the camera were tested as shown in Figure 5.12a. Positions 1 and 5 had the view least obstructed by chips between the camera location and those within the sensor volume. However, these two locations required a camera having a wider view angle, which was unavailable for these tests. At position 1, the chip stream came very close to the camera location and other chips not close to the camera were difficult to detect. Position 2 had a similar problem, but to a slightly lesser extent. For position 3, only portions (50% or less) of sensor cross-sectional area was viewable. Thus location 4 was chosen as the most appropriate place to install the camera. In this test, a *Logitech* HD Webcam c270 was selected to take videos at 100 frames per second. The results, however, failed to capture the cross-sectional images very well. When chips were fed continuously, the viewing area would be fully covered and obscured, as Figure 5.12b. An alternative calibration method

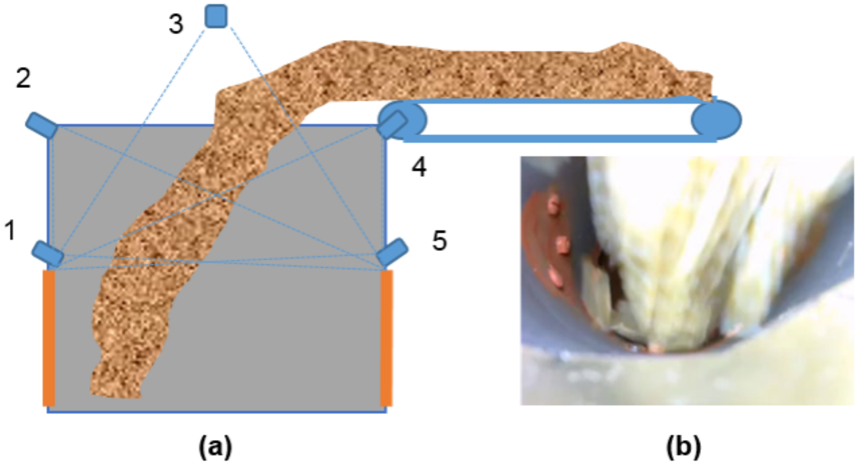

Figure 5.12: Test apparatus for calibrating ECT image volumetric estimates using a video camera. Points 1-5 were the locations evaluated for the camera positions to perform the tests.

was therefore taken that used a reduced quantity of chips - in fact, only a single chip. An very large green chip (38.5g) was chosen and dropped into the ECT singly using the conveyor belt. The camera was installed on the top of the sensor, as location 3. A circular light was placed around the camera to illuminate the measuring pipe.

A fixed, one-second delay was set between the video recording system and the LABVIEW program for ECT. The video record was processed as below.

1. Image extraction. Two images were extracted from each video recorded: one was a background frame (Figure 5.13a), and the other was the chip location within the sensing area (Figure 5.13b).

2. Image processing. This step included two major objectives: one was to measure the area of the sensing space (Figure 5.13c). Procedures used were to convert the color image to gray scale (using the *rgb2gray* function in MATLAB), then setting an appropriate threshold to turn the gray scale image to binary (MATLAB *im2bw* function, threshold set to 0.15), and removing noise areas using open and close operations (*imopen* and *imclose* MATLAB functions within the operating area using a 5×5 probe matrix).

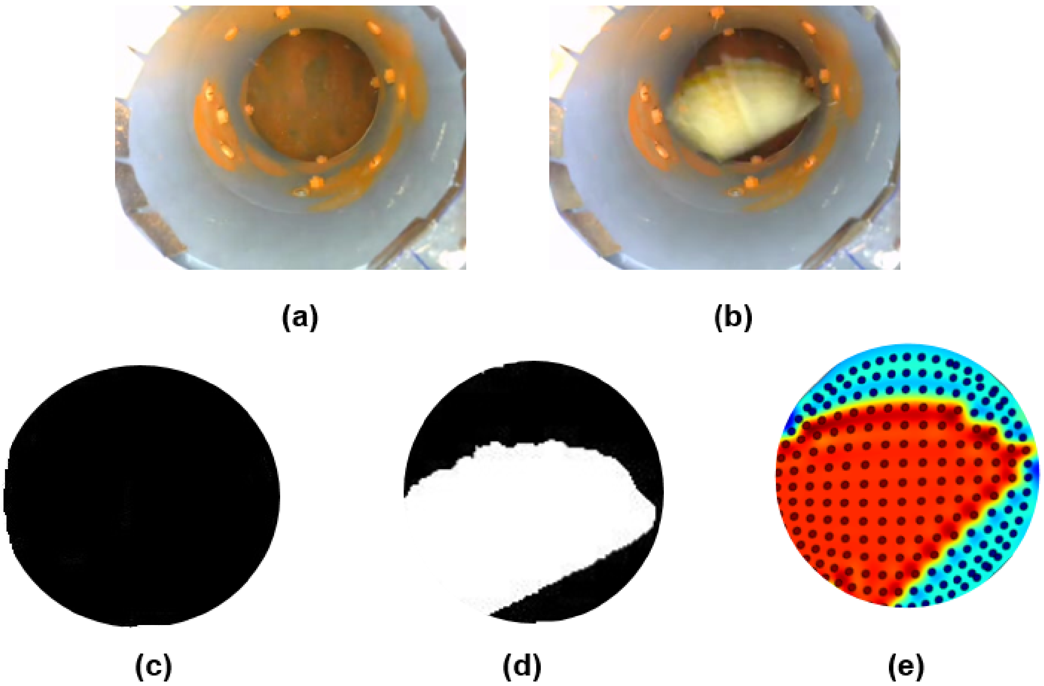

Figure 5.13: An illustration of the sequence of images resulting from the algorithm applied to correlate video and ECT images of a single chip falling through the ECT sensor.

Another was to measure area of chips (Figure 5.13d) in which similar processes were applied except with an additional step. After gray scale conversion, the background image was subtracted from the chip image to remove all background information, leaving the area difference between these two images, which was the chip itself.

3. Calculation. Computed the percentage of chip area, dividing chip area by background area.

The percentage of sensing area covered by the woodchip was calculated as 56.04%. Accordingly, the ECT image should also have the same covered area, which worked out to be a total of 126 pixels (225 pixel resolution) (Figure 5.13e). The test was repeated 5 times, and the threshold was set as the value 0.152 for ECT image processing.

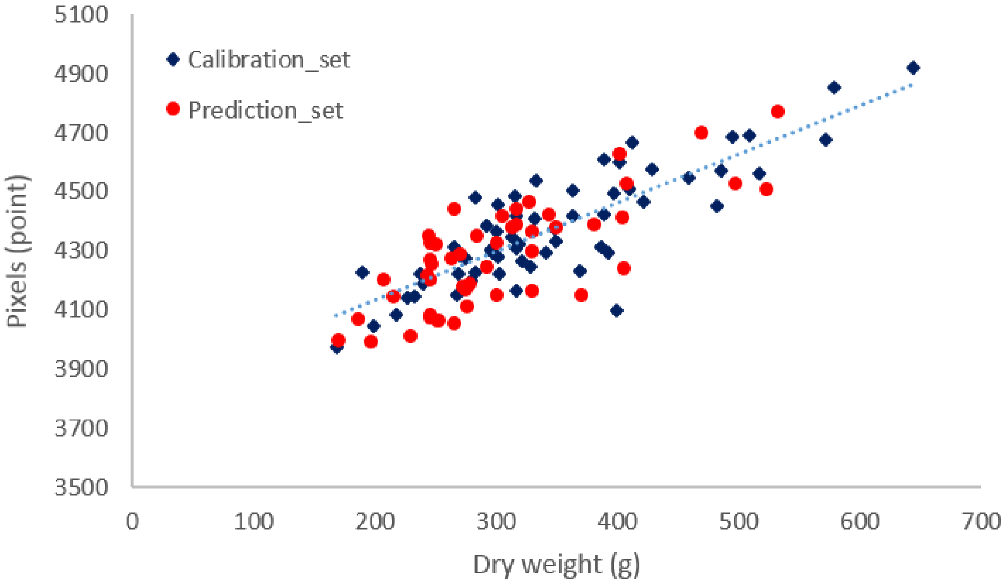

Figure 5.14: Regression result showing the relationship between area occupied in ECT images by wood material and the dry weight of the sample (R_c^2=0.71, R_p^2=0.60).

5.4.2 Mass Flow Measuring Result

These measurements differed from those using the impact mass flow approach in that dry weight, rather than wet, was necessary to predict moisture content. ECT readings of the impact method were directly used for this analysis. The regression result between measured dry weight and pixels on reconstructed image was as shown in Figure 5.14. RMSEC and RMSEP were 62.54 and 69.67 grams, respectively. The average dry weights of calibration and validation sets were 346.25 and 304.36 grams. The relative RMSEC and RMSEP were 18.06 % and 22.89 %. Relative measuring errors were about 1.7 times that of the impact method, though they were measuring weights in different states (wet vs dry). The major reasons for the relative inaccuracy in the predicted results were as follows.

1. Wood chip orientation. As Figure 5.15a, the same chip with different orientation had a significant effect on the cross sectional image. For the method outlined above, the

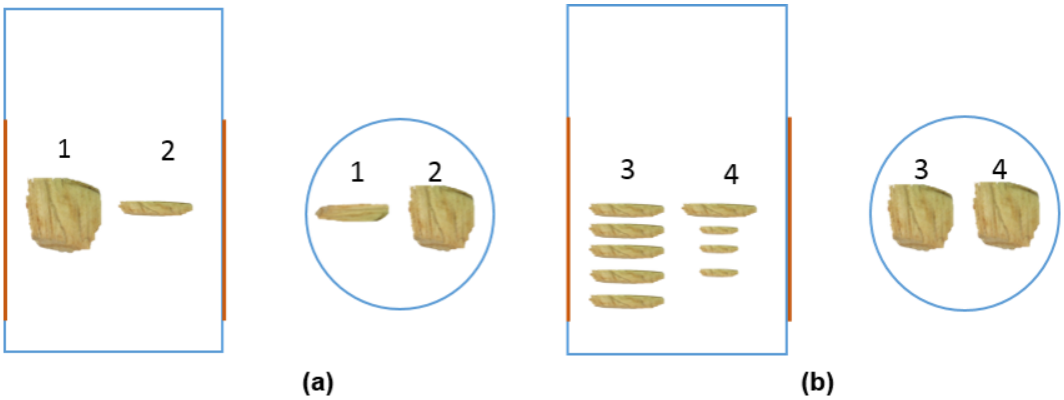

Figure 5.15: Error sources of using image to estimate mass.

moisture content prediction result of orientation 1 would be much higher than 2, while the estimated mass of position 1 was much smaller.

2. Overlap. The measuring volume was about 7.793×10^6 mm^3 and the dimensions of a typical pine chip was about 7.875×10^3 mm^3 (45mm×35mm×5mm), which means hundreds of chips could exist in the sensing area simultaneously. Some of the chips being obscured in the images was unavoidable. An extreme example would be as in Figure 5.15b where both stacks of chips would have the same cross-sectional area from the image. The ECT system would estimate dry matter based on the presumption that samples 3 and 4 had the same volume and the dry matter weights were equal. For a higher capacitance obtained in sample 3 (larger total mass), an inaccurate moisture content prediction, unfortunately, would be made.

3. Insufficient sampling rate. The frame rate of the designed data acquisition software was about 10 Hz. However, the minimum sampling rate was 20 Hz to capture all chips, as noted above.

The first two challenges would be reduced when the quantity of chips increased. The distribution of orientation and overlapping probabilities could be expected to become more normal for a field test, than in laboratory tests with a small sample quantity. The third

Table 5.4: MC measurement accuracy using ECT in tomographic mode to measure both permittivity and mass flow.

Method	R^2		RMSEC		RMSEP	
	Calibration	Prediction	Absolute	Relative	Absolute	Relative
Sum mode and True dry weight	0.76	0.60	10.68%	16.55%	14.18%	19.34%
Sum mode and Tomographic mode	0.71	0.57	12.38%	19.18%	17.71%	24.16%

point, however, would be the limitation of the designed ECT sensor. Neither hardware or software modification could solve the problem.

5.4.3 MC Measuring Result

The image based method was to predict dry mass of wood chips, equation 4.8 could not be applied directly. Going back to the original relationship, equation 4.3, dividing by the dry weight, the equation becomes:

$$\begin{aligned}\frac{V}{W_1} &= \alpha_0 + \beta_0 MC + \frac{\varepsilon_0}{W_1} \\ \text{MC} &= \frac{1}{\beta_0}\frac{V}{W_1} + \frac{\varepsilon_0}{\beta_0}\frac{1}{W_1} + \frac{\alpha_0}{\beta_0}\end{aligned}$$

Letting $\alpha^{'} = \frac{1}{\beta_0}$, $\beta^{'} = \frac{\varepsilon_0}{\beta_0}$, and $\varepsilon^{'} = \frac{\alpha_0}{\beta_0}$, the above becomes

$$\text{MC} = \alpha' \frac{V}{W_1} + \beta' \frac{1}{W_1} + \epsilon' \tag{5.5}$$

The W_1 here was the dry weight, which could be measured or estimated from imaging results. Measuring accuracy was summarized in Table 5.4. Both results were plotted in Figure 5.16.

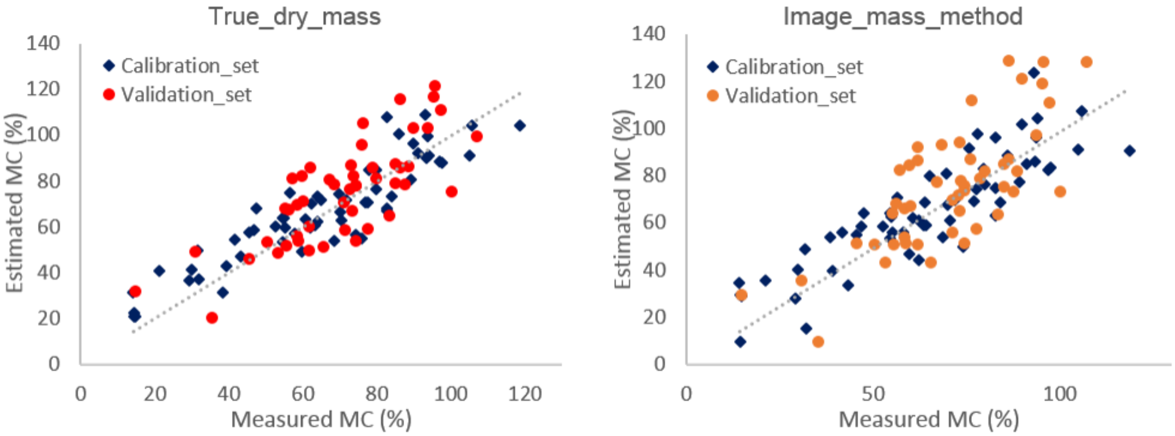

(a) **(b)**

Figure 5.16: MC prediction results for tests (a) using measured dry weight (R^2=0.76), and (b) those using the ECT image processing approach to estimate sample mass (R^2=0.71).

5.4.4 Method Discussion

As presented by Young *et al.* (1996) and Sun *et al.* (2008), measuring the mass information using ECT sensor was accurate and feasible when the particle density was uniform. Though the biomass chips have different densities when their MCs are distinct, their dry densities do not vary much. ECT tomography would have the capability to measure the dry mass. A linear relationship between binary ECT images and the dry weight of wood chips was found in Figure 5.14. However, with the sampling rate limitation, the accuracy was not as reported in the two papers cited above.

The error in measuring dry weight directly affected the MC prediction result, as in Table 5.4. In the impact test, a 13.42% relative error in estimating wet weight led to only about 1% increase in relative error of moisture measurement. The ECT imaging tests, however, resulted in a 22.89% relative error in dry weight, which added 5% relative error to MC estimation. Improvements in the imaging system, especially solving the sampling rate problem, would help ECT achieve better accuracy for dynamic MC determination.

The dry weight measuring method, however, could not provide an equivalent performance with wet weight model. When comparing the data obtained from scale estimates of weight (data for two tests were from the same chip samples), though the calibration result was close, the prediction error of using dry mass was 3% more than wet weight method. This extra error might be from three sources.

1. Water forms. This error source was mentioned in Chapter 4, and was concluded to be an ignorable influence. However, the contribution to capacitance from variation in dry weight was also small. Comparing to the dry mass variation, different effects of bound and free water might be significant. The relationship among ECT, wood and water should be:

   $$V = \alpha_0 W_w + \beta_0 W_f + \gamma_0 W_b + \varepsilon_0 \tag{5.6}$$

   where W_w is weight of dry wood, W_f and W_b are weight of free and bounded water separately. For the dry weight model, γ_0 was approximately equal to β_0 and that added some additional error. In the wet weight model as 4.5, it could be expressed as:

   $$V = \alpha_1 (W_w + W_f + W_b) + \beta_1 W_f + \varepsilon_0 \tag{5.7}$$

   $$V = \alpha_1 W_w + (\alpha_1 + \beta_1) W_f + \alpha_1 W_b + \varepsilon_0 \tag{5.8}$$

   The different slopes of bounded and free water might reduce the error compared to the dry mass model.

2. Interactions. Though the interaction between wet weight and water weight was found to be insignificant in the model for the parallel-plate ECT readings (Chapter 4), the interaction between dry weight and water was left out in deriving equation 5.5. Interactions from dry weight/water and wet weight/water were tested using the ECT readings, the P-values of which were found to be 0.1019 and 0.1132, respectively. Though both of them were not significant (95% confidence interval), the interaction between dry weight and water was slightly stronger than that for wet weight. Thus ignoring the

interaction term would probably affect the dry weight model more than the wet weight version.

3. Weight lost. Chips were transported from the conveyor belt to the ECT, impact surface, and finally collected by a plastic container. During that process, a portion of the small wood pieces/ powder was possibly not recovered. A non-uniform loss in weight between tests would increase the measuring error.

Though the final results for the ECT moisture predicting method were not very accurate, the method was proven as a feasible way to measure mass flow, moisture or maybe other components for dynamic biomass/bioproducts. The ECT sensor as built would have the capability to distinguish chips with big differences in MC and mass, or to tell the possible range of chip sample MC. However, dynamic sampling of MC distributed in a narrow range would be difficult to implement using the ECT sensor alone.

5.5 Conclusion

In this Chapter, two dynamic moisture determining methods were presented. One was the combined impact and capacitance method, another used ECT tomographic mode by itself. As weight information was crucial to MC prediction using the capacitance sensor, the basic principles for the two methods were to predict wet weight using a force sensor, and to predict dry mass from cross sectional images reconstructed from ECT data, respectively.

Both methods were feasible solutions to measure MC of moving biomass. The prediction result from the impact method achieved a higher accuracy than ECT measurement alone. Possible reasons were discussed. Since it introduced one more sensor and extra design work, the impact/capacitance method was more expensive than the ECT system. The combination of two sensors also required setting an appropriate time delay to match the two data sequences. However, if the velocity of chips were not constant, the delay would be difficult to determine, possibly increasing the measuring error. But if the velocity was constant, the method would be easier to use and modify. The ECT system did not have the measuring time issue. No extra structure was necessary to make it work. However the range of factors, and their interactions, affecting accuracy was complex. For example, the threshold to extract area information (and, hence, dry weight) might be changing with environmental factors such as humidity. As concluded in Chapter 4, the choice of sampling systems will be specific to an application and its operating conditions.

Chapter 6

CONCLUSION AND FUTURE WORK

Variation in MC has been identified as a potential problem in sourcing biomass for a conversion facility, both in deciding on a price for feedstocks and in control of the conversion process itself. A practical moisture sensor meeting the constraints required in this application would imply a system capable of measuring water content in moving streams of biomass, and one that is efficient and capable of operating without the necessity of additional handling of the material. As a step towards this end, we have begun development of a moisture measurement system (based on electrical capacitance tomography, ECT) the design of which we feel could be adapted to sensing water content of chips produced by an in-woods chipper and measured as they were being blown into a van.

6.1 Conclusion

In comparing ECT with other moisture sensing technologies, including X-ray, microwave, acoustic wave, radio frequency, and NIR, the ECT sensor was concluded as being rapid, robust and low cost and the method should be adaptable to dynamic measurements on wood chips. In this dissertation, an 8 electrode ECT system was built to measure MC of pine chips in both static (non-moving samples) and dynamic modes.

6.1.1 Hardware and Software

Creation of the sensor involved development of several key hardware components, and chief amongst those was a capacitance-to-voltage transducer. The transducer built for this work was based on circuits reported in other ECT applications and used a low-pass filtering approach tuned to the needs of this sensor. Operation of the transducer involved cycling among 28 different combinations of electrodes and a switching network was necessary to control the state of each electrode. The design of this network was driven by the need to minimize stray capacitance in the system. Multiple strategies were applied to stabilize power variations and minimize noise in all components. Results of tests on the system indicated it was a reliable and stable tool for capacitance measurements.

Capacitance measurements using the sensor required detecting the amplitude of a periodic waveform output by the capacitance-to-voltage circuits. Many approaches to measuring this amplitude were tried, including hardware detectors (envelope detection), and software methods based on sampling the waveform. Many of the methods, however, introduced spurious or biased elements into the output signal and were rejected. The final methods for amplitude detection chosen were based on two signal processing strategies: power spectral estimation, and autocorrelation. Both worked well, but the correlation approach achieved the highest precision in results.

Four different strategies for cycling among readings between the 8 electrodes were investigated, each having advantages and disadvantages. These sampling 'modes' affected accuracy and stability of the measurement circuits, but also influenced the rate at which measurements could be taken, which was a crucial limitation in later application of the ECT sensor in imaging applications. Based on numerous tests, a single source-single detector approach was found to be the mode having the least negative impact on system reliability and accuracy, but it was also the slowest. A second approach, single source-multiple detector mode, was quicker, but its sensitivity in detecting test material permittivity was lower. That approach was also unique and not previously found in the ECT literature.

The unique capability of ECT was its ability to generate maps of permittivity within an enclosed space. Imaging methods were developed for this research that were compatible with the types of measurements and speed requirements of this application. Techniques employed included Linear Back Projection for image reconstruction, plus a Landweber iterative method to refine images based on a mean-squared error protocol. The LBP approach was based on an estimate of the charge distribution within the sensor, and this estimate, called a sensitivity matrix, was calculated using a simulation generated using Ansys.

6.1.2 System Characteristics

The following tests of the performance of the sensor were conducted to verify its accuracy under controlled conditions.

1. Empty and full (wood chips) states of the ECT system were tested and the responses of all electrode combinations followed very well what the theory of capacitance suggested. In these measurements, it was observed the full state increased ECT readings about 13.0% above the background.

2. Repeatability tests for empty and full states indicated the ECT as designed had acceptably low noise present in readings. The minimum SNR for both states was 36.6.

3. Sensitivities for water, dry and green wood were measured. Results showed that the sensor had the capability to detect small objects, the size of which depended on the material's permittivity. Sensitivities to the same object in central and edge areas within the sensor were found to be different.

4. Though statistical analysis showed no significant difference (at 95% confidence interval) among readings taken at 15 different locations within the sensing volume, readings from the sensor's central area were uniformly smaller than those from the edges for the same object. A normalization method was introduced, the result of which reduced the difference between readings based on object location.

5. No significant difference was found in sensor output among three different dry wood samples having the same weight but different particle size distributions.

6. According to the requirements of two different data acquisition methods, two distinct sensitivity matrices were computed to implement the LBP image reconstruction

algorithm. Results derived from application of the methods (including Landweber iteration) showed that images of permittivity of wet and dry wood chips, plus PVC rods of various sizes, were accurate in the sense they reproduced the spatial structure and relative cross-sectional area of the samples as expected. Methods for real-time reconstruction of images for later ECT tests were developed, but were somewhat limited in frame rate because of limitations with sampling inherent in the ECT system.

6.1.3 Capability in Static MC Determination

Static measurements were made using the ECT system as effectively a single paired electrode capacitance sensor. A linear relationship between ECT output and weight of materials tested was observed. For pine chips, no significant interaction was observed between water and wood weights (both dry and wet state). A MC prediction model was derived and its parameters estimated based on the observed results.

Compared to the traditional NIR method, ECT achieved a better performance in measuring MC for bulk chips. However, the method failed to estimate the moisture for single chips accurately, due to the sensitivity issue. Though the ECT measurement was very fast, it required knowing the mass independently in order to estimate MC.

Two mass free methods were discussed. A dual frequency method was more accurate than an approach using a fixed sample volume. However, its sampling time was doubled.

6.1.4 Dynamic MC Measuring Methods

Knowledge of sample mass was required in all static estimates of MC, but it was impossible to measure mass using a normal scale in a dynamic application of the ECT sensor. Neither was it feasible to implement the mass-free estimation approaches developed for static tests. A mass flow sensor was therefore necessary in MC prediction of moving samples. A simple and robust method was to use an impact method to predict mass flow rate in concert with ECT estimates of moisture. Both field and laboratory tests indicated a load cell could be effectively used to measure mass flow accurately for pine chips. By combining the capacitance system with the force sensor, both mass flow and MC were determined.

The tomographic mode of ECT was also investigated as a possible means to measure the mass flow of solid materials. A volumetric method was used to estimate the dry mass of wood chips using the images generated with the ECT sensor. The cross-sectional permittivity images were calibrated using video images captured simultaneously of the actual flow through the ECT. An appropriate threshold was estimated to minimize the difference between reconstructed images and the real picture. Based on dry mass and capacitance, MC was measured, accuracy of which was 3% lower than the impact mass flow method. There might be weak interaction between dry mass and water that influenced the ECT readings. The ECT result, however, could definitely be improved by increasing the sampling rate.

Overall, the ECT sensor was shown to be a feasible way to measure MC for dynamic wood chip flows with acceptable accuracy. Comparing to the impact and capacitance methods, the ECT could also provide a real-time status and location of material within the measuring area. An extra application of ECT could be as a system failure check, for example, if the flow structure within a conveyance were indicative of a plugged conduit.

6.2 Future Work

The feasibility of using the ECT sensor to measure MC was well supported, the remaining hurdle limiting its application is accuracy. Future work should mainly focus on approaches to enhance system accuracy.

The most important point would be to increase the sampling rate. Much of the limitation in sampling speed with the current system was due to the software estimation of the output voltage amplitude in estimating capacitance. Switching to some kind of hardware detection would be a relatively simple and effective means of speeding up that process. Three simple options for doing that might be the following. Option (1): the AC/DC transducer introduced by Yang and York (1999) was a good way to improve sampling rate. Other amplitude extracting ICs, such as the AD 636 (true rms-to-DC converter), may also good to reduce the time cost of the ECT measuring period (28 readings). Option (2): If the AC/DC transducer has limitations, a new data processing algorithm will be worked on to extract useful information from the continuous sampling method. Option (3): Use another development environment, such as C++ , that should be much faster than LABVIEW in acquiring data and controlling switches.

A re-designed PCB layer, along with revised electrodes should also be considered. The cost of making a flexible PCB that would put encircle the sensor with the measurement electronics is about $900 for this ECT sensor. However, this approach in mounting the electronics provides more uniform and accurate locations of electrodes than the designed sensor. A driven guard is also a research direction to reduce errors by limiting noise side effects. It might also be included in the flexible PCB.

New methods, as in (Sun *et al.* 2008), will be tried using another single paired capacitance sensor. Different frequency excitation as in (Kandala & Sundaram 2010, Kandala & Puppala 2012) will be used in the modified sensor (and ECT) to measure MC and mass flow simultaneously. A 3-dimensional ECT sensor may also be a solution.

Another important connotation of this work will be testing an improved ECT sensor on other materials, such as corn or other cereal grains, for MC and mass flow. and dynamic modes.

6.2.1 Hardware and Software

Creation of the sensor involved development of several key hardware components, and chief amongst those was a capacitance-to-voltage transducer. The transducer built for this work was based on circuits reported in other ECT applications and used a low-pass filtering approach tuned to the needs of this sensor. Operation of the transducer involved cycling among 28 different combinations of electrodes and a switching network was necessary to control the state of each electrode. The design of this network was driven by the need to minimize stray capacitance in the system. Multiple strategies were applied to stabilize power variations and minimize noise in all components. Results of tests on the system indicated it was a reliable and stable tool for capacitance measurements.

Capacitance measurements using the sensor required detecting the amplitude of a periodic waveform output by the capacitance-to-voltage circuits. Many approaches to measuring this amplitude were tried, including hardware detectors (envelope detection), and software methods based on sampling the waveform. Many of the methods, however, introduced spurious or biased elements into the output signal and were rejected. The final methods for amplitude detection chosen were based on two signal processing strategies: power spectral estimation, and autocorrelation. Both worked well, but the correlation approach achieved the highest precision in results.

Four different strategies for cycling among readings between the 8 electrodes were investigated, each having advantages and disadvantages. These sampling 'modes' affected accuracy and stability of the measurement circuits, but also influenced the rate at which measurements could be taken, which was a crucial limitation in later application of the ECT sensor in imaging applications. Based on numerous tests, a single source-single detector approach was found to be the mode having the least negative impact on system reliability and accuracy, but it was also the slowest. A second approach, single source-multiple detector mode, was quicker, but its sensitivity in detecting test material permittivity was lower. That approach was also unique and not previously found in the ECT literature.

The unique capability of ECT was its ability to generate maps of permittivity within an enclosed space. Imaging methods were developed for this research that were compatible with the types of measurements and speed requirements of this application. Techniques employed included Linear Back Projection for image reconstruction, plus a Landweber iterative method to refine images based on a mean-squared error protocol. The LBP approach was based on an estimate of the charge distribution within the sensor, and this estimate, called a sensitivity matrix, was calculated using a simulation generated using Ansys.

6.2.2 System Characteristics

The following tests of the performance of the sensor were conducted to verify its accuracy under controlled conditions.

1. Empty and full (wood chips) states of the ECT system were tested and the responses of all electrode combinations followed very well what the theory of capacitance suggested. In these measurements, it was observed the full state increased ECT readings about 13.0% above the background.

2. Repeatability tests for empty and full states indicated the ECT as designed had acceptably low noise present in readings. The minimum SNR for both states was 36.6.

3. Sensitivities for water, dry and green wood were measured. Results showed that the sensor had the capability to detect small objects, the size of which depended on the material's permittivity. Sensitivities to the same object in central and edge areas within the sensor were found to be different.

4. Though statistical analysis showed no significant difference (at 95% confidence interval) among readings taken at 15 different locations within the sensing volume, readings from the sensor's central area were uniformly smaller than those from the edges for the same object. A normalization method was introduced, the result of which reduced the difference between readings based on object location.

5. No significant difference was found in sensor output among three different dry wood samples having the same weight but different particle size distributions.

6. According to the requirements of two different data acquisition methods, two distinct sensitivity matrices were computed to implement the LBP image reconstruction algorithm. Results derived from application of the methods (including Landweber iteration) showed that images of permittivity of wet and dry wood chips, plus PVC rods of various sizes, were accurate in the sense they reproduced the spatial structure and

relative cross-sectional area of the samples as expected. Methods for real-time reconstruction of images for later ECT tests were developed, but were somewhat limited in frame rate because of limitations with sampling inherent in the ECT system.

6.2.3 Capability in Static MC Determination

Static measurements were made using the ECT system as effectively a single paired electrode capacitance sensor. A linear relationship between ECT output and weight of materials tested was observed. For pine chips, no significant interaction was observed between water and wood weights (both dry and wet state). A MC prediction model was derived and its parameters estimated based on the observed results.

Compared to the traditional NIR method, ECT achieved a better performance in measuring MC for bulk chips. However, the method failed to estimate the moisture for single chips accurately, due to the sensitivity issue. Though the ECT measurement was very fast, it required knowing the mass independently in order to estimate MC.

Two mass free methods were discussed. A dual frequency method was more accurate than an approach using a fixed sample volume. However, its sampling time was doubled.

6.2.4 Dynamic MC Measuring Methods

Knowledge of sample mass was required in all static estimates of MC, but it was impossible to measure mass using a normal scale in a dynamic application of the ECT sensor. Neither was it feasible to implement the mass-free estimation approaches developed for static tests. A mass flow sensor was therefore necessary in MC prediction of moving samples. A simple and robust method was to use an impact method to predict mass flow rate in concert with ECT estimates of moisture. Both field and laboratory tests indicated a load cell could be effectively used to measure mass flow accurately for pine chips. By combining the capacitance system with the force sensor, both mass flow and MC were determined.

The tomographic mode of ECT was also investigated as a possible means to measure the mass flow of solid materials. A volumetric method was used to estimate the dry mass of wood chips using the images generated with the ECT sensor. The cross-sectional permittivity images were calibrated using video images captured simultaneously of the actual flow through the ECT. An appropriate threshold was estimated to minimize the difference between reconstructed images and the real picture. Based on dry mass and capacitance, MC was measured, accuracy of which was 3% lower than the impact mass flow method. There might be weak interaction between dry mass and water that influenced the ECT readings. The ECT result, however, could definitely be improved by increasing the sampling rate.

Overall, the ECT sensor was shown to be a feasible way to measure MC for dynamic wood chip flows with acceptable accuracy. Comparing to the impact and capacitance methods, the ECT could also provide a real-time status and location of material within the measuring area. An extra application of ECT could be as a system failure check, for example, if the flow structure within a conveyance were indicative of a plugged conduit.

6.3 Future Work

The feasibility of using the ECT sensor to measure MC was well supported, the remaining hurdle limiting its application is accuracy. Future work should mainly focus on approaches to enhance system accuracy.

The most important point would be to increase the sampling rate. Much of the limitation in sampling speed with the current system was due to the software estimation of the output voltage amplitude in estimating capacitance. Switching to some kind of hardware detection would be a relatively simple and effective means of speeding up that process. Three simple options for doing that might be the following. Option (1): the AC/DC transducer introduced by Yang and York (1999) was a good way to improve sampling rate. Other amplitude extracting ICs, such as the AD 636 (True rms-to-DC converter), may also good to reduce the time cost of the ECT measuring period (28 readings). Option (2): If the AC/DC transducer has limitations, a new data processing algorithm will be worked on to extract useful information from the continuous sampling method. Option (3): Use another development environment, such as C++ , that should be much faster than Labview in acquiring data and controlling switches.

A re-designed PCB layer, along with revised electrodes should also be considered. The cost of making a flexible PCB that would put encircle the sensor with the measurement electronics is about $900 for this ECT sensor. However, this approach in mounting the electronics provides more uniform and accurate locations of electrodes than the designed sensor. A driven guard is also a research direction to reduce errors by limiting noise side effects. It might also be included in the flexible PCB.

New methods, as in (Sun et al 2008), will be tried using another single paired capacitance sensor. Different frequency excitation as in (Kandala & Sundaram 2010, Kandala & Puppala 2012) will be used in the modified sensor (and ECT) to measure MC and mass flow simultaneously. A 3-dimensional ECT sensor may also be a solution.

Another important connotation of this work will be testing an improved ECT sensor on other materials, such as corn or other cereal grains, for MC and mass flow.

Bibliography

[1] Abdelrahman M.A., Sheta AF., Deabes W.A. 2009. Fuzzy mathematical modeling for reconstructing images in ECT of manufacturing processes. Computer Engineering & Systems. ICCES 2009. International Conference on, 461-468.

[2] Adepipe,O.E., Dawson-Andoh, B. 2008. Predicting moisture content of yellow-poplar veneer using near infrared spectroscopy. Forest Products Journal, 58(4): 28.

[3] Amoodeh, M.T., Khoshtaghaza M. H., Minaei, S. 2006. Acoustic on-line grain moisture meter. Computers and Electronics in Agriculture, 52 (1-2): 71-78.

[4] Angelovski A., Penirschke A., Jakoby R. 2011. CRLH-mass flow detector array for cross-sectional detection of inhomogeneous distributed flow regimes in pipelines. Microwave Conference (EuMC), 2011 41st European, 611-614.

[5] Arko A, Waterfall RC, Beck MS. 1999. Development of electrical capacitance tomography for solids mass flow measurement and control of pneumatic conveying systems. 1st World congress on industrial process tomography. 140-146.

[6] Axrup L., Markides K., Nilsson T. 2000. Using miniature diode array NIR spectrometers for analyzing wood chips and bark samples in motion. Journal of Chemometrics, 14: 561-572.

[7] Barale P.J., Fong C.G., Green M.A., Luft P.A., McInturff A.D., Reimer J.A., Yahnke M. 2002. The use of a permanent magnet for water content measurements of wood chips. Applied Superconductivity, IEEE Transactions on, 12 (1): 975-978.

[8] Birchall I., Spencer J.M., Tanner P.H. 1970. The measurement of transient mass flow rate in a gas using an ionization method. Review of Scientific Instruments, 41 (5): 782-783.

[9] Birrell S.J., Sudduth K.A., Borgelt S.C. 1996. Comparison of sensors and techniques for crop yield mapping. Computers and Electronics in Agriculture, 14(2-3): 215-233.

[10] Bochner S., Chandrasekharan K. 1949. Fourier Transforms, Princeton University Press.

[11] Boyarskii D. A., Tikhonov V. V., Komarova N. Y. 2002. Model of dielectric constant of bound water in soil for applications of microwave remote sensing. Progress in Electromagnetics Research, PIER 35, 251269.

[12] Brace J.G., Sanfelippo T.S., Joshi S.G. 1989. Mass flow sensing using surface acoustic waves. Ultrasonics Symposium, 1989. Proceedings, 1: 573-578.

[13] Brink M. Mandenius, CF., Skoglund, A. 2010. On-line predictions of the aspen fibre and birch bark content in unbleached hardwood pulp, using NIR spectroscopy and multivariate data analysis, Chemometrics and Intelligent Laboratory Systems, 103: 53-58.

[14] Bull, C. R. 1991. Wavelength selection for near-infrared reflectance moisture meters. Journal of Agricultural Engineering Research, 49(0): 113-125.

[15] Carter R.M., Yan Y. 2005. An instrumentation system using combined sensing strategies for online mass flow rate measurement and particle sizing. Instrumentation and Measurement, IEEE Transactions on, 54(4): 1433-1437.

[16] Chen DY., Shao L., Zhang Z., Yu XY. An image reconstruction algorithm based on artificial fish-swarm for electrical capacitance tomography system. Strategic Technology (IFOST), 2011 6th International Forum on, 2: 1190-1194.

[17] Chen DY., Tang WM., Wang LL., Yu XY. 2007. Hardware design and system calibration for electrical capacitance tomography system. Mechatronics and Automation. ICMA 2007. International Conference on, 3088-3093.

[18] Chen Y., Zhang J., Chen DY. 2009. Two-phase flow parameters measurement and Gauss-Newton image reconstruction algorithm for Electrical Capacitance Tomography. Industrial Mechatronics and Automation. ICIMA 2009. International Conference on, 192-195.

[19] Corluka, V., Filic, M., Mesic, M., Valter, Z. 2004. Near infrared based moisture meter. Electronics in Marine. Proceedings Elmar 2004. 46th International Symposium, 412-417

[20] Deans S.R. 1983. The Radon Transform and Some of Its Applications, New York: John Wiley & Sons.

[21] Defo M, Taylor AM, Bond B. 2007. Determination of moisture content and density of fresh-sawn red oak lumber by near infrared spectroscopy. Forest Products Journal. 57(5): 68.

[22] Demers A.M., Gosselin R., Simard J.S., Abatzoglou N. 2012. In-line Near Infrared Spectroscopy Monitoring of Pharmaceutical Powder Moisture in a Fluidized Bed Dryer: an Efficient Methodology for Chemometric Model Development, Canadian Journal of Chemical Engineering, 90, 299-303.

[23] Digman, M. F., Shinners, K. J. 2008. Real-time moisture measurement on a forage harvester using near-infrared reflectance spectroscopy. Transactions of the ASABE, 51(5), 1801-1810.

[24] Dong F., Xu YB., Hua L., Wang HX. 2006. Two methods for measurement of gas-liquid flows in vertical upward pipe using dual-plane ERT system. Instrumentation and Measurement, IEEE Transactions on, 55(5): 1576-1586.

[25] Enoksson P., Stemme G., Stemme E. 1996. A Coriolis mass flow sensor structure in silicon. Micro Electro Mechanical Systems, MEMS '96, Proceedings. An Investigation of Micro Structures, Sensors, Actuators, Machines and Systems. IEEE. The Ninth Annual International Workshop on, 156-161.

[26] Guo ZH,, Shao FQ., Lv DC. 2009. New calculation method of sensitivity distribution for ECT. Chinese Journal of Scientific Instrument, 30(10): 2023-2026 (in Chinese).

[27] Han J., Dong F. 2009. Mass flow rate measurement of Gas/liquid two-phase flow in horizontal pipe based on V-cone flow meter and adaptive wavelet network. Instrumentation and Measurement Technology Conference, 2009. I2MTC '09. IEEE, 1391-1396.

[28] Hanson C., Kelly D. 1998. Radio-frequency moisture determination of composite board products. Proceedings of the 1998 32nd International Particleboard/Composite Materials Symposium.

[29] Hansson L., Lundgren N., Antti A.L., Hagman O. 2005. Microwave penetration in wood using imaging sensor. Measurement, 38: 15-20.

[30] Huang SM., Plaskowski AB., Xie CG., Beck MS. 1988. Capacitance-based tomographic flow imaging system. Electronic letters. 24(7): 418-419.

[31] Huang YM., Zhang HJ., Sun ZQ. 2003. Measurement of mass flow rate using a vortex flowmeter. Sensors, 2003. Proceedings of IEEE, 1: 344-347.

[32] Huang ZY., Wang BL., Li HQ. 2003. Dynamic voidage measurements in a gas solid fluidized bed by electrical capacitance tomography. Chemical Engineering Communications, 190(10): 1395-1410.

[33] Jacobs T., Gomide A., Kaspereit M., Zeyer K.P., Kienle A., Hauptmann P. 2007. Inline analysis of chemical reactions in micro reactors using thermal mass flow sensors. EUROCON, 2007. The International Conference on "Computer as a Tool", 571-574.

[34] James W.L. 1998. Electric moisture meters for wood. Gen. Tech. Rep. FPL-GTR-6. Madison, 17p.

[35] Jenny N. Rapid measurements of the moisture content of biofuel. 2006. Mlardalen University Press Dissertations (Sweden), NO.24.

[36] Jensen PD, Hartmann H, Bhm T, Temmerman M, Rabier F, Morsing M. 2006. Moisture content determination in solid biofuels by dielectric and NIR reflection methods. Biomass and bioenergy. 30(11): 935-943.

[37] Jiang GW., Qiu BJ. 2011. Discrete element method simulation of impact-based measurement of grain mass flow. Computer Distributed Control and Intelligent Environmental Monitoring (CDCIEM), 2011 International Conference on, 419-422

[38] Jiang J., Wang HX. 2009. Electrical Capacitance Tomography system used in two-phase flow monitoring. Journal of test and measurement technology, 23(6): 540-544.

[39] Johana E., Yunus F.R.M., Rahim R.A., Seong C.K. 2011. Hardware development of electrical capacitance tomography for imaging a mixture of water and oil. Hurnal Teknologi, 54:425-442

[40] Johansson J. 2001. Property predictions of wood using microwaves. Licentiate thesis. Sweden: Department of Chemistry, Umea University, 1402-1757.

[41] John Deere HarvestLab. Sensor information management [Internet]. [Cited 2014 May 20]. Available from: *http* : $//www.deere.com/wps/dcom/en_{U}S/products/equipment/ag_{m}anagement_{s}olutions/information_{m}a$

[42] Kandala CV, Puppala N. 2012. Parallel-plate capacitance sensor for nondestructive measurement of moisture content of different types of wheat. Sensors Applications Symposium (SAS). 1-5.

[43] Kandala CV, Sundaram J. 2010. Nondestructive measurement of moisture content using a parallel-plate capacitance sensor for grain and nuts. Sensors Journal. 10(7): 1282-1287.

[44] Karim N.B.A., Bin I.I. 2011. Soil moisture detection using electrical capacitance tomography (ECT) sensor. Imaging Systems and Techniques (IST). 83-88.

[45] Kupnik M., Schroder A., O'Leary P., Benes E., Groschl M. 2004. An ultrasonic transit-time gas flowmeter for automotive applications. Sensors, 2004. Proceedings of IEEE, 1: 451-454.

[46] Lei J., Liu S., Li ZH., Sun M. 2008. Image reconstruction algorithm based on the extended regularised total least squares method for electrical capacitance tomography. Science, Measurement & Technology, IET, 2(5): 326-336.

[47] Leitner, R., Mairer H., Kercek A. 2003. Real-time classification of polymers with NIR spectral imaging and blob analysis. Real-Time Imaging, 9(4): 245-251.

[48] Lestander TA, Johnsson B, Grothage. 2009. NIR techniques create added values for the pellet and biofuel industry. Bioresource Technology, 100(4), 1589-1594.

[49] Li JW., Yang XG., Wang YH., Pan RZ. 2012. An image reconstruction algorithm based on RBF neural network for electrical capacitance tomography. Electromagnetic Field Problems and Applications (ICEF), 2012 Sixth International Conference on, 1(4): 19-21.

[50] Li X., Huang ZY., Wang BL., Li HQ. 2008. A new method for the on-line voidage measurement of gas-oil two-phase flow. Instrumentation and Measurement Technology Conference Proceedings, 2008, 1189-1193.

[51] Li Y., Yang WQ., Wu ZP., Tsamakis D., Xie CG., Huang SM., Lenn C. 2012. Gas/oil/water flow measurement by electrical capacitance tomography. Imaging Systems and Techniques (IST), 2012 IEEE International Conference on, 83-88.

[52] Liu HY., Chen DY. 2006. Image reconstruction algorithms of electrical capacitance tomography based on SVM. Journal Harbin Univ. Sci. & Tech, 1(4):13-17 (In Chinese).

[53] Liu L., Chen Y., Song YC. 2010. A novel Barzilai-Borwein image reconstruction algorithm for electrical capacitance tomography system. Machine Vision and Human-Machine Interface (MVHI), 2010 International Conference on, 385-388.

[54] Liu X., Zhang J., Patrick D.J., Steele P.H. 2010. In-Plane Moisture Content and Specific Gravity Evaluation of Oriented Strandboard Using a Radio Frequency Technique. Forest Products Journal, 60(7/8): 622-628.

[55] Lu G., Peng LH., Yao DY., Zhang BF. 2004. Practical system design for electrical capacitance tomography. ACTA metrological SINICA, 25(3): 241-261 (in Chinese).

[56] Marashdeh Q., Teixeira F. L. 2004. Sensitivity matrix calculation for fast 3-D electrical capacitance tomography (ECT) of flow systems. IEEE Transactions on Magnetics, 40(2): 1204-1207

[57] Mesic M, Corluka V, Valter Z. 2005. Analysis of some parameters influencing moisture quantity measurements in wheat with NIR technique. Applied Electromagnetics and Communications, 18th International Conference on. 1-4.

[58] Minamisawa A, Ozawa A, Sakai H, Takagi K. 1990. Moisture effects on the ultrasonic velocities in wood. Ultrasonics Symposium. 2: 1105 1108.

[59] Mohamad E.J., Marwah O.M.F., Rahim R.A., Leow PL. 2011. An analysis of sensitivity distribution using two differential excitation potentials in ECT," Sensing Technology (ICST), 2011 Fifth International Conference on, 575-580.

[60] Morrow R. 1980. Applications of radio-frequency power to the drying of timber. Physical Science, Measurement and Instrumentation, Management and Education - Reviews, IEE Proceedings A. 127: 394-398.

[61] Mou CH., Peng LH., Yao DY., Xiao DY. 2005. Image reconstruction using a genetic algorithm for electrical capacitance tomography. Tsinghua Science and Technology, 10(5): 587-592.

[62] Nordell A., Vikterlof, K.J. 2000. Measurements of moisture content in wood fuels with dual energy X-ray. Vaermeforsk Technical Report (Sweden), 41p.

[63] Norimoto M. 1976. Dielectric properties of wood. Kyoto University Research Information Repository, 108-152.

[64] Olmos A. M., Primicia J. A., Marron J. L. F., 2007. Simulation design of electrical capacitance tomography sensors, IET Sci. Meas. Techno, 1(4): 216223.

[65] Pan Y., Wang HX. 2004. Two-phase flow electrical capacitance tomography system. Journal of Tianjin University of Science and Technology, 19(4): 38-42 (in Chinese)

[66] Paz, A., Nystrom, J., Thorin, E. 2006. Influence of temperature in radio frequency measurements of moisture content in biofuel. Instrumentation and Measurement Technology Conference (IMTC 2006). Proceedings of the IEEE, 175-179.

[67] Peng LH., Ye JM., Lu G., Yang WQ. 2012. Evaluation of Effect of Number of Electrodes in ECT Sensors on Image Quality. Sensors Journal, 12(5): 1554-1565.

[68] Penirschke A., Angelovski A., Jakoby R. 2010. Moisture insensitive microwave mass flow detector for particulate solids. Instrumentation and Measurement Technology Conference (I2MTC), 2010 IEEE, 1309-1313

[69] Penirschke A., Jakoby R. 2010. Design of a moisture independent microwave mass flow detector for particulate solids. German Microwave Conference. 130-133.

[70] Rasteiro, M.G., Silva F.A.P.G., Faia P. 2011. Electrical Tomography: a review of configurations and applications to particulate processes. KONA Powder and Particle Journal, 29: 67-80.

[71] Reeb J. E. 1995. Wood and moisture relationships. Ext. Serv. EM 8600, Oregon State Univ. 7p.

[72] Reeb J.E., Milota M.R. 1999. Moisture content by the oven-dry method for industrial testing. 50th Western Dry Kiln Association Meeting.

[73] Roels S., Carmeliet J. 2006. Analysis of moisture flow in porous materials using microfocus X-ray radiography. International Journal of Heat and Mass Transfer, 49, 4762-4772.

[74] Saxena S.C. 1981. Capacitive moisture meter. Industrial Electronics and Control Instrumentation, IEEE Transactions on, 37-39.

[75] Schajer G. S., Orhan F. B. 2005. Microwave non-destructive testing of wood and similar orthotropic materials. Sensing and Imaging Series, 6: 293-313.

[76] Shao XY., Huang ZY., Ji HF., Li HQ. 2003. Study on flow pattern identification of gas-oil two-phase flow based on electrical capacitance tomography and fuzzy pattern recognition. Journal of chemical engineering of Chinese Universities, 17(6): 616-621.

[77] Siau J.F. 1984. Transport processes in wood. Springer-Verlag, NewYork, 245p.

[78] Steele P. H. and J. E. Cooper. 2003. Estimating lumber strength with radio frequency scanning. Computers and Electronics in Agriculture, 41(13): 77-83.

[79] Steiner G., Wegleiter H., Watzenig D. 2005. A dual mode ultrasound and electrical capacitance process tomography sensor. Sensors, 696-699.

[80] Sun M, Liu S, Lei J, Li ZH. 2008. Mass flow measurement of pneumatically conveyed solids using electrical capacitance tomography. Measurement science and technology. 19(4): 1-6.

[81] Thygesen L.G., Lundqvist, S.O. 2000. NIR measurement of moisture content in wood under unstable temperature conditions. Part 1. Thermal effects in near infrared spectra of wood, Journal of Near Infrared Spectroscopy, 8: 183-189

[82] Tormanen, V. O., Makynen, A.J. 2011. Determination of wood moisture content using angularly, spatially and spectrally resolved reflectance. Instrumentation and Measurement Technology Conference (I2MTC), 1-5.

[83] Vallejos C. G. 2009. Wood moisture content measurement at 2.45 GHz. Microwave and Optoelectronics Conference (IMOC), 2009 SBMO/IEEE MTT-S International, 221-225.

[84] Van D.J. 2005. Introduction of a 2 transducer ultrasonic mass flow meter. Instrumentation and Measurement Technology Conference. IMTC 2005. Proceedings of the IEEE, 2: 1369-1372.

[85] Vanarase A.U., Jackeline M.A., Rozo I.J., Muzzio F.J., Romaach R.J. 2010. Real-time monitoring of drug concentration in a continuous powder mixing process using NIR spectroscopy. Chemical Engineering Science, 65: 5728-5733

[86] Via B.K., Shupe T.F., Groom L.H., Stine M., So C.L. 2003. Multivariate modelling of density, strength and stiffness from near infrared spectra for mature, juvenile and pith wood of longleaf pine. Journal of near infrared spectroscopy, 11(5): 365-378.

[87] Wang BL., Huang ZY., Li HQ. 2009. Design of high-speed ECT and ERT system. Journal of Physics: Conference Series, 147(1).

[88] Wang F., Marashdeh Q., Fan LS., Warsito W. 2010. Electrical capacitance volume tomography: design and applications. Sensors, 10: 1890-1917

[89] Wang HC., Fedchenia I., Shishkin S., Finn A., Smith L., Colket M. 2012. Electrical Capacitance Tomography: A compressive sensing approach. Imaging Systems and Techniques (IST), 2012 IEEE International Conference on, 590-594.

[90] Xie CG., Atkinson I., Lenn C. 2007. Multiphase flow measurement in oil and gas production. Proc. 5th World Congress on industrial Process Tomography, 723-736.

[91] Xie CG., Huang SM., Hoyle BS., Thorn R., Lenn C., Snowden D., Beck MS. 1992. Electrical capacitance tomography for flow imaging: system model for development of image reconstruction algorithms and design of primary sensors. Circuits, devices and systems, 139(1): 89-98.

[92] Xie CG., Stott AL., Plaskowski AB., Beck MS. 1990. Design of capacitance electrodes for concentration measurement of two-phase flow, Meas. Sci. Technol. 1: 65-78

[93] Xu LJ., Carter R.M., Yan Y. 2005. Mass flow measurement of fine particles in a pneumatic suspension using electrostatic sensing and neural network techniques. Instrumentation and Measurement Technology Conference. IMTC 2005. Proceedings of the IEEE, 2: 1365-1368.

[94] Xu LJ., Weber A.P., Kasper G. 2000. Capacitance-based concentration measurement for gas -particle system with low particles loading. Flow Measurement and Instrumentation, 11(3): 185-194.

[95] Yan H., Shao FQ., Wang S. 1999. Simulation study of capacitance tomography sensors. 1st Word Congress on Industrial Tomography, Buxton, Greater Manchester, 388-394.

[96] Yan H., Shao FQ., Wang S., Wu EG. Analysis of soft field characteristics of capacitance tomography sensors. Journal of northeastern university, 20(5).

[97] Yan H., Tang DD., Zhang L., Cui KX. 2008. Research on the axial responses of ECT sensors. Intelligent Control and Automation, 2008. WCICA 2008. 7th World Congress on, 7762-7767.

[98] Yan H., Wang YF., Zhou YG. 2011. Research on direct 3D ECT imaging: sensor modeling and image reconstruction. Computational and Information Sciences (ICCIS), 2011 International Conference on, 95-98.

[99] Yan Y. 1996. Mass flow measurement of bulk solids in pneumatic pipelines. Measurement Science and Technology, 7(12): 1687-1706.

[100] Yang DY., Zhou B., Wang SM. 2009. Electrical capacitance tomography in dense-phase pneumatic conveying of pulverized coal under high pressure. Imaging Systems and Techniques, 2009. IST '09. IEEE International Workshop on, 41-46.

[101] Yang WQ.1996. Hardware design of electrical capacitance tomography systems. Meas. Sci. Technol, 7: 225232.

[102] Yang WQ. 2006. Key issues in designing capacitance tomography sensors. Sensors, 2006. 5th IEEE Conference on, 497-505.

[103] Yang WQ., Conway, WF. 1998. Measurement of sensitivity distributions of capacitance tomography sensors. Review of Scientific Instruments, 69(1), 233-236.

[104] Yang WQ., Liu S. 1999. Electrical capacitance tomography with square sensor. Electronics Letters, 35(4):295-296.

[105] Yang WQ., Spink DM., York TA., McCann H. 1999. An image reconstruction algorithm based on Landwebers iteration method for electrical capacitance tomography Meas. Sci. Technol. 10: 10651069.

[106] Yang WQ., York T.A. 1999. New AC-based capacitance tomography system. IEE Proc. - Sci. Meas. Technol, 146(1): 47-53.

[107] Yang YL., Huang M. 2007. Simulation study of sensor capacitance of ECT system based on ANSYS software. Electronic measurement technology, 30(3): 44-46 (in Chinese)

[108] Ye J., Wang H., Yang W. 2014. Image reconstruction for electrical capacitance tomography based on sparse representation. Instrumentation and Measurement, IEEE Transactions on , 99: 1.

[109] Young M., Pickup E., Deloughry R., Hartley T., Nixon S.A., Barratt L. 1996. Development of a variable density flowmeter for an industrial application using tomographic imaging. Advances in Electrical Tomography (Digest No: 1196/143), IEE Colloquium on, 14: 1-3.

[110] Zhang HF., Li YX., Jiang LC. 2010. Multivariate modeling Dahurian larch plantation wood density based on near infrared spectroscopy. Measuring Technology and Mechatronics Automation (ICMTMA), 2010 International Conference on, 2: 748-751

Appendices

Appendix A

ECT System Hardware Details

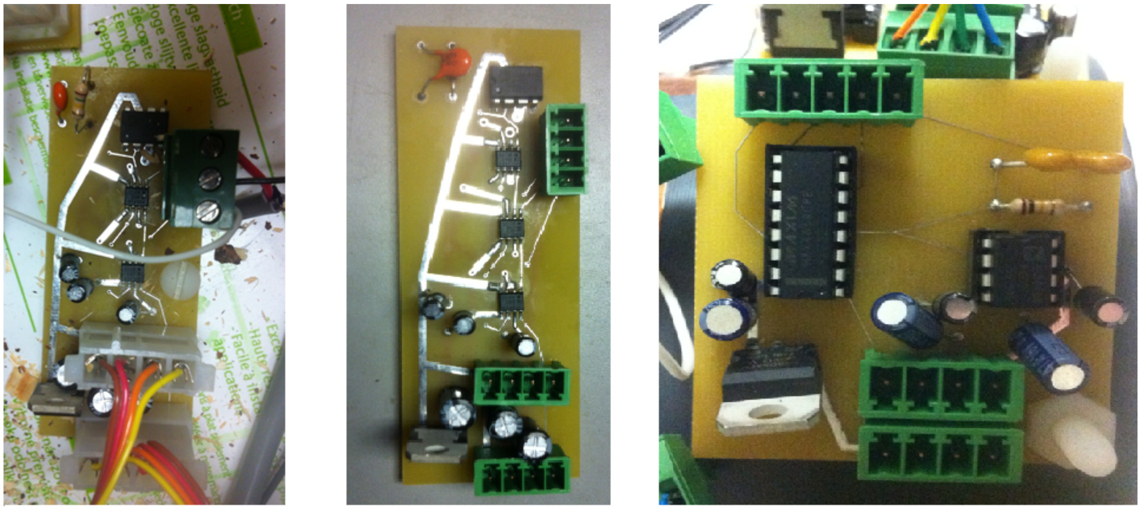

(a) (b) (c)

Figure A.1: Printed circuit board. (a) With two switches, (b) three swicthes, (c) three switches in a chip

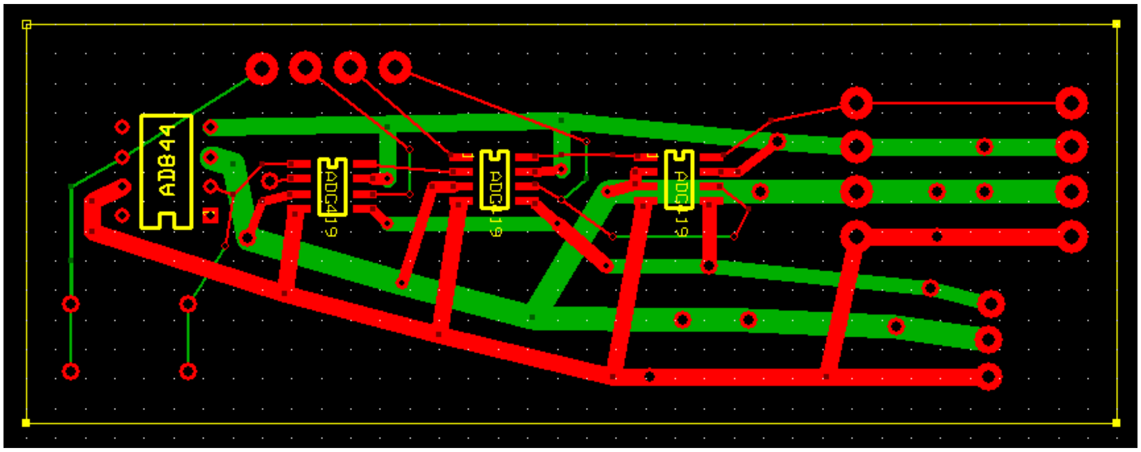

Figure A.2: Printed circuit board drawing of three separate switches as in figure A.1b

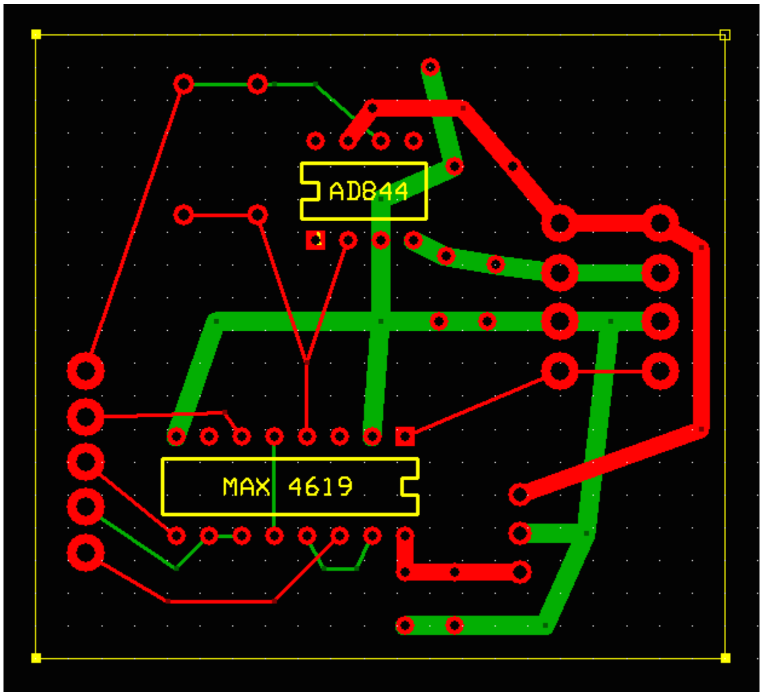

Figure A.3: Printed circuit board drawing of three switches in single chip as in figure A.1c

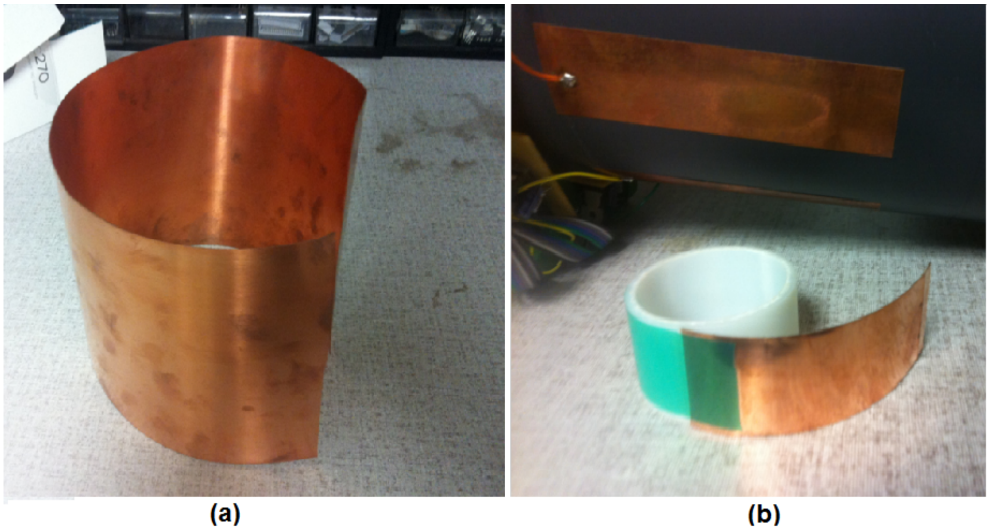

Figure A.4: Copper materials. (a) Copper shield, (b) sticky copper for electrodes

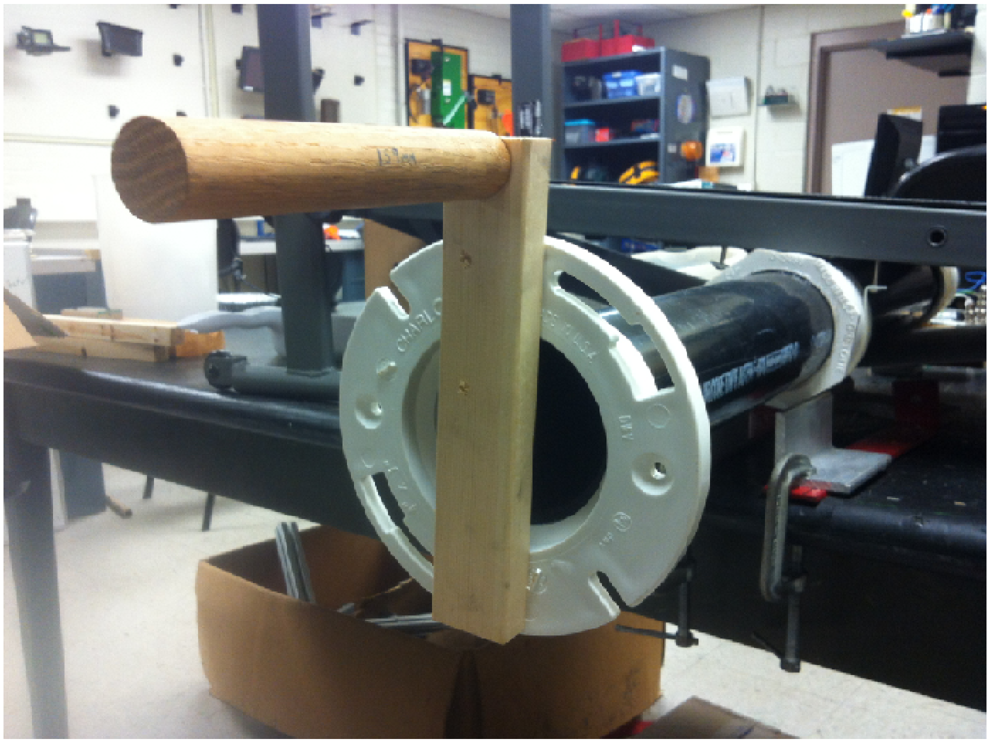

Figure A.5: Manual conveyor belt driver using a ABS pipe

Figure A.6: Mechnical treadmill used as woodchips feeding system

Figure A.7: Power supply, function generator and oscilloscope

Figure A.8: Data acquisition devices

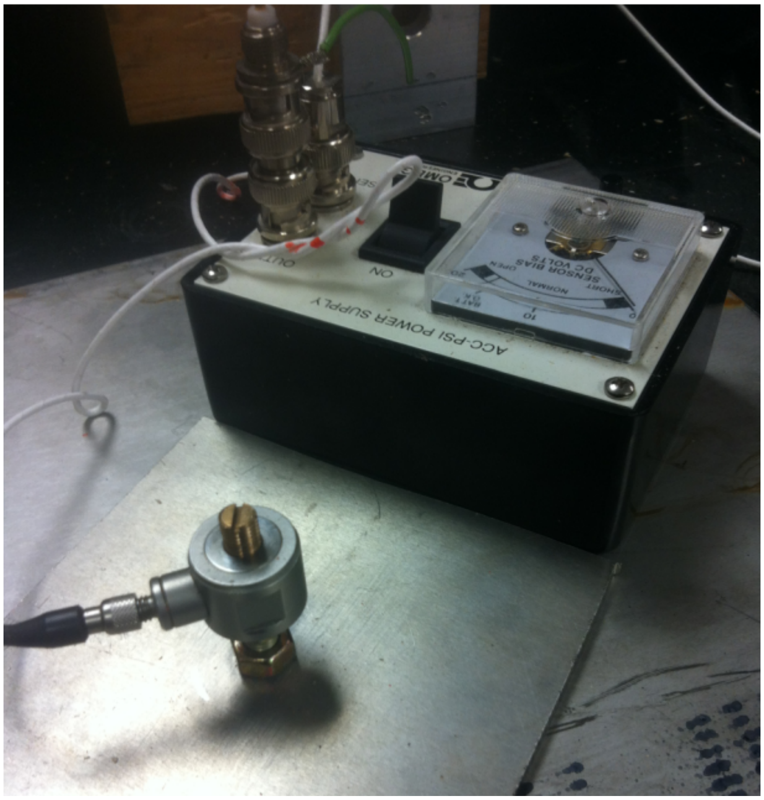

Figure A.9: Dynamic force transducer and the impact surface

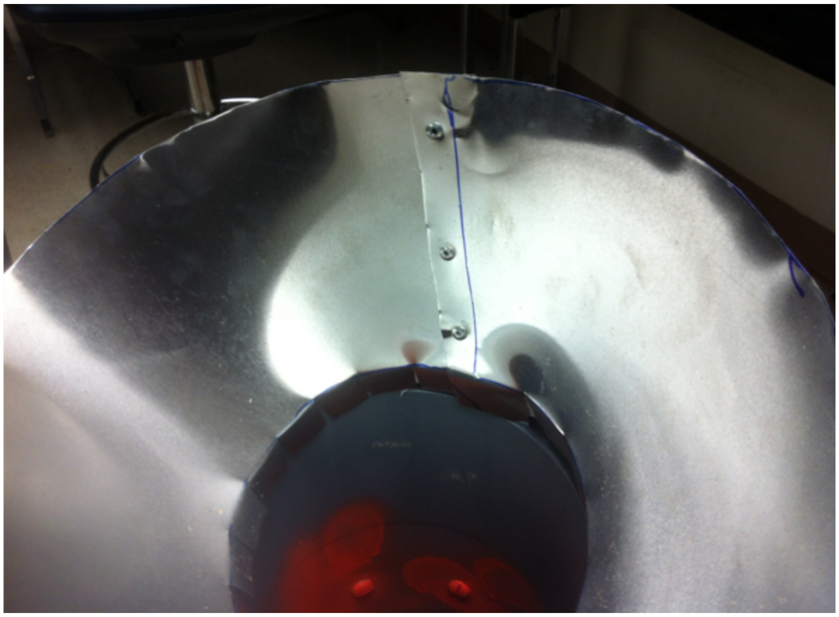

Figure A.10: Aluminium hopper above the ECT

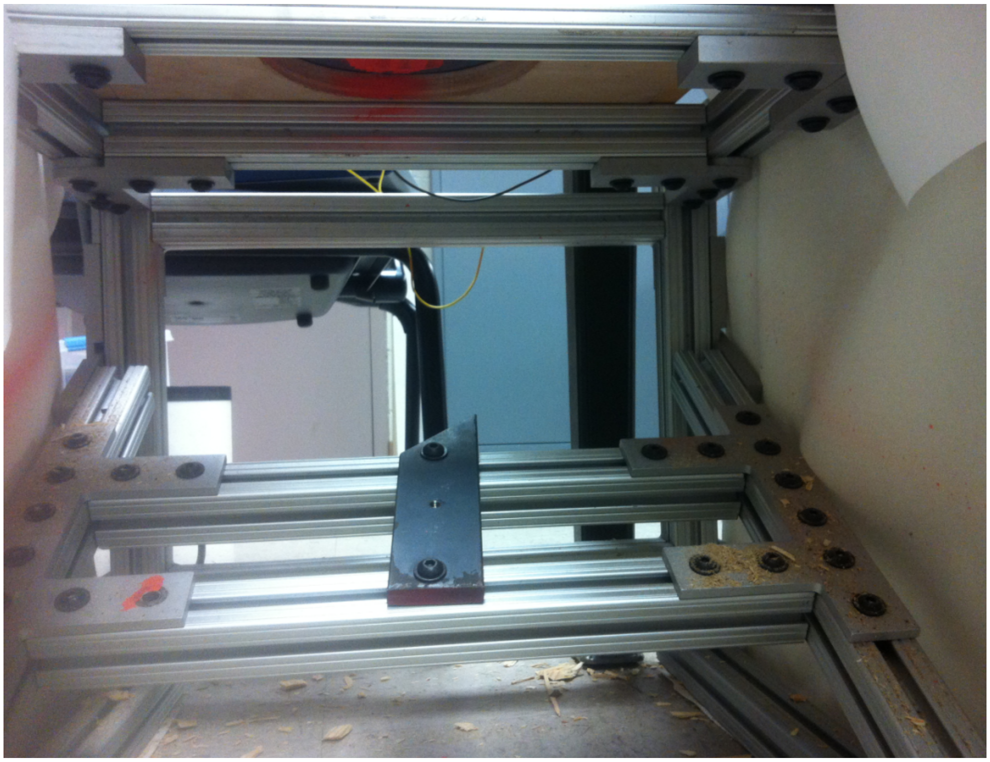

Figure A.11: Metal basis of the ECT system

Figure A.12: System illumination for image calibration

Figure A.13: Webcam for ECT image calibration

Appendix B

Related Equipments

Figure B.1: Computer for data processing and system control

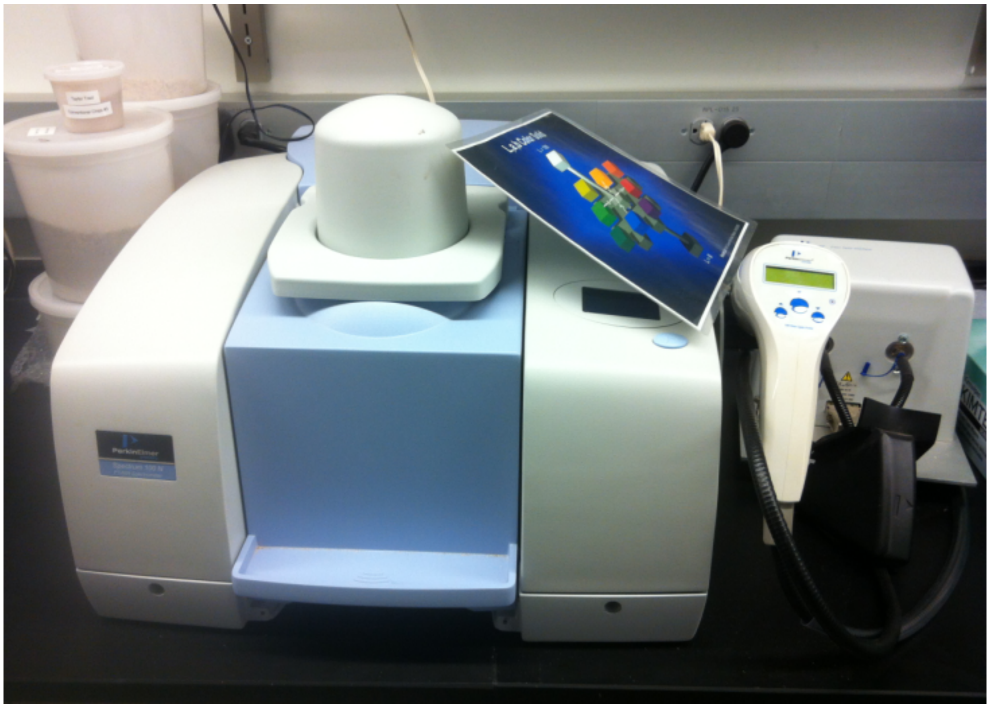

Figure B.2: PerkinElmer Spectrum 100N FT-NIR spectrometer

Figure B.3: Scale

Figure B.4: Oven for woodchips drying

Figure B.5: Walk-in freezer for woodchips storage

Appendix C

Tested materials

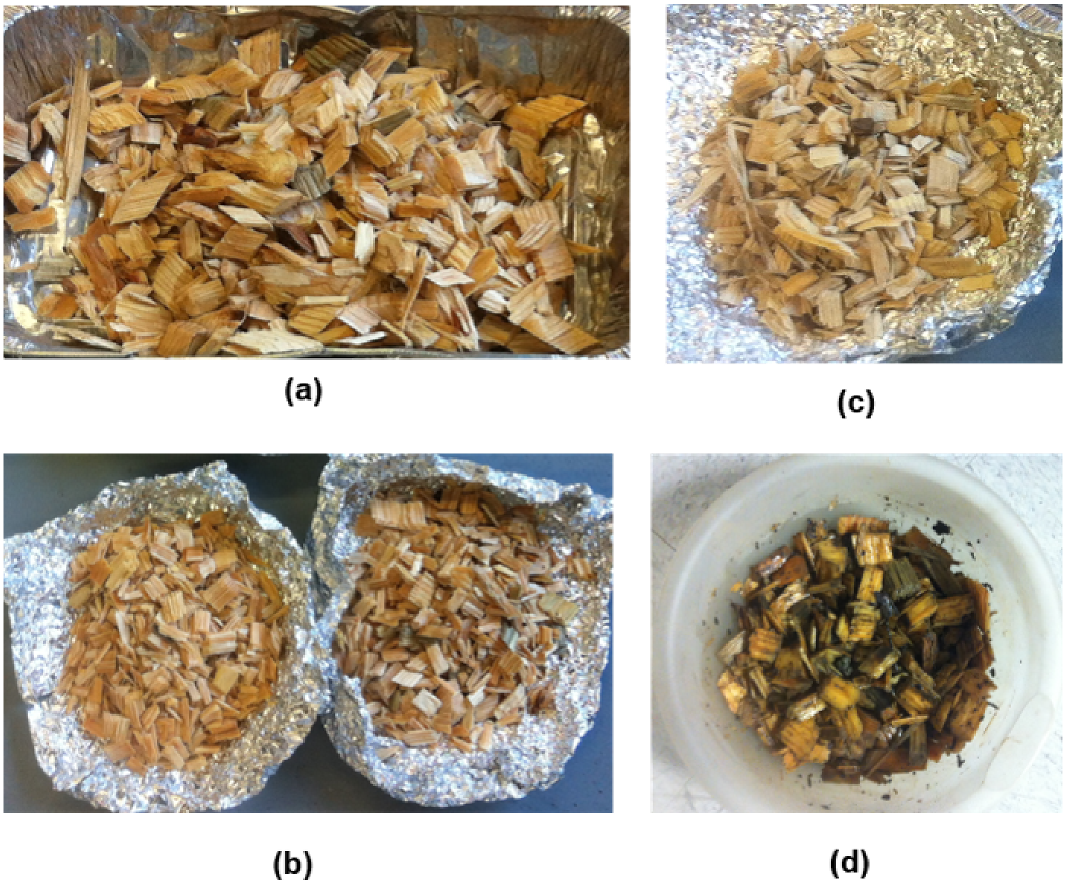

Figure C.1: Tested woodchip samples. (a) Batch 1&2, (b) batch 3&4, (c) batch 5, and (d) batch 6.

Figure C.2: Tested dried woodchips and wood powder

Figure C.3: Tested PVC rods

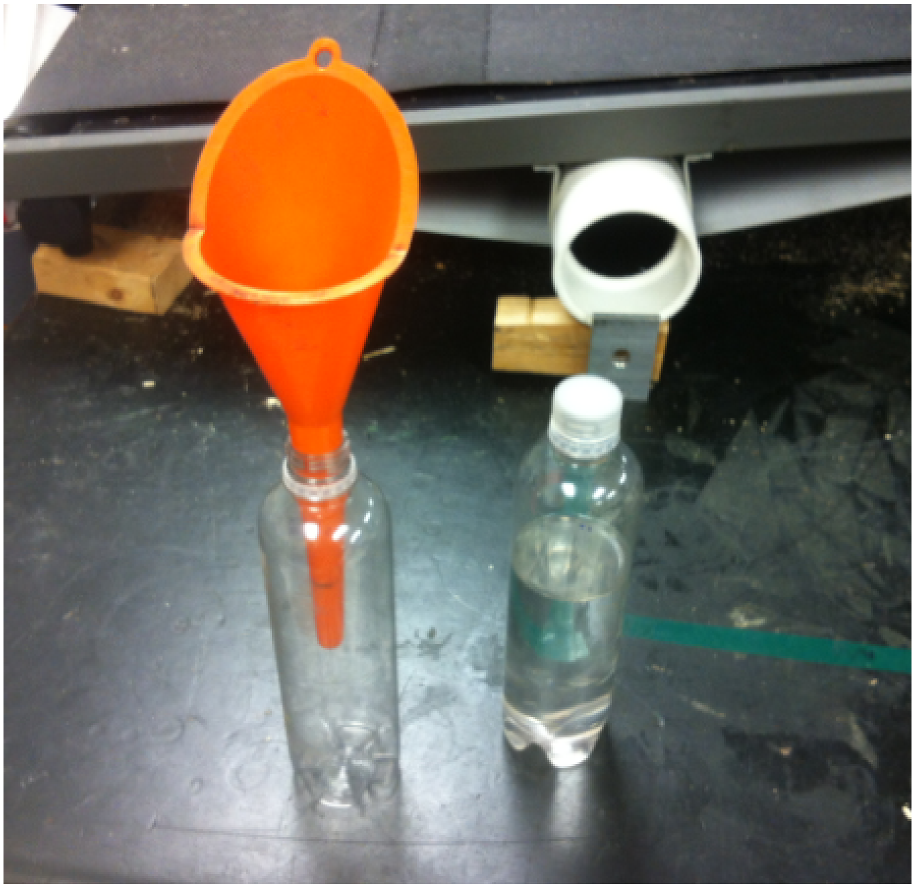

Figure C.4: Tested water in plastic bottles

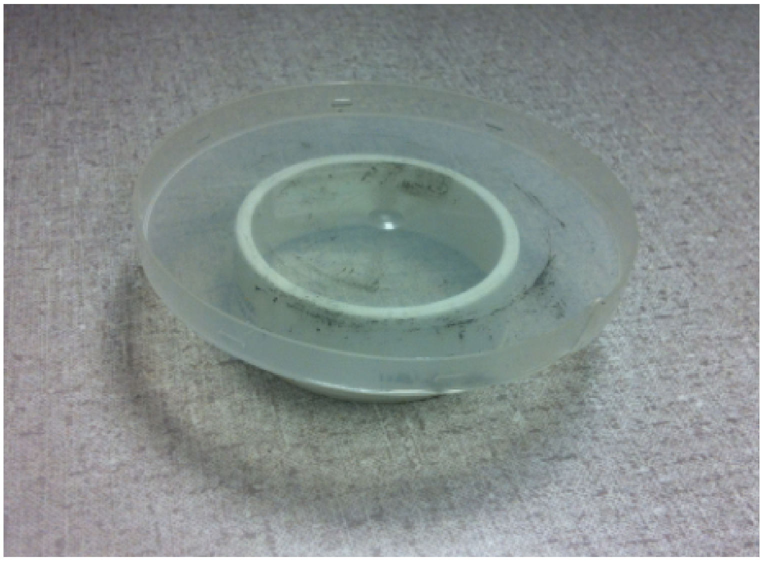

Figure C.5: Plastic container for material sensitivity tests

Appendix D

Softwares

Matlab codes

1. T-test: $[h, p, ci, stats] = ttest2(x, y, 0.05)$.
2. Anova: $p = anova1(x)$.
3. Stepwise: $stepwise(x, y, inmodel, penter, premove)$.
4. PCA: $[coeff, score, latent] = princomp(p)$;

   $PC = score * coeff' + repmat(mean(p), size(p, 1), 1)$;

   figure;

   $percent\_explained = 100 * latentsum(latent)$;

   pareto(percent_explained);

   xlabel('Principal Component');

   ylabel('Variance Explained (%)');

   print -djpeg 2;
5. Welch's power spectral density estimate: $pxx = pwelch(x, window, noverlap, nfft)$
6. Landweber:

   For i= 1:20

   $G = G + S^T(C - SG)$

   end

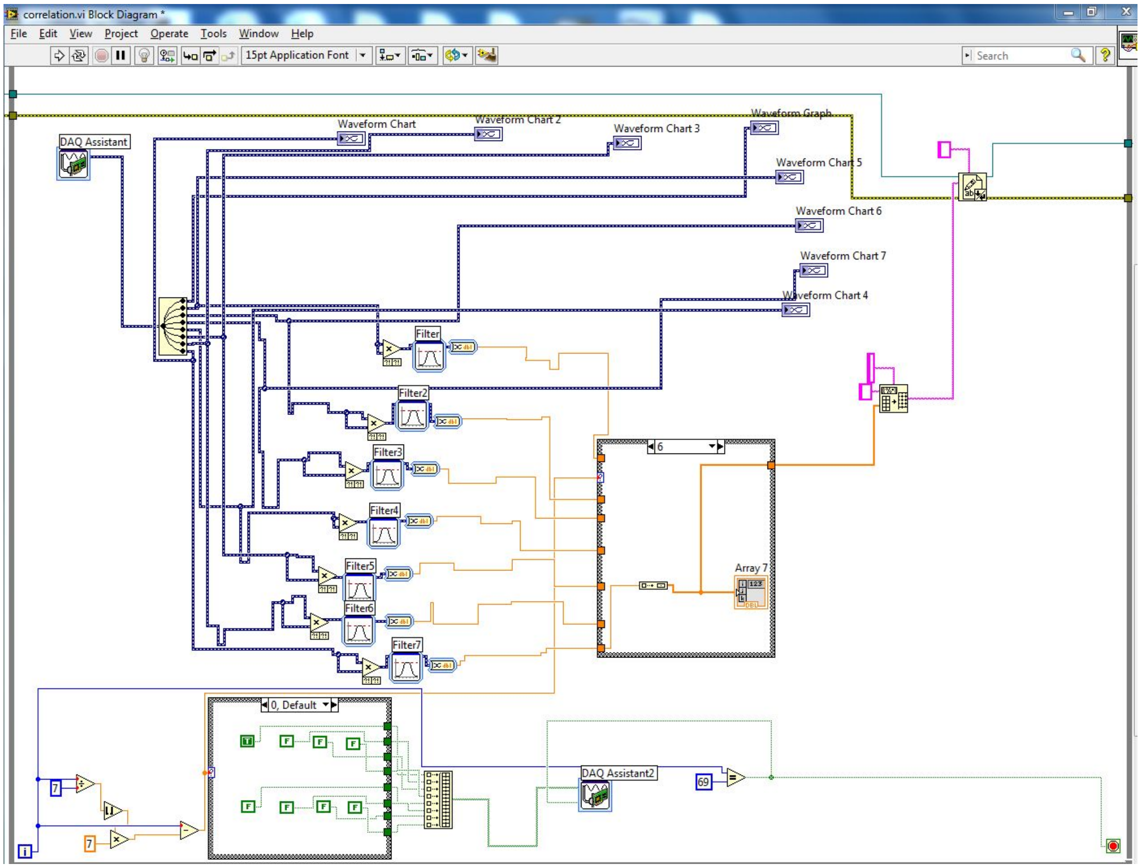

Figure D.1: Signal auto-correlation for amplitude extraction in Labview

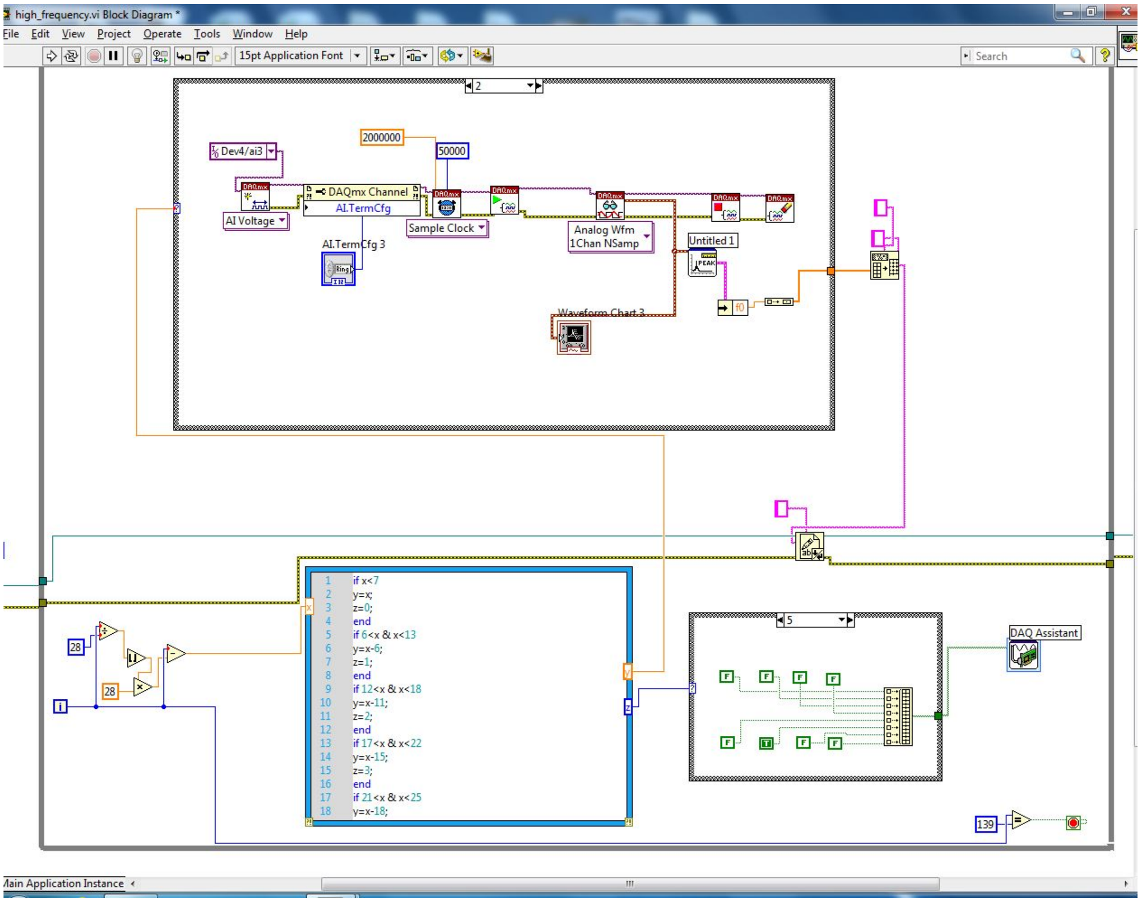

```
if x<7
y=x;
z=0;
end
if 6<x & x<13
y=x-6;
z=1;
end
if 12<x & x<18
y=x-11;
z=2;
end
if 17<x & x<22
y=x-15;
z=3;
end
if 21<x & x<25
y=x-18;
```

Figure D.2: One source one receiver mode and FFT amplitude extraction in Labview

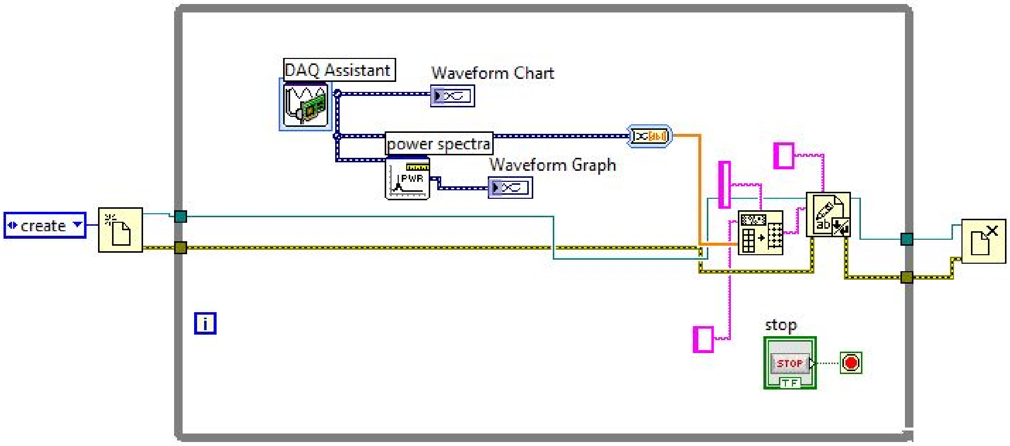

Figure D.3: Labview impact data collection

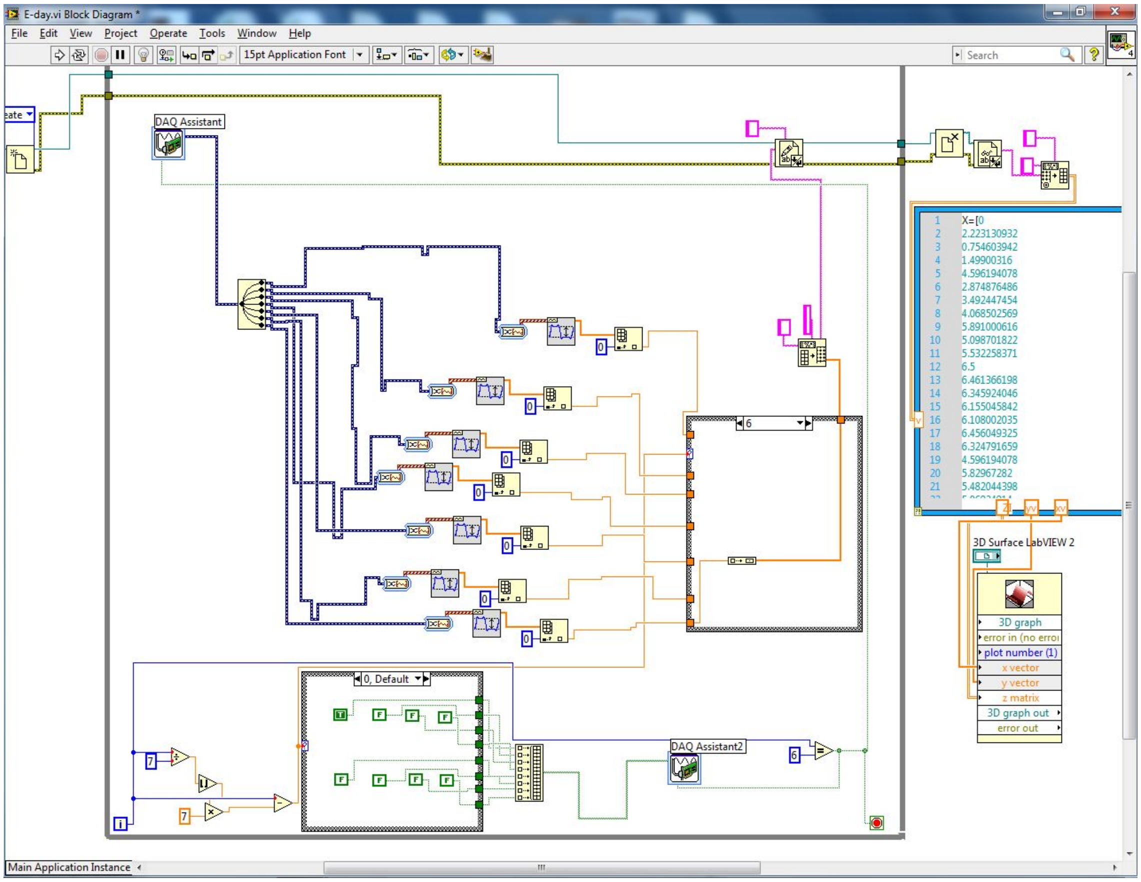

```
X=[0
2.223130932
0.754603942
1.49900316
4.596194078
2.874876486
3.492447454
4.068502569
5.891000616
5.098701822
5.532258371
6.5
6.461366198
6.345924046
6.155045842
6.108002035
6.456049325
6.324791659
4.596194078
5.82967282
5.482044398
```

Figure D.4: Labview real-time image reconstruction program

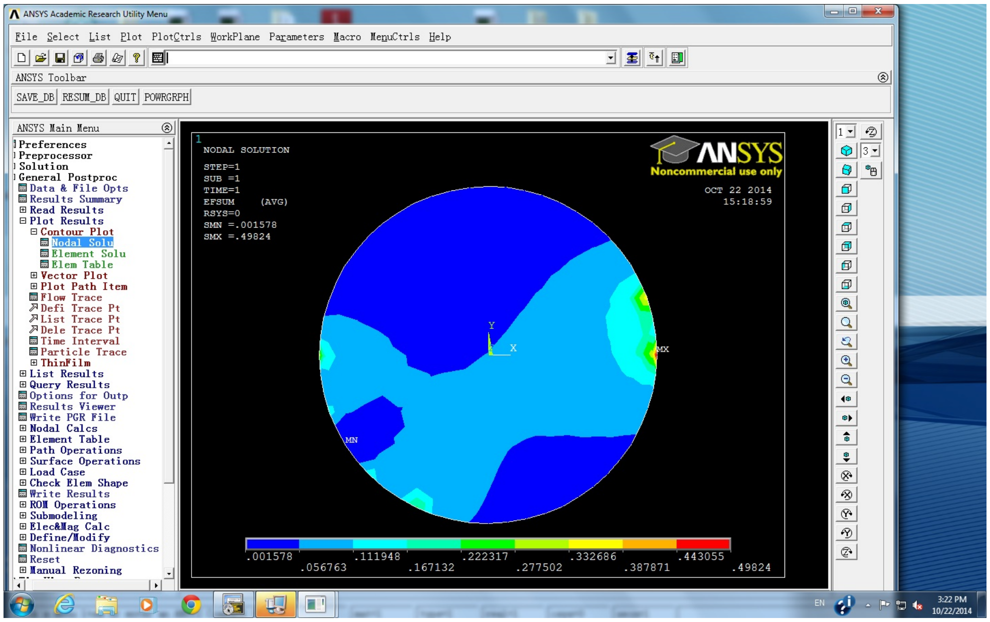

```
1
NODAL SOLUTION

STEP=1
SUB =1
TIME=1
EFSUM    (AVG)
RSYS=0
SMN =.001578
SMX =.49824
```

```
OCT 22 2014
15:18:59
```

Figure D.5: ANSYS user interface

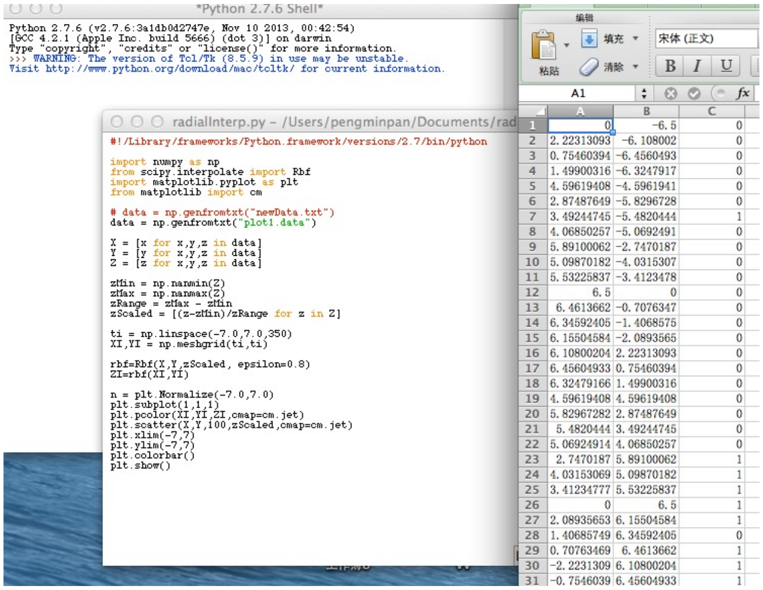

```
Python 2.7.6 (v2.7.6:3a1db0d2747e, Nov 10 2013, 00:42:54)
[GCC 4.2.1 (Apple Inc. build 5666) (dot 3)] on darwin
Type "copyright", "credits" or "license()" for more information.
>>> WARNING: The version of Tcl/Tk (8.5.9) in use may be unstable.
Visit http://www.python.org/download/mac/tcltk/ for current information.
```

```
#!/Library/frameworks/Python.framework/versions/2.7/bin/python

import numpy as np
from scipy.interpolate import Rbf
import matplotlib.pyplot as plt
from matplotlib import cm

# data = np.genfromtxt("newData.txt")
data = np.genfromtxt("plot1.data")

X = [x for x,y,z in data]
Y = [y for x,y,z in data]
Z = [z for x,y,z in data]

zMin = np.nanmin(Z)
zMax = np.nanmax(Z)
zRange = zMax - zMin
zScaled = [(z-zMin)/zRange for z in Z]

ti = np.linspace(-7.0,7.0,350)
XI,YI = np.meshgrid(ti,ti)

rbf=Rbf(X,Y,zScaled, epsilon=0.8)
ZI=rbf(XI,YI)

n = plt.Normalize(-7.0,7.0)
plt.subplot(1,1,1)
plt.pcolor(XI,YI,ZI,cmap=cm.jet)
plt.scatter(X,Y,100,zScaled,cmap=cm.jet)
plt.xlim(-7,7)
plt.ylim(-7,7)
plt.colorbar()
plt.show()
```

	A	B	C
1	0	-6.5	0
2	2.22313093	-6.108002	0
3	0.75460394	-6.4560493	0
4	1.49900316	-6.3247917	0
5	4.59619408	-4.5961941	0
6	2.87487649	-5.8296728	0
7	3.49244745	-5.4820444	1
8	4.06850257	-5.0692491	0
9	5.89100062	-2.7470187	0
10	5.09870182	-4.0315307	0
11	5.53225837	-3.4123478	0
12	6.5	0	0
13	6.4613662	-0.7076347	0
14	6.34592405	-1.4068575	0
15	6.15504584	-2.0893565	0
16	6.10800204	2.22313093	0
17	6.45604933	0.75460394	0
18	6.32479166	1.49900316	0
19	4.59619408	4.59619408	0
20	5.82967282	2.87487649	0
21	5.4820444	3.49244745	0
22	5.06924914	4.06850257	0
23	2.7470187	5.89100062	1
24	4.03153069	5.09870182	1
25	3.41234777	5.53225837	1
26	0	6.5	1
27	2.08935653	6.15504584	1
28	1.40685749	6.34592405	0
29	0.70763469	6.4613662	1
30	-2.2231309	6.10800204	1
31	-0.7546039	6.45604933	1

Figure D.6: Python image reconstruction code

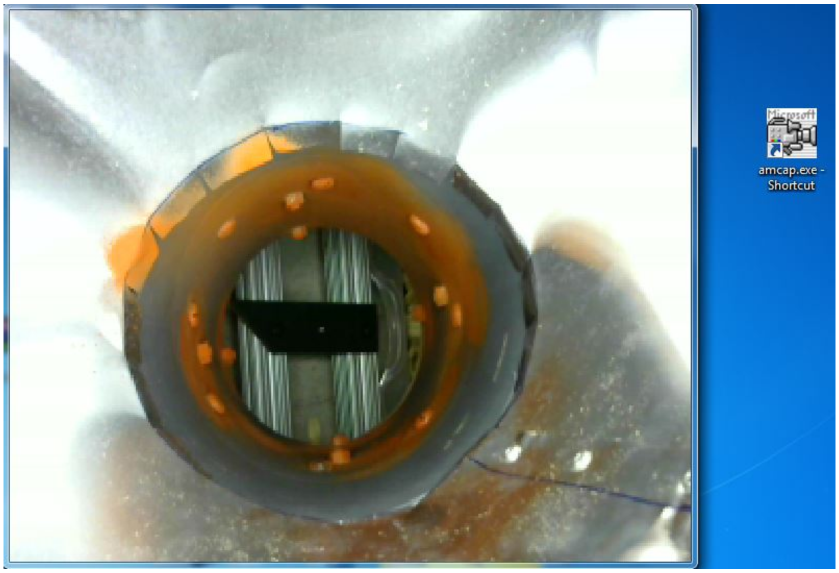

Figure D.7: Amcap software for webcam

Appendix E

Raw Data Examples

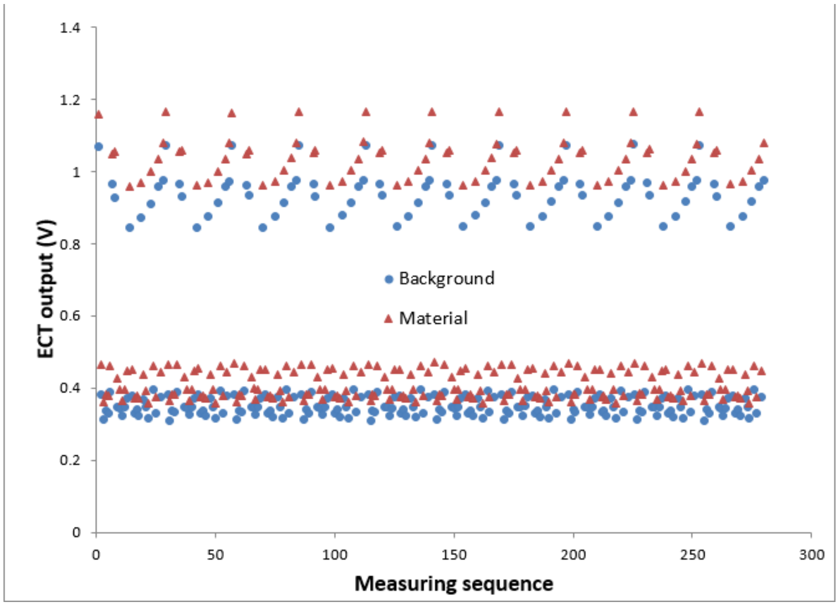

Figure E.1: 10 repeating readings from all electrode combinations at empty and full states

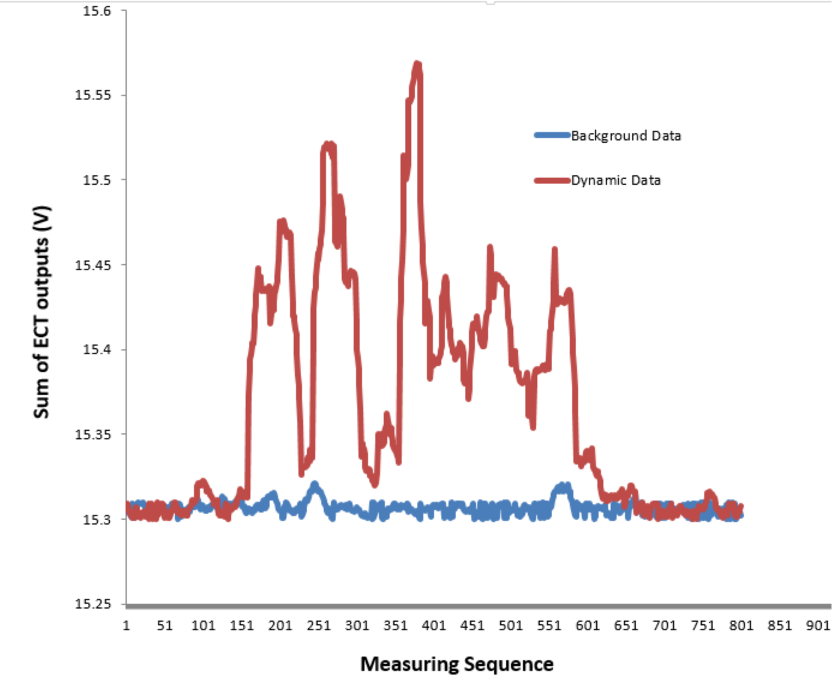

Figure E.2: Dynamic ECT readings in sum